THE UNIVERSITY OF HULL

An Evaluation of the Performance of Multi-static Handheld Ground Penetrating Radar using Full Wave Inversion for Landmine Detection

Being a Thesis submitted for the Degree of Doctor of Philosophy

in the University of Hull

by

Suki Dauda Sule, MSc, B.Eng. (Hons)

June 2018

Acknowledgments

I would like to begin by thanking my first supervisor, Dr. Kevin Paulson for his support and guidance before and throughout my research. His enthusiasm, optimism and availability have been critical to the completion of this work despite the challenges.

To my second supervisor Mr. Nick Riley whose persistent constructive criticism and suggestions always helped to point me in the right direction.

My special gratitude goes to my sponsor, the Petroleum Technology Development Fund (PTDF) of Nigeria for providing me with an exceptional full scholarship, one of the best in the world, without which this research would not have been possible.

I'm also grateful to the humanitarian demining research teams at the University of Manchester led by Professors Anthony Peyton and William Lionheart for their support.

I thank the Computer Simulation Technology (CST) GmbH technical support for the CST STUDIO SUITE.

I will not forget the administrative support of Jo Arnett and Glen Jack in processing my numerous requests, expense claims and other academic requisitions.

To my colleagues, my laboratory mate and other PhD students in the Electronic Engineering Department for their moral support and encouragement.

I'm very thankful to Pastor Isaac Aleshinloye and the Amazing Grace Chapel, Hull family for providing me with a place of spiritual support, friendship, opportunity for community service and a place to spend my time outside of academic study productively.

I need to thank my parents, Mr. and Mrs. S. S. Sule for their immense support in many ways and encouragement throughout my studies generally and my postgraduate study at the University of Hull. Special thanks also go to my sisters Suninba and Saundiba, as well as Aisha and my brother Saminu, who have also provided the motivation for me to succeed. I won't forget my extended family members, uncles, aunties and cousins who I can't mention by name but who have all contributed to my achievements in one way or the other.

Lastly, I want to appreciate my dear wife Ndepana for her encouragement and support and my wonderful daughter Sarah Azaria for arriving and inspiring me in the final stages of the project.

I cannot conclude this acknowledgement without a declaration of gratitude and praise to God who I firmly believe in and who is the source of my life and my driving force.

Abstract

This thesis presents an empirical study comparing the ability of multi-static and bi-static, handheld, ground penetrating radar (GPR) systems, using full wave inversion (FWI), to determine the properties of buried anti-personnel (AP) landmines. A major problem associated with humanitarian demining is the occurrence of many false positives during clearance operations. Therefore, a reduction of the false alarm rate (FAR) and/or increasing the probability of detection (POD) is a key research and technical objective. Sensor fusion has emerged as a technique that promises to significantly enhance landmine detection. This study considers a handheld, combined metal detector (MD) and GPR device, and quantifies the advantages of the use of antenna arrays. During demining operations with such systems, possible targets are detected using the MD and further categorised using the GPR, possibly excluding false positives. A system using FWI imaging techniques to estimate the subsurface parameters is considered in this work.

A previous study of multi-static GPR FWI used simplistic, 2D far-field propagation models, despite the targets being 3D and within the near field. This novel study uses full 3D electromagnetic (EM) wave simulation of the antenna arrays and propagation through the air and ground. Full EM simulation allows the sensitivity of radio measurements to landmine characteristics to be determined. The number and configuration of antenna elements are very important and must be optimised, contrary to the 2D sensitivity studies in (Watson, Lionheart 2014, Watson 2016) which conclude that the degree (number of elements) of the multi-static system is not critical. A novel sensitivity analysis for tilted handheld GPR antennas is used to demonstrate the positive impact of tilted antenna orientation on detection performance. A time domain GPR and A-scan data, consistent with a commercial handheld system, the MINEHOUND, is used throughout the simulated experiments which are based on synthetic GPR measurements.

Finally, this thesis introduces a novel method of optimising the FWI solution through feature extraction or estimation of the internal air void typically present in pressure activated mines, to distinguish mines from non-mine targets and reduce the incidence of false positives.

Table of Contents

List of Figures and Tables

List of Acronyms

1D, 2D, 3D	one, two and three-dimensional
ABC	absorbing boundary conditions
ALIS	advanced landmine imaging system
AP	anti-personnel mine
AT	anti-tank mine
AXO	abandoned explosive ordinance
CST	Computer Simulation Technology
DRH	double ridged horn
DRI	detection, recognition and identification
EM	electromagnetic
EMI	electromagnetic induction
ERW	explosive remnants of war
FABW	Find A Better Way
FAR	false alarm rate
FDTD	finite difference time domain
FIT	finite integration technique
FWI	full wave inversion
GPR	ground penetrating radar
HSTAMID	handheld standoff mine detection system
IED	improvised explosive device
IR	infra-red
L-BFGS	limited memory Broyden-Fletcher-Goldfarb-Shannon
LSQ	least squares
MD	metal detector

MMI	man machine interface
NQR	nuclear quadrupole resonance
PCA	principal component analysis
PEC	perfect electric conductor
PETN	Pentaerythritol tetranitrate
PML	perfectly matched layer
POD	probability of detection
RCS	radar cross section
RDX	explosive $\left(O_2NNCH_2\right)_3$
ROC	receiver operating characteristics
RX	receive/receiver
SAR	synthetic aperture radar
SCR	signal-to-clutter ratio
SFCW	stepped frequency continuous wave
SIMO	single input multiple output
SNR	signal-to-noise ratio
SVD	singular value decomposition
TEM	transverse electromagnetic
TNT	trinitrotoluene
TRL	technology readiness level
TX	transmit/transmitter
UN	United Nations
UWB	ultra-wideband
UXO	unexploded ordinance

Chapter 1 Introduction

1.1 The Humanitarian Demining Challenge

Landmines are man-made explosive devices that are deposited in areas that have been conflict zones, besieged by insurgency, war torn or experience military activity. Landmines have proven to be effective weapons that have ravaged communities and lives, causing destruction or serious damage without discrimination. They have adversely affected human populations, leading to displacement, disruption of way of life and almost irreversible effects on economic, social and environmental restoration (Daniels 2006). The two broad classifications of landmines are the anti-vehicle or anti-tank (AT) mines, and the anti-personnel (AP) mines. The latter are responsible for most civilian incidences (Daniels 2007)(Daniels 2006). It is reported that there are more than 2500 versions of mines and fuse setups that have been developed (Ho, Collins et al. 2004). Fuse mechanisms are typically pressure activated but may also be triggered by sound, magnetic fields, wireless systems or motion (Habib 2008). Other forms of man-made or homemade explosive devices that harm vehicles or persons are referred to as improvised explosive devices (IEDs), unexploded ordnances (UXOs), abandoned explosive ordnances (AXOs) and explosive remnants of war (ERW). An IED is a rudimentary version of a landmine. The UXO is an explosive device which failed activation at the time of use and is not evacuated from the field, constituting a future source of danger, whereas the AXO or ERW refers to an unused explosive device that is left behind (Monitoring and Research Committee, ICBL- CMC Governance Board 2016).

The United Nations (UN) Mine Ban Treaty (UNITED NATIONS 1997 (standard section 5, paragraph 10)) defines an antipersonnel mine as “a mine designed to be exploded by the presence, proximity or contact of a person and that will incapacitate, injure or kill one or more persons.” Curiously, a landmine costs between US$3 and US$30 to make, whereas it requires between US$300 and US$1000 to identify and remove a single mine (Habib 2007). In (UNITED NATIONS 1997 (standard section 5, paragraph 10)) the UN has prescribed a standard for the clearance of mines and UXOs under its control which includes a 99.6% landmine clearance rate. This was replaced by a new standard in (UNITED NATIONS 2003) which stipulates a minimum clearance depth of 130 mm below the ground surface and defines clearance thus: “Land shall be accepted as 'cleared' when the demining organisation has ensured the removal and/or destruction of all mine and ERW hazards, (including unexploded sub-munitions), from the specified area to the specified depth”. The regulations are mainly applicable to humanitarian or civilian demining as there is also military demining which is premised primarily on military tactics and mission requirements rather than total land clearance. A mine clearance rate of 80% is acceptable for military demining (Habib 2008).

The Landmine Monitor 2016 (Monitoring and Research Committee, ICBL- CMC Governance Board 2016) provides some of the most current information concerning global humanitarian demining activities and relevant data which covers the year 2015. The UN Mine Ban Treaty comprises 162 State Parties at the time of the report. The use of AP mines by non-state militia groups was reported in 10 countries. These include Afghanistan, Colombia, Iraq, Libya, Myanmar, Nigeria, Pakistan, Syria, Ukraine and Yemen. Global financial support for humanitarian demining plummeted to its lowest

over the previous 10 years and the number of casualties recorded was also the highest over the same period. Casualties escalated by 75% from the recorded numbers in 2014, due largely to unprecedented cases of casualties reported in Libya, Syria, Ukraine and Yemen. However, the casualties recorded were spread across 56 countries in total.

Humanitarian demining is a growing global problem. Two of the key objectives of humanitarian demining operations are increasing the probability of detection (POD) and reduction of the false alarm rate (FAR) (Daniels 2007). This translates to increasing the discrimination or distinguishability of targets and the reduction of false positives respectively. Typically, humanitarian or community demining operations are slow and tedious as many require handheld systems with human operators, with a variety of technical and human limitations. The effective reduction of false positives is critical to ensuring faster yet safer and more reliable AP mine clearance operations globally.

1.2 Landmine Detection Methods

Millions of mines have been deployed all over the world in the last two decades, mostly in developing or poorer countries. Land mines are being deployed much faster than they are removed. The process of AP landmine clearance involves detection, classification or discrimination and subsequent removal of all mines in an area. Therefore, detection is a critical first step to the solution. Methods used for AP mine detection include electromagnetic induction (EMI) such as the metal detector (MD), ultra-wideband (UWB) radar such as ground penetrating radar (GPR), acoustic, infrared, nuclear and biological detection (Dubey, Harvey et al. 2001)(Macdonald, Lockwood et al. 2003). AP mines are broadly classified into fragmentation and blast mines (Macdonald, Lockwood et al. 2003).

Fragmentation mines are larger, contain more metal and are designed to project or scatter pieces of the mine over a wide area. Blast mines are usually buried shallowly and are commonly cylindrically shaped and made of plastic or non-metallic material with a small metallic detonator which is pressure activated. Such mines are more difficult to detect because they have similar electromagnetic (EM) properties to the surrounding soil and so EM reflections from the target are easily obscured by surface and subsurface clutter (Sai, Ligthart 2004). This is especially the case in dry sand which has a relative permittivity of 2-6 (Daniels 2007). AP mines are typically buried at a shallow depth in rough, inhomogeneous soil that varies in nature across different geographical locations.

1.2.1 MD and GPR Sensor Fusion

The majority of mine detection programmes have used metal detectors (MDs) which are effective in identifying metallic objects under the ground. However, the placement of many plastic mines with very little metal content, coupled with the requirement to reduce false alarm rates, has necessitated the use of dual or multiple sensor fused systems that combine more than one type of detection technique. GPR is widely regarded as the most promising sensor for the detection of non-metallic mines (Dumanian, Rappaport 2005). GPR measures signals from targets by detecting changes in dielectric permittivity, and does not require conductive target components (Carin, Geng et al. 1999). GPR faces other difficulties associated with sub-surface wave propagation, primarily multiple reflections from the surface and soil inhomogeneities which obscure and confuse the target signal. The term *clutter* describes signals due to scattering from irregularities other than the target and artefacts due to the assumption that only single reflections occur. Clutter may be reduced by filtering or other

improvements in signal processing, but ultimately limits the ability of systems to estimate target parameters. Over the last decade, GPR has been developed as an effective method to improve AP landmine detection, particularly in combination with the MD. This has led to the development of dual or multiple sensor systems that are commercially available for humanitarian demining.

GPR systems can be classified by several characteristics. One is the mounting mode, which is either vehicle based or handheld (Takahashi, Sato 2008). The latter are necessary in areas that are difficult or to access by vehicle. Another important taxonomy is based on the antenna system, which may be mono-static, bi-static or multi-static (Karim, Malek et al. 2013). Mono-static systems use a single antenna to transmit and receive the probing EM signal. This presents difficulties in preventing the high power transmit signal damaging the sensitive receive electronics (Daniels 2007); but yields a very light and compact system. Most systems are bi-static and use separate transmit and receive antennas to isolate the receive electronics, but must be carefully designed to ensure low cross coupling between the antennas (Daniels 2007). More recently, multi-static systems have been deployed (Dumanian, Rappaport 2005), mostly vehicle based. These systems provide more information as pairs of antennas provide different views of the target. They can operate in several modes. The simplest configuration is multiple, concentric bi-static measurements from a linear array of antennas, providing views of the same central subsurface from different angles. Alternatively, two-dimensional (2D) array antennas can provide views from a range of directions. Potentially, array antennas could use beam steering to focus on a target. However, this would require arrays too large for a hand-held device, for frequencies that propagate

through soil yet can resolve objects as small as APs. In either configuration, each view of the target potentially adds new information and aids target discrimination (Counts, Gurbuz et al. 2007).

Operationally, handheld GPR landmine systems must be small and light to allow the operator to carry and use them in cluttered environments. They must also provide a means for fast and reliable mine detection decision making to enable operators work and cover larger areas more quickly. Typically, sensor data is converted to audio signals, time waveforms or images which are used to determine detection. Due to the severe consequences of failing to detect a mine, any extra information that can be acquired on the subsurface is valuable. This means increasing the POD and reducing the FAR or false positives. Sensor fusion methods have emerged to improve POD and FAR and optimize mine identification (Daniels 2008). Dual or multiple sensor systems, that combine two of the most mature techniques, the MD and GPR, have emerged as one of the most reliable, commercially available systems for humanitarian demining (Daniels 2008). These systems can operate the MD and GPR sequentially or simultaneously without interference (Steinway, Duvoisin et al. 1998). Three well-known handheld systems that have been developed and undergone field trials or evaluation are: the Advanced Landmine Imaging System (ALIS) (Sato, Fujiwara et al. 2004), MINEHOUND (Daniels, Curtis et al. 2005, Daniels, Curtis et al. 2007) and the Handheld Standoff Mine Detection System (HSTAMID) (Steinway, Duvoisin et al. 1998). However, the ALIS is not currently available commercially. The ALIS and MINEHOUND are based on a civil programme whereas the HSTAMID was developed in a military programme (Daniels 2004).

Like vehicle based systems, handheld systems could benefit from multiple antenna systems, although the weight and size constraints make this challenging. This project seeks to provide an extended evaluation of the performance of a handheld, multi-static GPR and MD system, operating in a dual sensor mode such as the MINEHOUND system which has been previously reported by (Watson, Lionheart 2014)(Watson 2016). Watson proposed an improvement in the reduction of false positives using the MINEHOUND system by imaging the detected target using full wave inversion (FWI), see Section 3.2. His work reports the results of 3D FWI for handheld GPR and an evaluation of multi-static, handheld GPR performance. Watson reported on a 2D singular value decomposition (SVD) analysis and a 2D FWI for verification. This project considers a more realistic 3D sensitivity study and FWI analysis. Based on the operation of the MINEHOUND system it is assumed that an object, potentially a landmine, has already been identified by the MD and localized in the middle or centre of the GPR antenna array. FWI (Watson 2016) is used to estimate several parameters of the object, allowing for the object to be classified as mine or not mine.

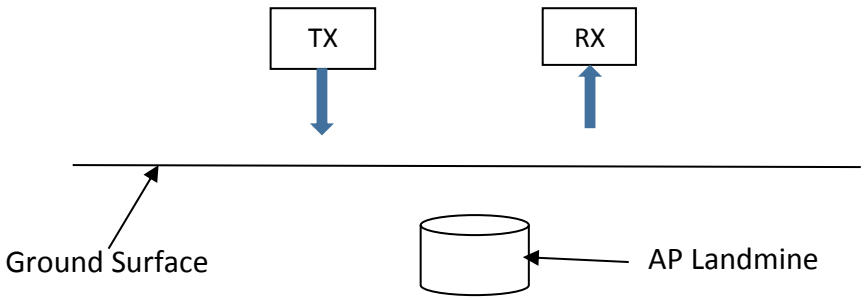

Figure 1 Landmine detection using a bi-static GPR system (TX=transmitter, RX= receiver)

1.2.2 GPR Signal Processing

GPR signal processing generally refers to the use of various techniques and methods to manipulate, convert or interpret the data that is obtained from the sensor

measurements. The aim is to acquire sufficient information about the target under consideration. Signal processing is also a means of clutter suppression (Daniels 2007). Generally, GPR data or received signals are either processed to produce an image that can be analysed or data that is characterised according to standard procedures by an operator. GPR data is represented in three different formats. These include the A-scan, B-scan and C-scan.

The A-scan, also called a trace, refers to a single time series, which varies with the recorded signal amplitude. It is the time series obtained at a single, fixed antenna position. The time and depth are both related to the velocity of propagation, see (2.4). The A-scan is a 1D plot. The B-scan is an ensemble of A-scans or traces obtained at several different points as the antenna is moved along a single straight line. The B-scan is a typically a 2D plot with the propagation time to the target and back plotted against the number of traces for a given distance. The C-scan refers to an ensemble of B-scans, collected alongside each other and is presented as a 3D plot.

Figure 2.2 presents an illustration of the GPR data forms of A-scan, B-scan and C-scan. Therefore, GPR data signal processing refers to application of algorithms to an A-scan, B-scan or C-scan which is referred to as A-scan processing, B-scan processing and C-scan processing respectively.

For A-scan processing, considered in this work, the GPR received impulse signal or time waveform is basically a convolution of several signal contributions in the time domain and is given by (Daniels, Gunton et al. 1988)

$$f_{rx}(t) = f_{source}(t) \otimes f_{imptx}(t) \otimes f_{cc}(t) \otimes f_{grtx}(t) \otimes f_{target}(t) \otimes f_{grrx}(t) \otimes f_{imprx}(t) + n(t) \quad (1.1)$$

where $f_{rx}(t)$ = received signal, $f_{source}(t)$ = transmitted signal from antenna (Gaussian impulse), $f_{imptx}(t)$ and $f_{imprx}(t)$ = transmit and receive antenna impulse responses respectively, $f_{cc}(t)$ = response from antenna cross-talk, $f_{grtx}(t)$ and $f_{grrx}(t)$ = forward and return ground impulse responses respectively, $f_{target}(t)$ = target impulse response and $n(t)$ = noise signal.

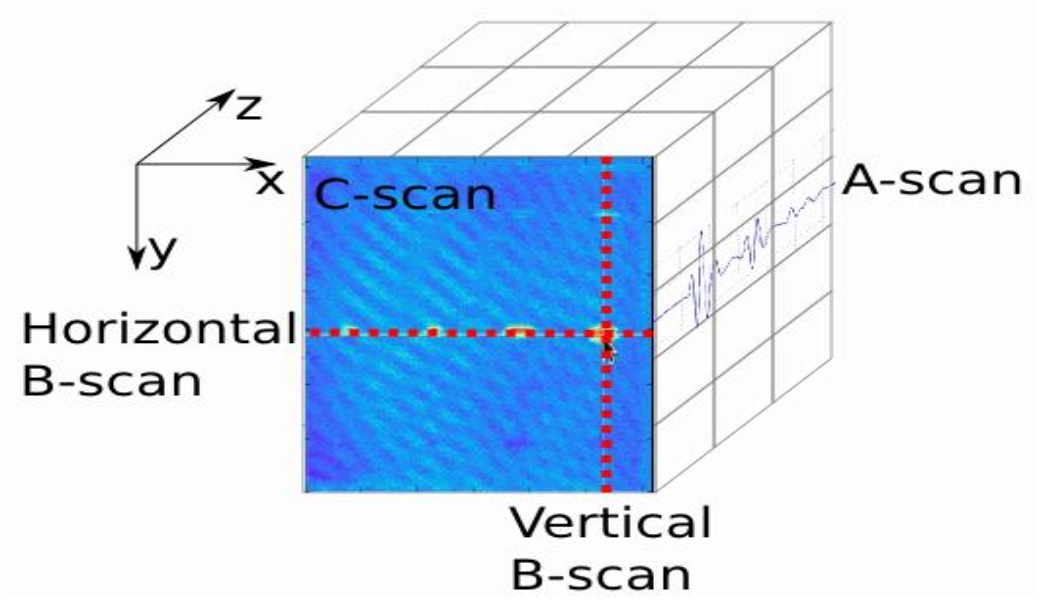

Figure 2.2 GPR data forms (Texas Research Institute Austin, Inc. 2017)

1.3 Research Motivation and Background

Demining activities occur in areas in the aftermath of war or other conflicts and most of these areas are in emerging or developing countries. The terrains are often rugged, making vehicle based methods impractical and even posing serious challenges to handheld systems. For instance, sensor scanning at a constant height above the ground, which is necessary for various image or data processing algorithms (Tantum, Morton et

al. 2012), is unachievable in many cases. This may be compounded by variation in soil composition, weather and other environmental conditions, flora and fauna, as well as the types of mines deposited from place to place. The Sambisa Forest located in North Eastern Nigeria where the use of IEDs and AP mines has been reported (Monitoring and Research Committee, ICBL- CMC Governance Board 2016) is an example of a difficult terrain populated with trees and thick vegetation. Handheld sensors are required as vehicular systems are impractical without extensive land clearance. Similar environments are commonly found in other under-developed or developing countries.

The Find a Better Way (FABW) charity was established in the United Kingdom (UK) in 2011 by Sir Bobby Charlton to support victims of landmines and ERWs; and to fund innovative research into the improvement of humanitarian demining in affected communities, globally. Several universities across the UK were competitively selected to undertake research in various aspects targeted at developing technologies to assist landmine clearance. One of the focus areas at the University of Manchester was on the improvement of the humanitarian demining procedure using a handheld dual sensor system (Daniels, Curtis et al. 2007) through the introduction of GPR data imaging (Watson, Lionheart 2014, Watson 2016). The demining procedure involves the use of the MINEHOUND handheld dual sensor system first in MD mode and then subsequently in GPR mode to scan a mined field divided into lanes (Daniels, Curtis et al. 2005).

The procedure can be summarised accordingly:

1. The area to be cleared is divided into lanes and the operators start their search along a safe or cleared lane and scan in MD mode along each lane. All points with positive audio signals indicative of metal mass are marked.
2. Operators repeat the preceding procedure this time with the system in GPR mode and investigate the points previously marked. Positive GPR responses over those locations are marked in a new and distinctive manner.
3. The targets at the points marked in step (2) are treated as mines and the ground is excavated and cleared.
4. All other marked points without a positive GPR audio signal are regarded as false positives or detections and are treated in a manner that prevents further false alarms if the clearance were to be repeated.

An operator uses audio signals obtained from both sensors to identify possible mine locations and the ground is carefully excavated when both signals are positive. A major limitation in this procedure is the occurrence of many false positive identifications requiring careful excavation but leading to the discovery of objects other than mines e.g. nails, drink cans, shrapnel, roots and rocks. The GPR can effectively reduce the FAR by rejecting non-mine metallic objects. However, a further reduction in the FAR is required to speed up the process, decrease the risk of accidental mine activation and increase the productivity of the operators.

Watson (2016) proposed reducing this problem by more sophisticated GPR signal processing with FWI to identify object parameters. Objects with parameters that did not match mines could be eliminated without excavation and hence speed up mine clearance operations without compromising safety. However, FWI is computationally

very expensive and the hardware that can perform the calculations in a reasonable amount of time is too large and heavy to be carried by an operator. The practical application of the method relies upon advances in computing and telecommunications, allowing the computation to be performed online. Furthermore, his work also concluded that multi-static (multiple transmit or/and receive) systems provide more information than bi-static (single receiver) systems which he demonstrated principally through a sensitivity analysis. His analysis was based on a simplistic 2D model, dipole antennas with no coupling, and far-field propagation assumptions. This work extends the work of Watson using an industrial standard EM simulation package to test his conclusions with realistic antennas and a radio propagation environment. The ultimate objective is to contribute to the reduction of demining costs. Though this project is not formally a part of the FABW research teams, there has been informal collaboration and it is believed that the goal to improve the lives of communities and people endangered through landmines around the world is a worthy common goal for all.

1.4 Thesis Aim and Objectives

This thesis builds on previously reported results and seeks to reduce the costs of AP demining through the reduction of false positives in procedures utilising handheld dual or multiple MD and GPR sensor systems. Specifically, the aim is to produce empirical analysis data that improves the reduction of the FAR or false positives in mine detection and make FWI practical through the following ways:

1. Enhanced target discrimination using multi-static antenna arrays;

2. Enhanced feature extraction or target classification based on FWI quantitative data which can be fused with image reconstruction to increase the reliability of detection.

Therefore, the objectives are focused on the enhancement of two key components and the achievement of the following:

1. Comparison of the ability of multi-static and bi-static handheld GPR systems to accurately estimate object parameters for a realistic 3D setup;
2. Classification of mines and non-mines, with a focus on the internal structure, based on the numerical FWI quantitative data.

Three fundamental research questions will be considered:

1. What improvements in land mine detection can be achieved using multi-static antenna, compared to the standard bi-static antenna?
2. What improvements in the discrimination between landmine and clutter can be achieved?
3. Are these improvements generally plausible and consistent with the constraints on system complexity, cost and ease of use?

Previously, parameter sensitivity analysis for GPR handheld antennas systems has not been carried out for a 3D EM forward problem which also considers GPR antenna radiation characteristics, cross-coupling, configuration and orientation. Sensitivity analysis comparing GPR antenna systems had been undertaken but was limited to a 2D forward problem and linear arrays of dipole antennas.

Therefore, this thesis shall provide a more realistic characterisation of the performance of multi-static antennas and bi-static antennas in handheld GPR systems. The potential of GPR systems using directional multi-static antenna will be explored and compared to bi-static systems in both noise limited and clutter limited conditions.

1.5 Thesis Methodology

Sensitivity analysis and the estimation of model parameters that best fit measured GPR data, requires the calculation of accurate EM fields in a computationally efficient forward model. Methods of GPR modelling include those based on individual frequencies, time domain methods, ray tracing, transmission line models, the method of moments (MOM) and discrete elements i.e. finite or boundary element methods (Daniels 2007). In this project, a time domain method is used to simulate propagation of a band-limited pulse. Most commercial GPR systems broadcast impulses, rather than carrier-wave, chirp or pseudo-random sequence signals. This is particularly true for systems designed for mine detection (Daniels 2007, Tesfamariam 2013), for example the MINEHOUND handheld dual sensor impulse GPR (Daniels, Curtis et al. 2005). Additionally, UWB signals, such as those produced by short-impulse GPR systems, can be simulated in the time domain with a single execution. GPR system data is nonlinear, therefore the time domain impulse response is typically a time-series waveform. The ground is also typically inhomogeneous, which refers to the non-uniformity caused by different materials buried and on the surface. GPR system data analysis is less computationally expensive in the time domain than the frequency domain (Miller 1994, Teixeira 2001).

Discrete methods for EM wave propagation and scattering simulation are generally classified into finite difference (FD), finite element (FE) and finite volume (FV), with the finite-difference time domain (FDTD) regarded as simpler conceptually (Teixeira 2008). Time domain methods are widely used for GPR (Daniels 2007). Additionally, the time domain analysis enables optimal A-scan data analysis with the limited computer resources available for the simulated experiments in this work.

There are various EM simulation software tools that could be used for 3D GPR modelling based on the methods previously outlined and specifically using time domain methods. This thesis uses the Computer Simulation Technology (CST) STUDIO SUITE 3D EM design environment, which relies on a different time domain technique for high frequency structures, the finite integration technique (FIT), and the Antenna Magus software tool used widely for GPR/UWB applications and UWB antenna design respectively (Ozdemir, Yilmaz et al. , Oloumi, Mousavi et al. 2013, Mohamed, Elsadek et al. 2012, Jamali, Marklein 2011, Panzner, Jostingmeier et al. 2010, Hertl, Strycek 2007, Hertl, Strýček 2009). The software also enables the design and prototyping of UWB antennas for GPR applications from scratch or automatically with selected parameters. The time domain FIT and FDTD have a similar performance of speed and accuracy (Munteanu, Hirtenfelder 2005). The FIT also provides accurate modelling of complex 3D structures and domains and can accommodate curves and nonlinear boundaries.

1.6 Thesis Contributions

The contributions to research and knowledge provided by this project are:

1. A novel evaluation of the performance of handheld multi-static GPR versus a bi-static handheld GPR for mine detection using 3D sensitivity analyses and FWI with realistic antenna designs and heterogeneous soil.
2. The evaluation of the performance of handheld multi-static GPR systems for mine detection using 3D FWI in a cluttered domain which shows that they achieve an improvement of less than 5% in accuracy of parameter estimation over handheld bi-static GPR systems for A-scan data.
3. An estimation of POD based on distinguishability, with the preclusion of FWI, for bi-static and multi-static systems for a flat, homogeneous domain. For omni-directional (dipole) antennas, the bi-static system achieved a higher POD by 9.6%. For directional (Vivaldi) antennas, the multi-static systems achieved a higher POD of less than 2%. However, for directional antennas and a cluttered domain with mean scan subtraction clutter, distinguishability for a multi-static system was greater than that of the bi-static system by over 10%. Furthermore, a novel investigation of antenna tilting for a handheld GPR system with directional antennas shows that based on an SVD analysis, tilting achieves a nonlinear but significant improvement in parameter sensitivity if the antenna radiation is aimed at the subsurface target. The results reported are for a bi-static horn antenna system and flat, homogenous media. However, with the application of appropriate clutter reduction schemes, the outcome is expected to be similar for a rough, heterogeneous medium.
4. A novel procedure for selection of the initial parameter for the non-linear optimisation for landmine detection that is closer to the global optimum, which

can reduce the computational time and number of iterations of the algorithm. This involves the generation of a database of multiple sets of forward model time domain impulse responses for a range of parameters based on *a priori* data, produced in a one-off training phase preceding the mine clearance operation. Each GPR time domain impulse response obtained during the clearance operations is first measured with the time domain impulse responses in the database to determine the response that is closest to the former, numerically.

5. A novel technique for optimising the FWI parameter estimation by considering the air void parameter, included in the optimisation as the relative permittivity of free space parameter. This is preceded by the successful mapping of the sensitivity data singular values of this parameter to the presence or absence of a void, hence mine or no-mine detection. Further experiments with the non-linear optimisation algorithm for a cluttered domain showed that this parameter in the FWI solution converges closer to the true value of 1 with a percentage error of 10% when a void is present in the mine surrogate and diverges significantly from this value with a percentage error exceeding 100% when there is no void present in the subsurface target.

1.7 Publications

The following journal article has been produced during the PhD research:

1. SULE, S.D., 2017. Handheld Sensor Fusion for Landmine Detection Using Metal Detector and GPR. Frontiers in Science, **7**(4), pp. 51-56. DOI:10.5923/J.FS.20170704.01

The following internationally reviewed conference articles have been produced during the PhD research:

1. SULE, S.D. and PAULSON, K.S., 2017. A comparison of bistatic and multistatic handheld ground penetrating radar (GPR) antenna performance for landmine detection, Radar Conference (RadarConf), IEEE, pp. 1211-1215, May, Seattle. DOI: 10.1109/RADAR.2017.7944389
2. SULE, S.D. and PAULSON, K.S., 2017. Enhanced feature extraction for landmine detection using handheld ground penetrating radar (GPR) based on full wave inversion (FWI), Radar Symposium (IRS), 2017 18th International, IEEE, pp. 1-6, June, Prague. DOI: 10.23919/IRS.2017.8008194
3. SULE, S.D. and PAULSON, K.S., 2017. Performance measurements for full wave inversion (FWI) based multistatic handheld ground penetrating radar (GPR) for landmine detection, Circuits, System and Simulation (ICCSS), International Conference on, IEEE, pp. 45-48, July, London. DOI: 10.1109/CIRSYSSIM.2017.8023179

1.8 Thesis Structure

This section provides a summary of the thesis structure and an outline of each chapter. The current chapter introduces the concept of landmine detection and describes the global demining problem. Landmine detection methods are briefly listed followed by a short introduction to MD and GPR sensor fused systems. The subsequent sections provide the background to the research, aim and objectives and a short summary of the research methodology.

Chapter two presents a more detailed description of landmine detection methods and their strengths and limitations. Sensor fusion for landmine detection is introduced and a description of handheld MD and GPR dual/multiple sensor systems is provided. This is followed by a discussion of several operational elements and working principles of GPR.

The third chapter provides background to FWI and a technical description of the bi-static and multi-static GPR systems that have been evaluated. Several example sensitivity analyses are reported. POD is calculated based on distinguishability.

FWI numerical complexity analysis data is presented in chapter four. Optimisation is achieved using a derivative free nonlinear optimization technique, with simulated data for the measured and forward model GPR data. The analysis provides a comparison of bi-static and multi-static GPR for 3D, homogeneous and inhomogeneous domains.

Distinguishability of mines in a cluttered domain is considered in chapter five to further compare bi-static and multi-static systems. The results of a novel sensitivity analysis to determine the impact of antenna tilting in handheld GPR systems are also presented.

Chapter six includes the results of a novel feature extraction and mine classification procedure using FWI optimisation. The procedure attempts to estimate the air void in pressure activated blast AP mines, from the FWI optimisation with A-scan data.

The seventh chapter which is divided into three sections. The first section provides the research and thesis conclusions, which outlines the research novel accomplishments and contributions to knowledge. The second section discusses several key limitations of the research and assumptions that have been considered in arriving at the conclusions of the studies conducted. The final section presents areas of further work or study.

Chapter 2 Landmine Detection Using Handheld GPR

2.1 Introduction

This chapter provides an overview of landmine detection methods and introduces sensor fusion for handheld landmine detection systems, with a focus on current systems that combine MD and GPR. An emphasis is placed on handheld, combined MD and GPR sensor systems considered technologically mature, or are commercially available. This is followed by an overview of GPR with a focus on selected working principles and elements of system design.

2.2 Landmine Detection Methods

This section briefly outlines several landmine detection methods. Most methods utilise a range of sensors based on acoustic waves, infrared waves, chemical detection, thermal detection, gamma rays, ultra-wideband (UWB) microwave radar and electromagnetic induction (EMI). Some of the major techniques that have been tested or validated experimentally are presented.

2.2.1 Nonlinear Seismo-acoustic Technique

The nonlinear seismo-acoustic technique (Donskoy 1998)(Donskoy, Ekimov et al. 2002) relies on the mechanical properties of mines and senses the vibrations between buried mines and the surrounding medium. Seismic or acoustic waves below 1000 Hz are used for the buried object measurements while the laser-Doppler or microwave vibrometers

are used for the remote ground surface measurements. Mines are typically geometrically simple containers of explosive with resonant modes of vibration quite distinct from those of other buried objects such as rocks, roots and metal fragments with no air void. Experiments reported in (Donskoy 1998, Donskoy, Ekimov et al. 2002) confirmed that the ground surface vibrations in the presence of buried geometrically simple objects with a void are distinctly different from those when there is no object or irregular objects in the ground. This allows the detection of the presence of AP mines of any material type. However, the system is expensive, vehicle based and not currently available commercially for humanitarian demining.

2.2.2 Gamma Rays

Gamma rays generated from soil irradiated with neutrons have been used by (Witten 2005) to detect anti-tank (AT) mines. Voltage sources of hundreds of kilovolts are required to produce neutrons with the required energy. Different elements can be distinguished from the returning gamma ray energy spectrum. The soil spectrum depends upon soil composition and is measured to produce baseline data. Soil containing a mine yields a different return spectrum, with gamma energies linked to the presence of explosives. Mine explosives typically contain carbon, nitrogen, oxygen and hydrogen. Soil has a lower nitrogen content than air, therefore the detection of a significant volume of nitrogen in the energy spectrum is indicative of a mine. The detection of large volumes of carbon or iron are also indicative of possible mines. However, the nitrogen detection was weak and not visible over a wide spectrum for the AT mine tested, making the technique ineffective for non-metallic mine detection.

2.2.3 Passive Infrared (IR) Polarization

The passive infrared (IR) polarization (Barbour, Jones et al. 1998) is a further development of IR imaging which relies on the polarimetric properties of scattered and reflected radiation from mines and the associated clutter sources. It assumes that mines are artificial objects and therefore have known physical properties and regular dimensions whose polarization features can be distinguished from that of the non-deterministic soil, subsurface clutter and foliage. Incident light on a lossy material that is reflected and refracted at a boundary produces backscattered or transmitted waves that possess orthogonal polarization properties with varying levels of intensity. These properties are measured and then used to reconstruct images of the target or object under test. A special IR camera is used to produce the incident electromagnetic radiation and a sensor collects the polarization data which is processed in real time with a computer system. The polarimetric IR camera has been shown to yield greater resolution and discrimination of targets than a standard IR camera (Barbour, Jones et al. 1998).

2.2.4 Active Thermal Sensing

The active thermal sensing method (Poulain, Schaub et al. 1998) uses an IR camera to acquire images of a buried mine target, like the IR polarization method. A high-power laser, greater than 1 kW, is used to produce a thermal impulse on the ground surface of interest. The laser beam is scanned over a surface area on the ground using special gold mirrors to ensure a constant thermal impulse spread. Information on the subsurface is deduced from the time evolution of the surface temperature, measured using an IR

camera. Experimental data reveals that the laser impulse based IR imaging also yields better imaging quality than the basic IR camera radiation based imaging. Nevertheless, the result is limited to the copper mines and sandy soil that were tested. Plastic mines are expected to yield greater challenges in detection as they possess thermal properties that are closer to soil.

2.2.5 Nuclear Quadrupole Resonance

The nuclear quadrupole resonance (NQR) method (Hibbs, Barrall et al. 1998) relies solely on the detection of explosive charges which are components of all mines, due to the unique properties of charges when exposed to incident low frequency EM radiation in the amplitude modulated (AM) radio frequency bands. The NQR procedure can detect the charge deposits in mines. The system can be operated on a handheld platform that indicates to the operator either a positive or negative detection. Measurements can easily and quickly be repeated for a specific location and the results are obtained immediately. Two major technical challenges of the NQR method are the limitations in antenna design and the poor detectability of Trinitrotoluene (TNT) which is the most common mine explosive. Signals suffer significant interference from external or background noise sources which can completely mask the backscattered charge radiation. As a result, the NQR systems have been applied with greater success to explosive charge detection in applications such as airport baggage screening. The complex energy emission spectrum of the TNT explosive renders detection prohibitive in comparison to other common mine explosives such as RDX $(O_2NNCH_2)_3$ and Pentaerythritol Tetranitrate (PETN).

2.2.6 Ultra-wideband (UWB) Radar

UWB systems for land mine detection are usually GPR. GPR relies on the analysis of backscattered EM waves which are incident on the ground and are also transmitted into the soil subsurface. Reflection occurs at boundaries between materials with different intrinsic impedances, determined by the EM properties of the materials. More than one boundary can lead to multiple reflections of the transmitted signal. The total returning signal is received at the antennas and processed using various signal and data processing schemes to determine the target's features. Typically, a 2D/3D image or audio signal is used to detect the presence of a mine. The antenna system and the frequency of operation of a GPR system, are critical to its detection performance. Image resolution improves with higher frequencies and smaller wavelengths closer in magnitude to the dimensions of the mine. However, signal attenuation by the soil also increases with frequency. A significant system design challenge is achieving a suitable balance between the frequency of operation and sufficient penetration of the signal in the ground. This challenge is further compounded by the fact that these criteria are largely influenced by the type of soil, nature of the environment and properties of the mine, all of which vary between and within areas of demining interest. Signal processing schemes that can suppress unwanted signals from the ground or other objects in the soil are also critical to mine detection using GPR.

2.2.7 Electromagnetic Induction (EMI)

The EMI method (Yamazaki, Nakane et al. 2002) for mine detection refers to the use of the classical MD method. The system typically uses two wire coils which function

separately as transmit and receive coils. When the detector is placed near the ground area of interest, electrical current in the first or transmit coil induces an initial time dependent, usually sinusoidal, magnetic field in the ground. This field induces electrical currents in buried conductive objects, usually metallic, which generate their own magnetic field. A time varying voltage is induced in the second receiver coil by the total magnetic field i.e. the sum of the first coil field and that due to buried conductors. Variation in this voltage is transformed to audio signals that are used to detect the presence of metals. The MD method is useful for the detection of metallic mines only and is ineffective in the detection of non-metallic mines which have become commonplace. Most mines contain at least a small conductive element that may be detected.

2.2.8 Summary

The methods outlined above provide a summary of some of the major sensing techniques for landmine detection. There are also biological methods such as the use of dogs or rats to detect mines by smelling explosives (Macdonald, Lockwood et al. 2003). Many improvements and alternative methods are under investigation, or have achieved limited levels of maturity. Nevertheless, no single system is capable of detection under all environmental conditions, soil moisture levels and types of mines. Systems may also not be commercially available in the open market without restrictions or special regulatory control. Each technique possesses a weakness that limits detection performance driving interest in the integration or combination of dual or multiple sensor techniques. Furthermore, while all the methods described may be deployed on vehicle based platforms, only the NQR, MD and GPR have been deployed as handheld systems.

2.3 Sensor Fusion

The limitations of individual or single sensor systems, and the need to increase the detection metric (POD) and reduce false positives (FAR) for humanitarian demining, has led to the exploration of data fusion (Macdonald, Lockwood et al. 2003). Data fusion generally refers to the combination of different sources of information with the aim of system performance optimization. For landmine detection, this is commonly referred to as sensor fusion, which is the deployment of two or more sensing techniques in the same instrument. Data from all the sensors are combined, either sequentially or concurrently, for target discrimination. Data fusion may also refer to the combination of multiple interpretations of data from a single sensor, by operators or experts to produce a single result (Tesfamariam 2013).

2.3.1 Types of Sensor Fusion

Sensor fusion can be classified into three levels: the data level, feature level and decision level (Waltz, Llinas 1990).

Data level fusion refers to the combination of different aspects of data from a single or set of similar sensors. In landmine detection, this type of fusion typically occurs with several sensors that produce similar data with variations only in aspects such as wavelength and polarization (Clark, Hernandez et al. 1991, Earp, Hughes et al. 1996). An example is that of camera images where images from different angles, or different illumination or with different filters, may be combined into a single image for interpretation.

Feature level fusion combines features of a target obtained from different sensors, such as dimensions, shape, texture and material. This method fuses all the features data by linking them or choosing features from individual sensors. Subsequently, the features are either formed into a single result (feature extraction) or used to determine detection through classification (feature classification).

Decision level fusion combines all the detection data or decisions obtained from multiple sensors. This typically occurs when feature extraction or classification is limited or not possible. The data considered from the sensors is raw data or other outputs such as waveforms or quantitative data that can be used by operators to determine the POD. There are various methods of decision level fusion. Examples are the Bayesian approach, fuzzy logic, rules and voting methods (Macdonald, Lockwood et al. 2003). Decision level fusion also includes the fusion of multiple signal processing schemes applied to data from a single sensor (Tesfamariam 2013).

The sensor fusion levels are generally implemented based on the type of sensor. Feature level fusion is most suited to data obtained from a variety of sensors. This information can be merged into a single data set that enables the categorisation of the target. Data fusion is most applicable to data obtained from similar types of sensors. On the other hand, data obtained from different types of sensors would require the application of decision fusion. Decision fusion enables different sensing techniques and the data they produce to be combined separately or simultaneously by multiple operators or technical experts.

It has been reported that a comparison of the three types of sensor fusion for landmine detection with MD and GPR sensors showed that feature level fusion yielded more information about buried targets necessary for the reduction of the FAR or false positives (Stanley, Gader et al. 2002)(Gunatilaka, Baertlein 2001).

2.3.2 Current Handheld MD and GPR Systems

Sensor fusion methods for landmine detection have received considerable attention in the last few decades. The most widely studied and cited are systems combining GPR and a MD (Bruschini, Gros et al. 1998)(Collins, Huettel et al. 2002)(Liao, Nolte et al. 2007)(Kim, Kim et al. 2009, Masarik, Burns et al. 2016)(Knox, Rundel et al. 2017). Other combinations considered include heated water jets and IR sensors (Mitchell, Herrick et al. 1998), and MD and gas fused sensor (Prado, Cabrita et al. 2013). Typically, the MD measures returns from any metallic objects while the GPR provides information to help classify the object as a mine or not a mine. Mines with no metal content can only be detected by the GPR and not the metal detector.

Three handheld MD and GPR fused sensor systems have achieved the highest technical maturity and have been successfully used in mine field trials (Daniels 2004). These include the HSTAMID, used in Namibia (Doheny, Burke et al. 2006) and Thailand (Doheny, Burke et al. 2005) and the MINEHOUND, used in Cambodia, Bosnia and Angola (Daniels, Curtis 2006)(Daniels, Braunstein et al. 2015). The third system, the ALIS, has also undergone field evaluations in Afghanistan (Sato, Fujiwara et al. 2004)(Sato, Feng et al. 2005) and Croatia (Takahashi, Sato 2008). However, only the HSTAMID and MINEHOUND are commercially available. The HSTAMID is also the product of a USA

military programme whereas the other two are targeted at humanitarian demining. Table 2.1 provides a summary of known global GPR programmes in the last decade.

The MINEHOUND (Daniels, Curtis et al. 2005) is a handheld MD and GPR dual sensor system, designed for humanitarian demining. The MINEHOUND has physical dimensions of 170 x 305 mm for the active search component, weight of 4.75 kg and power consumption of less than 7W. Proprietary software is used for A-scan processing and the time-series measurements are obtained from both sensors in the form of audio signals. The MD acquires information on metal content and positioning while the GPR provides information on target position, depth and radar cross section (RCS).

This project aims to undertake an extended evaluation of the handheld multi-static GPR using a SVD and FWI analysis for a 3D domain. The focus is on MD-GPR systems where the MD detects the possibly, very small conductive part of the mine while the GPR is used to determine if a volume of mine-like permittivity exists around the conductive object. Additionally, the thesis looks at improving the ability of FWI imaging to identify this region of permittivity through enhanced feature extraction, given that feature level classification or fusion has been found to significantly reduce the FAR. Very importantly, the deployment of a satellite communications network is proposed to overcome the prohibitive costs of FWI and enable its current application.

Country	Programme	Type (Military/Civilian)	System Platform (Handheld, H or Vehicle, V)	Maturity (High/Medium/Low)
Australia	HILDA	Military	H	Medium
Australia	RRAMNS	Military	V	High
Belgium	HUDEM	Military	V	High
Canada	ILDP	Military	V	High
EU	GEODE	Civilian	V	Medium
EU	LOTUS	Civilian	V	Medium
EU	DEMINE	Civilian	H	Low
EU	MINEREC	Civilian	H	Low
EU	DEMINE	Civilian	H	Low
EU	HOPE	Civilian	H	Low
EU	PICE	Civilian	H	Low
France	SALAMANDER	Military	V	Medium
Germany	MMSR	Military	V	Medium
Israel	ELTA	Military	V	High
Japan	MEXT-SENCION	Civilian	H	High
Netherlands	ARMSBLD	Civilian	H	Low
Sweden	PICE	Civilian		Medium
UK	MINETECT	Civilian	H	High
UK	DCMC	Military	H	Unknown
UK	MCMC	Military	V	Medium
USA	HSTAMIDS	Military	H	High
USA	GSTAMIDS	Military	V	Medium

Table 2.1 Global programmes on landmine detection using GPR

2.4 GPR System Overview

This section provides an overview of general GPR system design and the principles of operation, largely based on (Daniels 2007). GPR has many applications including archaeology, medical imaging, geophysical investigations, road condition survey, planetary exploration, landmine detection and other security applications. GPR is a type of radar (Radio Detection and Ranging) system that is used to determine the position, and possibly other features, of subsurface objects. System design is often tuned to the

application i.e. the target depth and type, and the subsurface material e.g. sand, rubble, marsh etc. Radar systems generally operate by broadcasting an EM signal and detecting the signal that returns after scattering by objects. The delay between broadcast and detection indicates the range of the object and the angle of arrival indicates its direction. GPR differs only in that the propagation path is through the ground. Daniels (2007) listed four conditions that needed to be met to allow GPR imaging of a buried object:

a) Sufficient EM energy coupling into the ground;
b) Sufficient ground penetration of the EM radiation in the direction of the target;
c) Acquiring an adequate back scattered signal from the target or other impedance contrasts in the ground; and
d) A large enough bandwidth in the received signal to provide the resolution required.

Furthermore, the GPR needs to also achieve sufficient levels of:

a) Signal to clutter (SCR) and signal to noise (SNR) ratios; and
b) Target spatial and depth resolution;

The selection of a GPR system is largely based upon the nature of the target, desired resolution, expected associated clutter and attenuation (Skolnik 2008). The summary of the necessary design factors in a GPR system are provided in Figure 2.1 by Daniels (2014). Many parameters describe the operation of a GPR for a given situation including: range and path loss, system loop gain, velocity of propagation, depth and plan resolution, clutter, antennas and signal processing. The paragraphs below define these terms based on (Daniels 2014).

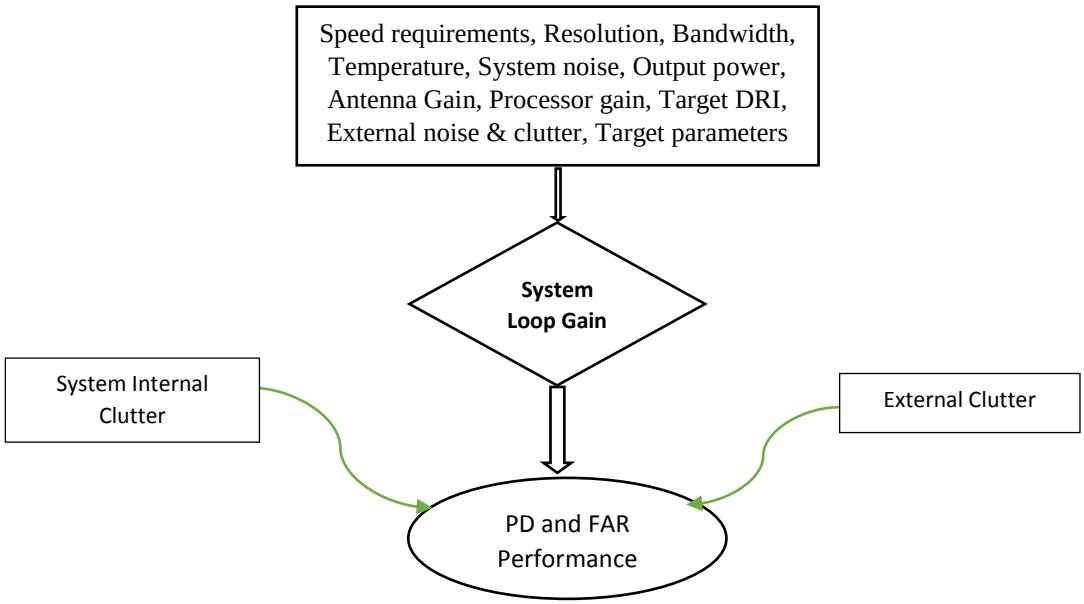

Figure 2.1 GPR system design elements (Daniels 2014) (DRI = detection, recognition & identification, PD = probability of detection, FAR = false alarm rate)

2.4.1 Physics of Operation

Of primary importance is the detection of the scattered EM signal. This signal is determined by the radar cross section (RCS) of the target, propagation losses to the object and back, SCR and SNR. The broadcast EM signal is incident on the ground surface and some of the signal is reflected. A portion is transmitted into the ground where it may encounter the target. Some of the transmitted signal may be scattered by the object back to the GPR receiver after undergoing further partial-transmission at the air-ground interface and additional losses. The RCS is a measure of the backscattered energy that a target scatters towards the radar receiver. For GPR, the RCS depends upon the size parameter, which is the ratio of the physical dimensions of the target to the transmitted signal wavelengths in the medium. Models of EM scattering can be divided into three domains based on the dimensionless size parameter, α which is defined as:

$$\alpha \equiv \frac{\pi D}{\lambda} \tag{2.1}$$

where D is the diameter of an object and λ is the wavelength of incident radiation. Three scattering domains can be considered, depending on the size parameter:

$\alpha \ll 1$: Rayleigh (reactive) region scattering where the object is much smaller than a wavelength;

$\alpha \approx 1$: Mie/resonance (near field) region scattering where the object and wavelength are of the same magnitude;

$\alpha \gg 1$: optical (far field) region scattering where the object is much larger than a wavelength.

Exact scattering fields are known in the limits of very large and very small α. Mie scattering theory refers only to scattering from spheres, although colloquially all scattering from objects of this size parameter is called Mie scattering. Conventional radars operate in the optical region where target dimensions are several times larger than the wavelength of the transmitted signal. However, GPR typically operates in the Mie or Rayleigh regions. Here, target dimensions are like the signal wavelengths. In the Mie region, scattering is highly anisotropic and frequency sensitive, and so interpretation of the scattered signal is difficult.

2.4.2 Range and Path Loss

Several loss mechanisms reduce received signal power of a GPR and hence determine the maximum depth of detectable objects (Daniels 2007). The dominant losses are the

antenna spreading loss, material attenuation loss and target scattering loss. The target scattering loss is a function of the scattering at the interface between the target and a different material or surrounding medium, as well as the influence of the target RCS. For GPR, reflection from the air-soil interface may also be very large. In classical radar propagation in free space, where the target is in the far field, the spreading loss is directly proportional to the inverse fourth power of the range. The range is the distance between the radar and the target. Spreading loss is always present but may be mitigated by transmitting more power in the target direction with the use of more directional antennas or antenna arrays. Material attenuation loss refers to EM powers transformed to heat by Ohmic heating of conductive media. This may be significant for wet or salty soil, or soil with a large iron content.

2.4.3 System Loop Gain

The use of GPR systems globally are subject to regulatory control and licensing depending on the region. Regulatory organisations include the European Telecommunications Standards Institute (ETSI) for Europe, Federal Communications Commission (FCC), for USA and The Office of Communications (OFCOM) for the United Kingdom. GPR systems transmit an average power of <1 milliwatt ($10^{-3}W$) (Daniels 1999)(Daniels 2006). The United Kingdom limits effective isotropic radiated power (EIRP) for 150 MHz – 4 GHz for GPR systems, given by (Daniels 2014):

- Total radiated power: ≤250 microwatts
- Radiated spectral line power: ≤100 nanowatts
- Maximum leakage power from antenna shield: ≤10 nanowatts

Typical GPR signal level that a receiver can acquire is within the range of picowatts ($10^{-12}W$) and femtowatts ($10^{-15}W$). The exact figure would be set by the system design parameters. The system loop dynamic range is determined by

$$\frac{TxPower_{mean}(W)}{RxPower_{minimum}(W)} \tag{2.2}$$

This value is usually within 10^8 and 10^{12} which corresponds to 80 dB and 120 dB. The thermal noise, external noise (clutter) and the bandwidth, determine receiver sensitivity.

2.4.4 Velocity of Propagation

Radars measure the propagation time for a signal to travel from antenna to target and return. To turn this propagation time into a distance requires knowledge of the phase velocity in the propagation media. The EM phase velocity or velocity of propagation, V_p, for homogeneous, isotropic non-magnetic materials is given by (Daniels 2007):

$$\mathrm{V_p} = \frac{\mathrm{c}}{\sqrt{\varepsilon_\mathrm{r}}}\,\mathrm{ms}^{-1} \tag{2.3}$$

and the depth, d is given by

$$\mathrm{d} = \mathrm{V_p}\frac{\mathrm{t}}{2}\,\mathrm{m} \tag{2.4}$$

where ε_r is the relative permittivity, t is the propagation time to the target and back and c is the propagation velocity in free space or air ($3 * 10e08\ \mathrm{ms}^{-1}$).

The phase velocity is a function of frequency since permittivity varies with frequency in wet lossy materials, and so these materials are often referred to as dispersive. However,

this variation is small for most soils types and the frequencies used in GPR. Propagation velocity varies inversely with relative permittivity and directly with wavelength in a material. This relationship is given by

$$\lambda_m = \frac{V_p}{f} \tag{2.5}$$

where λ_m = material wavelength and f = frequency.

2.4.5 Depth and Plan Resolution

Depth or range resolution refers to the detection of target features, structure and differences between targets. It is mainly determined by the received signal bandwidth. For impulsive systems, higher bandwidth yields shorter duration pulses and hence better return time resolution. The soil acts as a low pass filter as it typically becomes more absorbing at higher frequencies. Low bandwidth systems may be adequate in some applications such as in road condition surveys where a single interface or layer is targeted. Material with high water content, particularly salty water, cause greater attenuation hence limiting the effective bandwidth. Furthermore, parallel surfaces may lead to destructive interference at some frequencies due to superposition of the signals reflected off the two surfaces.

Plan resolution is required where multiple targets at the same depth need to be discriminated. In this case, greater spatial information is required, and this is primarily achieved by moving the GPR in a scanning fashion over the area of interest. Higher gain antennas provide better plan resolution but at the cost of larger antenna apertures which may be undesirable. Smaller antennas therefore come at the cost of lower gain

which may be compensated using a high carrier frequency. However, this produces the downside of decreased ground penetration. It is necessary to have a balance between the plan resolution, antenna dimensions, signal processing scheme and material penetration.

2.4.6 Clutter

Clutter refers to any reflections that are not relevant to the target of interest but are also received in the sample time frame and received bandwidth of the GPR. Clutter in air borne radar differs from that of sub-surface radar. Clutter arises from reflections from the ground surface and other objects or features on or underneath the ground such as cracks, rocks, roots, pieces of metal and other materials other than the soil, embedded or on the surface. This masks the signal from the target of interest and clutter may vary from one environment to another or even from one point to another in the same area. A sufficient SCR is required for successful target detection.

2.4.7 Antennas for GPR

Antennas for GPR systems require optimisation of various factors or technical considerations in line with the physics of propagation, and generally the choice is a trade-off between competing factors. UWB antennas are necessary to obtain fine depth resolution, which is important when differentiating targets from clutter. Higher frequencies also enable more directional antennas and hence greater plan resolution. This also aids the differentiation of different objects positioned in the same area of interest and depth. However, signal attenuation also increases with higher frequencies. Therefore, the acquisition of high quality images, or data that discriminates targets from

other clutter, requires high bandwidth and this is constrained by soil absorption at the higher frequencies. GPR antenna must be designed to maximise the information in the measured signal in multiple types of soils and environmental conditions. The latter is especially important as the ground couples with the antenna current distribution, affecting the performance of the antenna. This makes it difficult to optimise the antenna for a range of conditions (De Jongh, Ligthart et al. 1999). Characterisation of the GPR antenna radiation properties are complicated by the target's location which is often in the Rayleigh region or Mie region, rather than the optical region as is the case for traditional radar (Daniels 2007). Other factors in the antenna design are the minimization of the effects of side lobes and mutual coupling between antenna elements. GPR antennas can be classified into two broad groups. These include dispersive antennas where there is no linear change of phase with frequency and non-dispersive antennas (Neto, Monni et al. 2010). Dispersive GPR antennas include the Archimedean spiral, the Vivaldi antenna and exponential horn whereas non-dispersive antennas include the transverse electromagnetic (TEM) horn antenna, element antennas (bow-tie antenna, monopoles, and dipoles), the bi-cone antenna and lumped element loaded antenna (Daniels 2007).

2.4.8 System Operating Frequency and Domain

GPR systems generally operate in the frequency range of 10 MHz to 5 GHz (Daniels 2007). The desired application imposes constraints on the number, sizes and types of antennas that can be used. Variations in the system range are dependent on the design requirements. The centre frequency is the most significant design parameter, according to Sato (2009) who reports that the optimal GPR centre frequency range for landmine

detection is in the range of 1 to 4 GHz. Witten (1998) on the other hand specifies the GPR frequency range for landmine detection as 0.2 to 8 GHz and emphasizes the 0.75 to 2.5 GHz frequency range as the most widely used. GPR can also be generally classified based on the time domain or frequency domain systems. The time domain system, or impulse radar, transmits short pulses, typically of about a nanosecond duration. The received backscattered signals from the target are time-series that require processing to identify significant scatter returns. Frequency domain systems transmit individual frequencies sequentially, or alternatively sweep the frequency range. For ideal stationary systems and target, the time-series and frequency-series are a Fourier transform pair. The frequency domain signal is typically converted to a time domain signal by inverse Fourier transform for analysis. Impulse radars are cheaper, simpler in design and widely used for commercial GPR. Frequency domain radars are more complicated and expensive but typically have a larger operating frequency bandwidth and higher SNR as the longer duration frequency sweep allows more signal power to be broadcast.

2.4.9 Signal Processing

One signal processing goal is to estimate the target impulse response through a process of deconvolution applied to the received signal. This is done through various methods such as complex resonances, wavelet deconvolution, neural networks and statistical methods. A-scan (1D) processing is typically applied to handheld GPR data where imaging is not implemented as easily as for vehicular systems which deploy larger antenna arrays and record a greater number of measurements. Signal processing for vehicular systems requires larger datasets and allows for a variety of B-scan (2D) and C-

scan (3D) data processing. Migration, inversion and synthetic aperture methods are commonly used for 2D and 3D imaging. Migration is a process that combines signals from many measurements to localise scatterers, in 2D or 3D, that are inclined or outside the volume under the measurement system. Inversion is a technique that is used to quantitatively estimate subsurface information by fitting GPR measured data with synthetic data from a numerical forward model. Synthetic aperture processing is like the synthetic aperture radar (SAR) technique for remote sensing where an antenna is moved along a direction with measurements acquired at different positions and the measurements are combined in a way that resembles a single narrow beam. The SAR and migration methods are similar (Sato 2009). Clutter reduction is a critical aspect of signal processing and is also achieved through various schemes. Common examples of clutter reduction algorithms are the conventional mean subtraction methods or background removal, (Abujarad, Jostingmeier et al. 2004) and statistical methods of principal component analysis (PCA) (Tebchrany, Sagnard et al. 2014) and independent component analysis (ICA) (Hyvärinen, Oja 2000).

This work considers improvements in handheld GPR data processing, and is constrained to A-scan data and the inversion technique, which is reported to achieve better subsurface parameter estimation than migration and SAR (Watson 2016).

2.5 Conclusion

This chapter provided a general outline of landmine detection methods. The major methods of sensor fusion have been reviewed. Handheld sensor fused systems for landmine detection with a focus on MD and GPR sensors has been presented. These

systems represent the most cited and actively researched handheld fused systems intended for humanitarian demining. Feature level fusion has been reported to provide more information for discrimination in landmine detection using MD and GPR sensors, compared to data level and decision level fusion methods. Three handheld MD and GPR fused systems for landmine detection with the highest levels of technical maturity have been discussed. These are the HSTAMID, MINEHOUND and ALIS. However only the HSTAMID and MINEHOUND are currently commercially available. An overview of the GPR system was presented, with a focus on several principles of operation and technical aspects.

A recent study by Watson (2016) proposed the improvement of subsurface parameter estimation using FWI imaging with the MINEHOUND dual sensor handheld system to enhance target discrimination for humanitarian demining. Results from the study show that multi-static systems perform better than bi-static systems, when simplistic radio propagation models are used and that FWI is currently impractical for handheld field equipment due to the price, weight and power consumption of portable high-performance computing systems. This project shall undertake a more realistic evaluation of multi-static handheld GPR through a sensitivity study and FWI analysis in 3D analysis which considers full EM wave propagation. A remote FWI imaging implementation on supercomputing systems through a satellite communications link is also considered to enable the current application of the technique for mine clearance operations. The major aim is to achieve an enhancement in the reduction of false positives and cost of humanitarian demining. The research contributions emanating from this study are described in more detail in the following chapters.

Chapter 3 Parameter Sensitivity Comparison between Bi-static and Multi-static GPR

3.1 Introduction

This chapter explores the extra information that can be provided by handheld GPR multi-static systems compared to bi-static systems, in a dual or multiple sensor system with a MD. The aim is to verify the results of previous studies using 2D simulation, but using a more realistic 3D simulation and antennas. A sensitivity analysis is applied to data from simulated bi-static and multi-static GPR systems, most of which is reported in (Sule, Paulson 2017a, Sule, Paulson 2017c). Imaging is achieved by non-linear optimization, also known as FWI, which have been used widely for seismic data, which refer to measurements obtained from vibrations in the earth. This method was used by Oberrohrmann et al (2013) for seismic GPR measurements which showed that a multi-static acquisition system yielded greater acquisition than a bi-static system, making it less expensive. Silvestrov and Tcheverda (2011) performed seismic data processing using 2D FWI for surface and subsurface acquisition systems and used a SVD analysis of the inverse problem to show that the properties of the inversion are influenced significantly by the configuration of transmitters and receivers. However, a portable, handheld, multi-static system analysis was not considered. Meles et al (2012) used SVD to analyse GPR images calculated using FWI for a multi-antenna system, and developed a novel method to determine the sensitivity function of conductivity and permittivity based on the forward problem Jacobian. Watson (2014) performed a similar experiment

and additionally considered the singular vectors for a 2D FWI image analysis. This work focused on a handheld GPR system and compared the performance of a bi-static system with a multi-receiver system with 2 to 4 elements. He implemented a SVD analysis of the Jacobian matrix to determine FWI images of subsurface AP mines for bi-static and multi-static handheld GPR. The study showed that the singular values characterise the ill-posed nature of the linearised inverse problem and that the right singular vectors reveal the image space. His SVD analysis was based entirely on a 2D domain and a 2D solution of Maxwell's equations. The 3D SVD analysis is expected to reveal the more highly ill-posed inverse problem due to the greater spreading loss. His acquisition system assumed a simple dipole array and did not consider the complexity of real radio systems, such as antenna radiation characteristics, cross-talk, physical antenna geometry and configuration. For the systems considered the antennas are electrically large and scattering occurs in the near-field. For accurate simulation the antenna radiation characteristics need to be understood (Busch, van der Kruk et al. 2012). Lastly, only a flat, 2D homogenous ground domain was considered.

This chapter presents a sensitivity analysis of realistic multi-static handheld GPR systems, compared with bi-static systems. The sensitivity analysis is carried out in three phases with three different types of antennas, under varying conditions and parameters. Initially, Watson's results are verified before more realistic bi-static and multi-static systems are investigated. Uncertainties in soil and mine parameters are tested to identify the precision to which they can be estimated from GPR measurements using non-linear FWI. SVD is applied to the finite differences approximation of the Jacobian and simulated impulsive GPR A-scan data, from a single fixed location i.e. no SAR. This

is consistent with the MINEHOUND system GPR data processing (Daniels, Curtis et al. 2005). The aim is to estimate how much more information about the subsurface can be obtained with a handheld GPR with more receivers in a realistic 3D domain. The sensitivity analysis will be preceded by an overview of FWI, SVD and the finite difference derivative approximation method. Finally, POD is estimated for the GPR systems based on distinguishability and FAR reduction is validates using singular values from sample data. All modelling and simulation is performed using the 2016 and 2017 versions of the CST STUDIO SUITE EM software produced by CST, Computer Simulation Technology GmbH, owned by the Dassault Systemes Deutschland GmbH organisation.

3.2 Full Wave Inversion (FWI)

FWI is an EM parameter estimation technique that is used to obtain quantitative estimates from measured data. Typically, this requires the minimization of a non-linear error functional that is solved through the iterative minimization of linearized problems or numerous evaluations of an objective function (Plessix 2006). The parameters of a forward model are adjusted so the output fits measured data (Busch, van der Kruk et al. 2012)(Virieux, Operto 2009).

Consider an error functional $f(\mathbf{x})$ which is a measure of the distance between the GPR output and the output of a numerical forward model of the GPR measurement of a ground described by a parameter vector $\mathbf{x}$. The parameter vector $\mathbf{x}^*$ that is a local minimum of the function $f(\mathbf{x})$ yields the smallest value of $f(\mathbf{x})$ in a neighbourhood of $\mathbf{x}^*$:

$$f(\mathbf{x}^*) \leq f(\mathbf{x}) \text{ for all } \left\|\mathbf{X}-\mathbf{X}^*\right\| < \varepsilon \tag{3.1}$$

where ε is a positive number possibly small.

If $f(\mathbf{x})$ is twice continuously differentiable in the neighbourhood of $\mathbf{x}^*$ then two conditions will be satisfied at the local minimum. The necessary condition $\nabla f(\mathbf{x}^*) = 0$ shows that $\mathbf{x}^*$ is a stationary point. For $\mathbf{x}^*$ to be a minimum then the Hessian matrix of second derivatives needs to be positive definite. For GPR FWI, the parameter vector $\mathbf{x}^*$ contains parameters that specify the geometry and electrical properties of the ground, and possibly the mine. The accuracy of the inversion process is dependent on an accurate forward model i.e. FWI depends upon the ability to accurately estimate the GPR output measured on a ground described by the parameter vector $\mathbf{x}$. Any error in the forward model leads to errors in the estimates of the ground parameters. A wide range of optimisation algorithms exist to find the minima of $f(\mathbf{x})$. The choice depends upon the availability and cost of evaluating derivatives, the cost of function evaluation and other *a prioiri* information on the features of the error functional. The convergence of these methods to the desired minima depends upon an initial estimate of the minima. If the initial estimate is too far from the desired minima, it may converge to some different minima or even diverge. Derivative-free methods typically require more iterations to converge but each iteration requires less computation (Rios, Sahinidis 2013).

GPR FWI begins with a GPR measurement of the subsurface yielding a data vector **d**. This vector could be the voltage time-series at the output of a receiver system i.e. an antenna, amplifier, filter and possibly some signal conditioning relying on *a priori* information. The parameter vector $\mathbf{x}^*$ which yields a forward model $f(\mathbf{x})$ closest to the

data vector **d**, is assumed to be a good description of the subsurface. The FWI method is distinctly different from the historical approach known as the direct-solution. This group of methods is based on a range of heuristics allowing measured electrical time-series to be directly transformed into ground depth-series of electrical parameters. The direct solver method is considerably less computationally intensive but the heuristic assumptions, e.g. that single scattering dominates the return signal, limit the accuracy, (Plessix 2006, Erlangga, Herrmann 2008)(Riyanti, Kononov et al. 2007). FWI does not make these assumptions, but is vulnerable to errors due to inaccurate forward modelling and the restricted range of subsurfaces described by the finite parameter vector. The FWI problem is ill-posed. The ill-posedness tells us that small errors in the data vector, or the forward model, translate into arbitrarily large errors in the solution. Methods such as regularisation are required to control these errors (Watson, Lionheart 2014, Daniels 2007).

Gradient based methods rely on the Jacobian matrix of first derivatives, and the Hessian matrix of second derivatives, of either the objective function or the forward model. The first and seconds derivatives of either are very computationally expensive to calculate. Methods exists that use just first derivatives or first and second. Newton's method requires both and yields quadratic convergence whereas Steepest Descent method requires only the first derivatives and yields linear convergence. Quasi-Newton methods may be applied to least squares (LSQ) problems and rely upon an approximation of the Hessian to achieve quadratic convergence near the minimum (Fike, Jongsma et al. 2011).

FWI methods have been widely used for seismic geophysical exploration where inversion can occur off-line. However, FWI for AP demining GPR has not been used as immediate results are required and the computing equipment required has precluded handheld devices. Ernst et al (2007) and Kuroda et al (2007) used a 2D finite-difference time-domain method (FDTD) to produce FWI results for seismic radar experiments whereas Meles et al (2010) performed similar experiments with the addition of further electric field properties. Klotzsche et al (2010) used FWI with borehole GPR data whereas Ellefsen et al (2011) and Klotzsche et al (2012) successfully applied FWI 2D parameter fields in seismic radar experiments. Ground surface conductivity and permittivity estimation data have been produced by Busch et al (2012) using a 3D forward model. In the landmine detection application area Lopera et al (2007) and Soldovieri et al (2011) used FWI in estimating ground surface relative permittivity to mitigate surface and antenna reflections for landmine detection. Their work utilised a mono-static antenna and 2D data. More recently, Watson (2016) produced numerical 3D FWI data for AP landmine detection based on a handheld GPR acquisition setup. However, his antenna performance analysis was based entirely on 2D simulation.

3.2.1 FWI for Multi-static Handheld GPR

This section presents the FWI solution by iterative linearization as described in (Watson, Lionheart 2014). This provides the background required for the sensitivity analysis presented later. Watson used simplified modelling to test the ability of GPR FWI to distinguish between AP mines with different geometric and electrical parameters. He concluded that small scale arrays with multiple receivers could distinguish mine

parameters under these simplified situations. The formal definition of distinguishability is given later.

The GPR FWI problem may be posed as a regularised LSQ non-linear optimisation problem:

$$\mathbf{X}_{im} = \arg\min_{\mathbf{x}} \frac{1}{2}\left\|GPR(\mathbf{X}) - \mathbf{d}\right\|_2^2 + \lambda T(\mathbf{X}) \tag{3.2}$$

where $\mathbf{X}_{im}$ is a vector of geometric and electrical parameters describing the ground, **d** is the GPR measured data, $GPR(\mathbf{X})$ is a forward model that returns the GPR measurement that would be made for a subsurface with parameter vector $\mathbf{X}$, (Watson, Lionheart 2014). The GPR inverse problem is ill-posed as arbitrarily large changes in $\mathbf{X}$ can have negligible effect on the error $\left\|GPR(\mathbf{X}) - \mathbf{d}\right\|_2^2$. The regularisation term is required to control the size of components of $\mathbf{X}$ with little or no effect on GPR data. The function $T(\mathbf{X})$ introduces a penalty based on the size of these components and is a way to introduce prior information. For Tikhonov regularisation $T(\mathbf{X}) = \left\|\mathbf{\Gamma X}\right\|^2$ and often $\mathbf{\Gamma}$ is chosen to be the identity matrix. The regularisation or Tikhononv factor $\lambda \geq 0$ is often adjusted dynamically during the iterative optimisation process to control convergence.

The GPR forward model is non-linear and so (3.2) is often solved by iterative linearization. Watson used an iterative, quasi Newton method known as the Limited Memory Broyden-Fletcher-Goldfarb-Shannon (L-BFGS) nonlinear optimisation algorithm (Nocedal, Wright 2006). The solution requires a calculation of the gradients of the LSQ

error function $\left\|GPR(\mathbf{X})-\mathbf{d}\right\|_2^2$. Due to the special form of the LSQ error function, these derivatives can be directly related to the derivatives of the forward model.

FWI for GPR imaging relies upon the availability of a forward model that can accurately predict the measurements that would be made by the physical GPR on ground described by a particular set of subsurface parameters. Any difference in behaviour between the forward model and the physical GPR will lead to convergence to the wrong parameter vector. The inverse problem is ill-posed and so small errors in such things as modelling cross-coupling between antennas, can result in very large errors in the calculated image. For this reason, a very sophisticated and well calibrated EM simulation is required.

3.2.2 Sensitivity Analysis of GPR Measurements

The bi-static GPR measurement yields a vector of samples from the temporally discretized output of the receive antenna due to a pulse transmitted from the transmit antenna. For a given subsurface parameter vector $\mathbf{X}_s$ of *n* parameters, see (3.15), we denote this time-series vector: $GPR^B(\mathbf{X}_s)$. The subsurface without a mine, with parameter vector $\mathbf{X}_0$, yields measurement $GPR^B(\mathbf{X}_0)$, whereas subsurface with a mine $\mathbf{X}_m$ yields a measurement $GPR^B(\mathbf{X}_m)$. The distinguishability is a measure of the ability of a GPR measurement to distinguish between the subsurface with and without a mine and is defined numerically by

$$\left\|GPR^B(\mathbf{X}_m)-GPR^B(\mathbf{X}_0)\right\|_2^2 \tag{3.3}$$

A large distinguishability is associated with GPR experiments that yield information that would allow the user to determine whether a mine is present in the presence of noise.

In the multi-static case, $GPR^M(\mathbf{X}_s)$ is the concatenation of the independent discretized pulse responses.

The LSQ subsurface imaging is achieved by minimizing the sum square difference error between the measured data GPR_{meas} and the results of a CST forward model $GPR(\mathbf{X})$:

$$E(\mathbf{X}) = \|GPR_{meas} - GPR(\mathbf{X})\|^2 \tag{3.4a}$$

$$\mathbf{X}_{imag} = \arg\min_{\mathbf{X}} E(\mathbf{X}) \tag{3.4b}$$

The function $E(\mathbf{X}): \Re^N \rightarrow \Re^1$ is known as the error or objective function and is a time-discretized approximation to the equivalent functional. For the numerical experiments reported in this document, $GPR_{meas} = GPR(\mathbf{X}_s)$. This would be an inverse crime (Kaipio, Somersalo 2007) if the results were used to evaluate the imaging algorithm. However, the focus of this study is a comparison of the information that can be obtained by bi-static and multi-static GPR. Consider the Taylor expansion of the error function, around the global minimum at $\mathbf{X}_{imag} = \mathbf{X}_s$, and truncating at the quadratic term:

$$E(\mathbf{X}) \cong \frac{1}{2}(\mathbf{X} - \mathbf{X}_s)^T \mathbf{H}_E (\mathbf{X} - \mathbf{X}_s) \tag{3.5}$$

The constant and linear terms are both zero as $E(\mathbf{X}_s) = 0$, and all the first derivatives are zero as $\mathbf{X}_s$ is the global minimum. The Hessian matrix is defined by

$$\mathbf{H}_E \equiv \left[\frac{\partial^2 E}{\partial X_i \partial X_j} \right] \tag{3.6}$$

For a LSQ objective function the Hessian matrix may be estimated from the first derivatives of the forward model. Define a Jacobian matrix of the forward model to be:

$$\mathbf{J} : \mathbf{J}_{ij} \equiv \frac{\partial GPR_i(\mathbf{X})}{\mathbf{X}_j} \tag{3.7}$$

i.e. the derivative of the *i*th component of the GPR forward model discrete time series w.r.t. the *j*th subsurface parameter. Using a first order Taylor expansion to provide a linearization of the forward model around a subsurface parameter vector $\mathbf{X}_s$ yields:

$$GPR(\mathbf{X}) \cong GPR(\mathbf{X_s}) + \mathrm{J}(\mathbf{X} - \mathbf{X_s}) \tag{3.8}$$

Substitution of (3.8) into (3.4a) yields:

$$\begin{aligned} E(\mathbf{X}) &= \left| GPR(\mathbf{X_s}) - (GPR(\mathbf{X_s}) + \mathrm{J}(\mathbf{X} - \mathbf{X_s})) \right|^2 \\ &\cong \left| GPR(\mathbf{X_s}) - GPR(\mathbf{X_s}) - \mathrm{J}(\mathbf{X} - \mathbf{X_s}) \right|^2 \\ &\cong (\mathbf{X} - \mathbf{X}_\mathrm{s})^\mathrm{T} \mathrm{J}^\mathrm{T} \mathrm{J}(\mathbf{X} - \mathbf{X_s}) \end{aligned} \tag{3.9}$$

Comparison of (3.5) and (3.9) yields:

$$\mathbf{H}_E \cong 2\mathbf{J}^T\mathbf{J} \tag{3.10}$$

This is an approximation as the second derivatives of the forward model have been neglected, given the assumption that the forward model is smooth. The sensitivity of the imaging process to the parameters in the state vector $\mathbf{X}$ can be explored by singular value decomposition of the Hessian matrix. As $\mathbf{H}_E$ is symmetric non-negative definite, it may be decomposed into: $\mathbf{H}_\mathrm{E} = \mathbf{V}\Lambda\mathbf{V}^\mathrm{T}$ where $\mathbf{V}$ is an orthonormal matrix whose columns are the singular vectors of $\mathbf{H}_E$ and Λ is a diagonal matrix of non-negative

singular values. Consider the singular value decomposition of $\mathbf{J}$: $\mathbf{J} = \mathbf{U\Sigma V^T}$. It is assumed that the singular values are ordered from largest singular value to smallest. Due to the factorization in (3.10):

$$\mathbf{H_E} \cong 2\mathbf{J^T J} \cong 2\mathbf{V\Sigma U^T U\Sigma V^T} \cong 2\mathbf{V\Sigma^2 V^T} \tag{3.11}$$

Therefore, the singular values of $\mathbf{H}_E$ are twice the squared singular values of $\mathbf{J}$. The singular vectors with smallest singular values correspond to combinations of parameters with relatively small effect on the error function, and so have large uncertainty after the imaging process. To illustrate, consider subsurfaces that vary from the no-mine case by variation of subsurface parameters along singular vector directions, i.e.

$$\mathbf{X} - \mathbf{X}_s = \varepsilon \mathbf{V}_i \tag{3.12}$$

where ε is a small scalar and $\mathbf{V}_i$ is the *i*th singular vector. The change in the objective function is:

$$\begin{aligned} E(\mathbf{X}) &\cong \frac{1}{2} \varepsilon \mathbf{V}_i^T 2\sigma_i^2 \varepsilon \mathbf{V}_i \\ &\cong \varepsilon^2 \sigma_i^2 \end{aligned} \tag{3.13}$$

where $\mathbf{V}_\mathrm{i}^\mathrm{T}\mathbf{V}_\mathrm{j} = \sigma_\mathrm{ij}$ due to the orthonormality of **V**. If the noise in the measurements has a power equal to N^2, then the uncertainty of subsurface parameters along the *i*th singular vector direction has size $\varepsilon = \sqrt{N^2/\sigma_i^2}$. Uncertainty is large along directions associated with small singular values of the forward model around the no-mine condition. Subsurface variation along directions with zero singular values is completely

invisible to GPR measurements. The objects that GPR can most reliably distinguish are associated with the largest singular values.

This section has shown how to estimate the sensitivity of GPR measurements to uncertainty in the subsurface parameters. There are changes in the subsurface that cannot be seen by GPR. An advantage of multi-modal imaging is that the modes can be chosen to be sensitive to different variations in the subsurface, reducing the uncertainty in object identification. The following sections use SVD to estimate the singular values and singular vectors of the objective function and hence to determine the uncertainty in subsurface variation. The number of singular values above the noise floor of GPR measurements indicates the number of subsurface parameters that can be imaged. Right singular vectors associated with large singular values indicate variation of subspace parameters that can be imaged with some certainty. Right singular vectors with small or zero singular values are components that cannot be imaged by GPR. It is important that both these cases are explored so we can understand what features of mines can be seen and what cannot.

3.3 Finite Difference Partial Derivatives

The Hessian of the LSQ error function can be calculated from the Jacobian of the GPR forward model. This section discusses the estimation of the derivatives in the Jacobian. The derivatives required are those in the forward model i.e. $\mathbf{J}_{ij} \equiv \frac{\partial GPR_i(\mathbf{X})}{\mathbf{X}_j}$. Numerically, these can be estimated using a wide variety of finite difference formulae. The Central Difference estimate is known to have quadratic convergence to the first derivatives:

$$\frac{\partial GPR_i(\mathbf{X})}{\mathbf{X}_j} = \frac{GPR_i(\mathbf{X} + h\mathbf{I}_j) - GPR_i(\mathbf{X} - h\mathbf{I}_j)}{2h} + O(h^2) \quad (3.14)$$

where $\mathbf{I}_j$ is the *j*th column of the identity matrix. When the forward model is evaluated numerically and the value of $GPR_i(\mathbf{X})$ contains random noise, then an optimal value of the perturbation factor or step size *h* exists that balances the evaluation errors and the finite difference approximation. A single run of a numerical EM simulation yields a time-series vector of GPR output, and with *N* subsurface parameters, 2*N* simulations are required to estimate all the derivatives in the Jacobian matrix. In the following sections, the Jacobian matrix has been calculated using a value of *h* for each subsurface parameter that has been estimated by testing a range of values to identify the optimal size, see (De Pauw, Vanrolleghem 2006) and (Iott, Haftka et al. 1985).

3.3.1 Interpretation of the 3D Simulation, Sensitivity Analysis and FWI Workflow

The numerical EM solution is produced in the CST environment which is used to model the landmine scenario in 3D, see 3.4.1. The CST setup enables a graphical development of the antennas, ground and mine with the inclusion of electromagnetic parameters for the ground and other material properties which may be also be specified as required. Equation 1.1 is simulated numerically with the CST software. The transmitted impulse is a Gaussian impulse from the modelled antennas into the modelled ground and the received GPR impulse response is an A-scan time domain impulse response which is numerically a time series stored in the ASCII format. MATLAB scripts are used to import the time domain impulse response and compute the Jacobian matrices and finally the SVD which provides the data for the sensitivity analysis. The SVD data are then

interpreted based on the explanation provided in 3.2.2. The sensitivity analyses are performed in this chapter. For the FWI solution, the optimization algorithm is embedded in the CST STUDIO SUITE software. Therefore the time domain impulse response data from the numerical 3D simulations are automatically exported to the optimization algorithm, the Nelder Mead Simplex algorithm, which performs the optimization and presents the quantitative FWI data, which are the estimated parameters of the subsurface. This is outlined in more detail in chapters 4 and 6.

3.4 Sensitivity Analysis for the Dipole Antenna

This first phase aims to verify the results presented in (Watson, Lionheart 2014), of a sensitivity analysis on a simulated multi-static GPR system, assuming dipole antennas and a 2D propagation environment. The results demonstrated that multi-static systems performed better than bi-static, but concluded that the results needed to be verified in 3D using more sophisticated EM modelling. This section addresses these limitations, and further presents a sensitivity analysis based on 3D CST modelling of a notional GPR system consisting of dipole antennas. A comparison is made between different antenna array configurations which are not considered in Watson. A prior FWI solution is assumed and the Jacobian matrix is calculated using the central finite difference approximation (3.14).

3.4.1 Modelling and Simulation

The model in Watson (2014) used a 2D linear array of dipole antennas, vertically positioned, for 1 to 4 receivers (RXs). A 2 GHz frequency range of 1GHz to 3GHz was simulated at 100 discrete frequencies, for a frequency domain solver. The ground was a

parallelogram with horizontal dimensions of 1 m and depth of 30 cm, with 2 low contrast square shaped targets buried at some depth. Absorbing boundary conditions (ABC) were imposed on the sides and bottom. The entire model and experiment was conducted in 2D.

On the other hand, the GPR system models for this study are shown in Figure 3.1 with linear antenna arrays positioned with dipoles at a fixed distance above the surface in a vertical orientation. This is equivalent to the antenna configuration and orientation used by Watson and is aimed at verifying his work. The antennas are end-fed (coaxial) dipole antennas designed and optimised using the Antenna Magus software for a centre frequency of 2.5 GHz and frequency range of 1.75-3.25 GHz. The dipole antenna is a metallic wire of 25 mm (vertical) length fed by a coaxial cable of 86 mm total length. Assuming the same offset of 20 cm used by Watson, an antenna element spacing of 5 cm was deduced for 4 RXs and used in all configurations. Antenna mutual coupling, hence cross-coupling losses are significant with this spacing which is less than half a wavelength. The antennas are placed initially at a height of approximately 3.76 cm above the ground surface. The transmitting element is at the extreme left end of the array and the time series measured at each receive antenna are concatenated into a single data vector **d**. Sensitivity analyses are performed for the target object placed in the middle or centre of the array, see Figure 3.1, and with the target placed directly under the antenna next to the transmitting antenna. For the bi-static system the latter would imply either antenna. Both mine positions assume that the MD has located a conducting part of the device. The aim is to compare the performances of the mine's position w.r.t the antenna system.

To reduce the computational cost, the ground size for this study is 3D but smaller, with a 31 cm by 29 cm box with a depth of 9 cm. Since the emphasis of this study is limited to detection and not clearance, the 9 cm depth is used which is sufficient for detection of pressure activated AP mines which need to be concealed on the ground surface or buried very shallowly to be useful. The UN 13 cm clearance specification applies to excavation of mines in general after detection. The subsurface parameters are the soil relative permittivity $\varepsilon_{r,s}$=2.53 and loss tangent $tan\sigma$=0.0036 based on a practical setup at Manchester (Podd, Peyton et al. 2015). The target is a single AP mine which is modelled as a plastic cylinder with relative permittivity $\varepsilon_{r,m}$=2.8 (typical US M14 mine). The diameter and height are 7cm and 6cm respectively, closer to a Colombian military (INDUMIL) MN-MAP-1 mine (Lopera, Milisavljevic 2007). The mine also contains a tetryl charge (US M14) with relative permittivity $\varepsilon_{r,t}$=2.163 and an air void of free space relative permittivity. The subsurface parameter vector for the models is therefore given by

$$X_s = \left[\varepsilon_{r,s},\ tan\sigma,\ \varepsilon_0,\ \varepsilon_{r,m},\ \varepsilon_{r,t}\right] = [2.53,\ 0.0036,\ 1,\ 2.8,\ 2.163] \qquad (3.15)$$

Instead of ABC boundary conditions (used by Watson), perfectly matched layer (PML) boundary conditions are applied on all faces of the box (ground) for all models in this study with added space above the antennas on the top of box to simulate the antenna to antenna and antenna to ground propagation. Numerical modelling and solutions of wave propagation and EM scattering problems require a truncation of the otherwise infinite boundaries to a finite computational domain which can then be analysed. To minimise reflections at the newly created domain boundaries, special boundary

conditions need to be imposed. The ABC and PML are the most widely used for EM numerical analysis or simulation (De Hoop, Van den Berg, Peter M et al. 2002)(Nataf 2013). ABC boundary conditions have been studied longer and are generally easier to implement but the PML region achieves less boundary reflection (Nataf 2013).

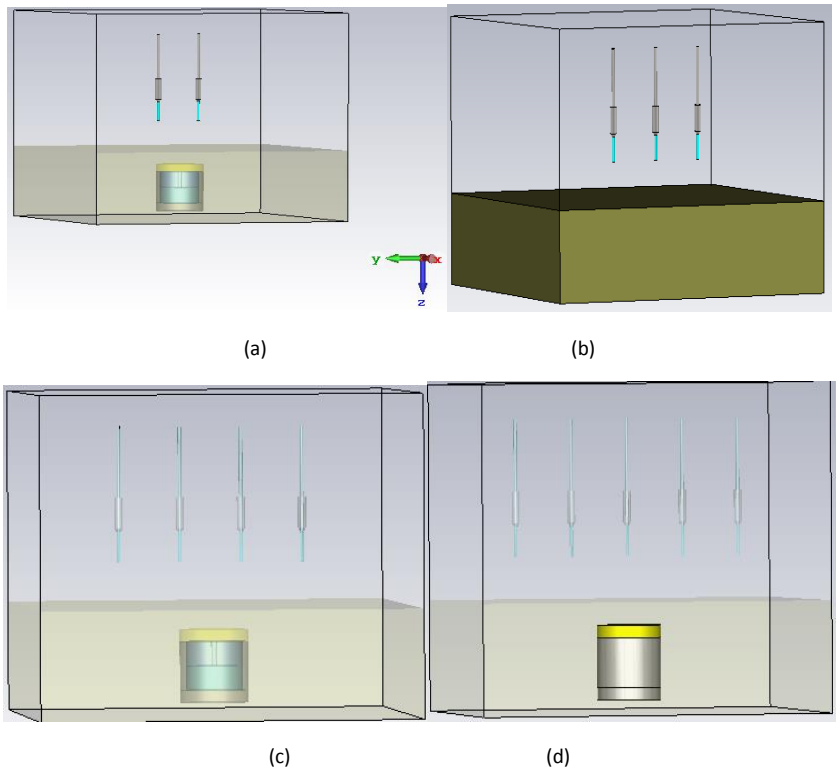

Figure 3.1 Different views of the dipole antenna system: a. bistatic b. 2 RXs c. 3 RXs d. 4 RXs

3.4.2 Results and Discussion

Results of the sensitivity analysis produced from the dipole antenna array simulations for the subsurface parameter vector in (3.15) are presented in Figures 3.2a, 3.2b, 3.3 and 3.4 respectively. In each graph, the magnitudes of the singular values are converted to the natural logarithm (ln) on the y-axis and are plotted against the singular value index on the x-axis, which corresponds to the individual singular values for each of the 5 parameters in 3.15. The singular values of GPR experiments with linear arrays of dipoles like Watson's are presented in Figure 3.2a, with the mine placed in the middle of the

array, and in Figure 3.2b, with the mine placed directly under an antenna element. The system with the mine placed in the middle achieves the largest singular values, and hence more information than the system with the mine placed under an antenna. Therefore, the former system shall be used for subsequent analysis throughout the thesis. The antenna patterns in the system with the mine placed under an antenna produce a striking result, as seen in the third singular values for the 3 RX and 4 RX systems. Otherwise, the singular values decay exponentially but tend to increase in value with increasing numbers of antenna elements. This is consistent with Watson's conclusion that multi-static systems with more receivers yield more information on the mine and subsurface than bi-static systems. However, it can also be seen that the improvement is not consistent or monotonic with increasing receivers, across the imaged parameters. For example, the second singular value for the 2 RX system is significantly larger than that of the 3 RX systems. Since the right singular vectors show us the data to image map (Watson, Lionheart 2014) then it means the 2 RX system provides more information on at least one subsurface parameter than the 3 RX system. These comparisons are complicated by the different geometries of the arrays with different numbers of antenna elements. Dipole antennas radiate little energy in the axis direction i.e. towards the ground. Initially, as receive antennas move further from the target, more of the transmitted energy reaches the target and received at RX, leading to a larger signal. This effect is stronger than the near-field spreading loss for the antenna separations considered. Additionally, the sensitivity analyses were repeated with no mine in the ground, yielding null singular values for each system and configuration. This verifies the accuracy of the simulation results for the sensitivity analysis, underpinning

the relationship between the singular values and the number of parameters that the GPR can sense or estimate quantitatively.

The impact of different configurations of 4 RX systems is seen in Figure 3.3. The line configuration outperforms the diamond and square configurations in terms of the magnitude of the singular values. Apart from the influence of the radiation patterns, this suggests the importance of the antenna cross coupling effects. Mutual coupling decreases in independence between signals recorded by each antenna and so reduces the total information gathered. There is a need to balance the antenna isolation while still maintaining physical dimensions that are suitable for a handheld system, which is also lightweight and possesses low power consumption. The 6 RX line configuration system achieves only a marginal increase in performance over the 4 RX equivalent and hence more elements would not be expected to yield significant improvements. Therefore, it is necessary to optimize the number of receiver elements with reference to not only detection performance but also cost, system complexity, power consumption and size or weight.

The effect of the antenna to ground spacing was also analysed by first placing the 4 RX antennas at a position of 7.5 cm above the ground surface, which is twice the distance of the original setup and secondly, in direct contact with the ground surface. The results are compared as seen in Figure 3.4. As expected, as an indication of the amount of electromagnetic energy coupled into the ground (Daniels 2007), it is noticed that the singular values of the system at the 7.5 cm above the ground decay consistently quicker and yield less quantitative information on parameter sensitivity or the subsurface.

Achieving maximum proximity to the ground without contact is therefore another factor necessary for optimal multi-static handheld GPR performance.

The preceding analyses have been for a flat, homogeneous ground, which was also used by Watson. In real environments, the signals produced from the air-ground reflections easily obscure the subsurface backscattered signals from the mine (Dumanian, Rappaport 2005). Generally, the rough ground surface is considered the dominant source of clutter signal (Gonzalez-Huici, Uschkerat 2010, Giannopoulos, Diamanti 2008)(Rappaport, El-Shenawee et al. 2003). Placing the GPR system in contact with the ground is expected to suppress such clutter signals. Nevertheless, this is impractical due to the dangerous implications of triggering a mine accidentally. This underlines the fact that clutter reduction is critical in estimating the parameter sensitivity for a typical, heterogeneous ground. FWI for a heterogeneous medium shall be considered in the next chapter.

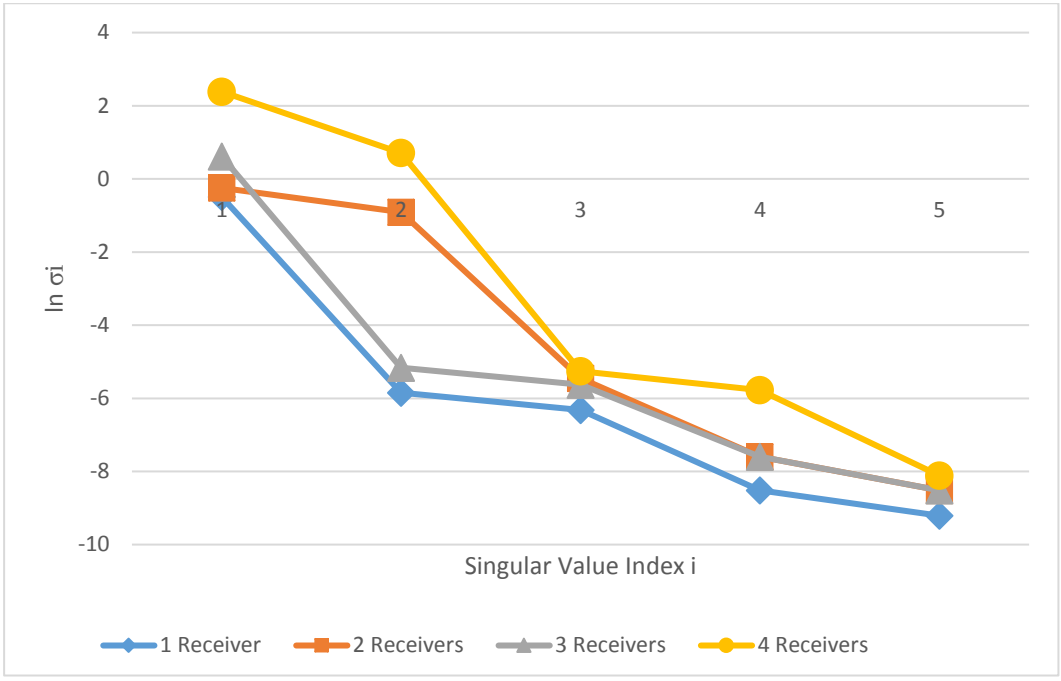

Figure 3.2a Singular values for linear dipole antenna system with 1-4 RXs for a mine placed in the middle of the array

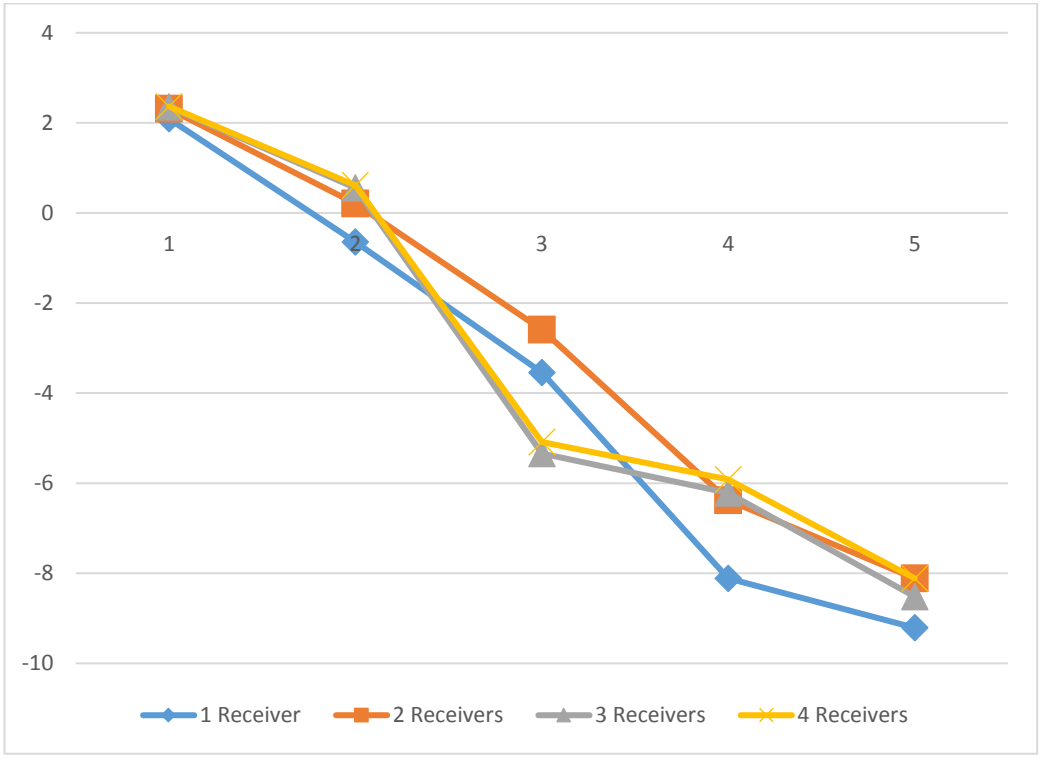

Figure 3.2b Singular values for linear dipole antenna system with 1-4 RXs for a mine placed under an antenna

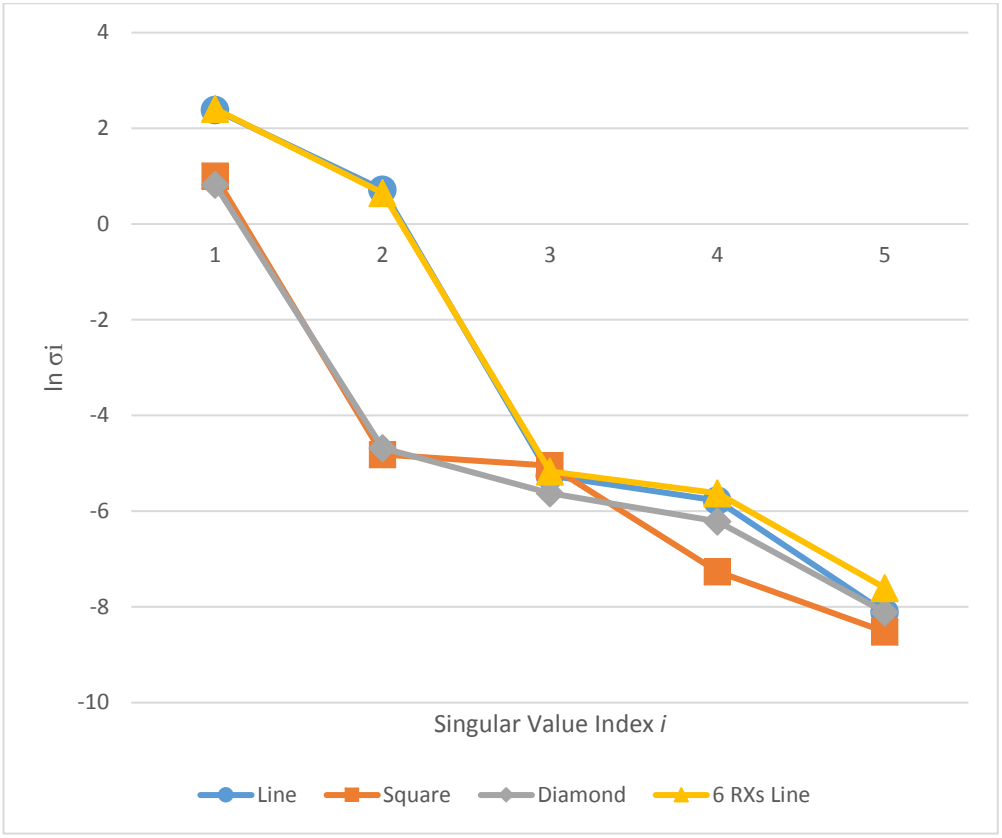

Figure 3.3 Singular values for different 4 RX dipole configurations and a 6 RX dipole configuration (the line configuration plot is largely obscured by the other 3 configurations)

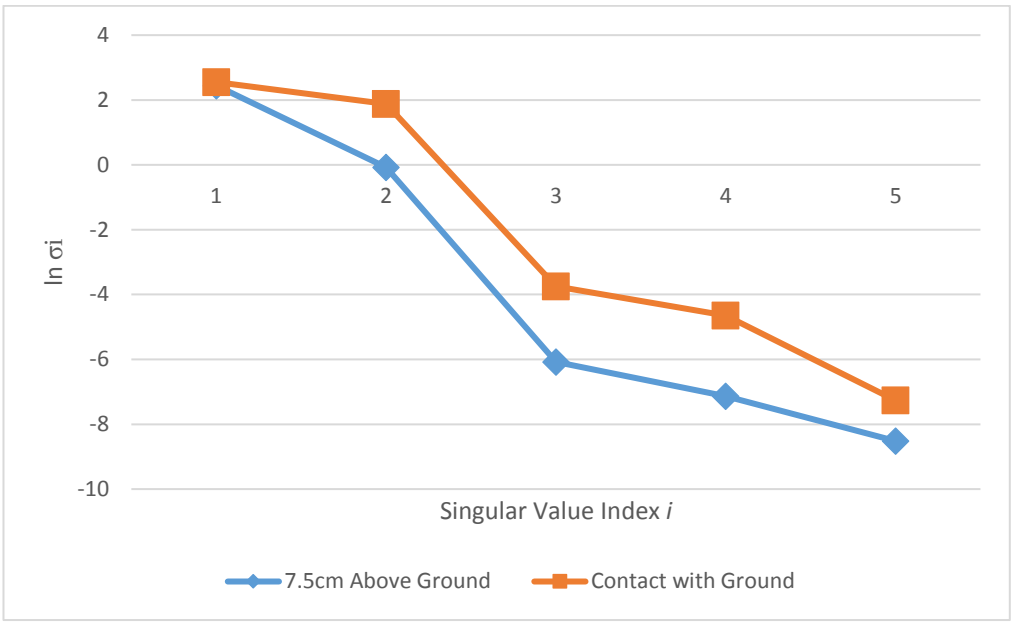

Figure 3.4 Singular values for a dipole 4 RX system for a. 7.5cm above the ground surface b. in contact with the ground

3.5 Sensitivity Analysis for the Double Ridged Horn Antenna

The second phase of the sensitivity analysis compares realistic, handheld bi-static and multi-static GPR systems for flat, homogeneous soil using simulation data for a 3D double ridged horn (DRH) antenna. A mine is modelled as a plastic sphere to reduce the computational cost. The primary distinguishing characteristic, between a mine and another small conductive target, is the permittivity of the surrounding volume. The simulation volume is a box of length and width: 61 cm by 49 cm, containing a 15 cm depth of homogeneous, flat dry sandy soil with relative permittivity $\varepsilon_{r,s}$=2.53 and conductivity σ_s= 0.001 S/m. This model is also based on a test rig at the University of Manchester (Podd, Peyton et al. 2015), and validates the simulation results of the sensitivity analysis for the DRH antenna. Figure 3.5 illustrates the simulated target. PML boundary conditions are imposed on the sides and bottom of the box. The AP mine target was modelled as a dielectric plastic sphere with radius R= 3.5 cm, relative permittivity $\varepsilon_{r,m}$=2.8 (US M14 plastic mine) and its top surface 5 cm below the soil surface, corresponding to a *z* coordinate of Z_m= 29. These are the 5 parameters that describe the unknowns in the GPR simulation, and they are collected into a state vector given by

$$X_s = \left[\sigma_s, \varepsilon_{r,s}, \varepsilon_{r,m}, R_m, Z_m\right] = [0.001, 2.53, 2.8, 3.5cm, 29] \qquad (3.16)$$

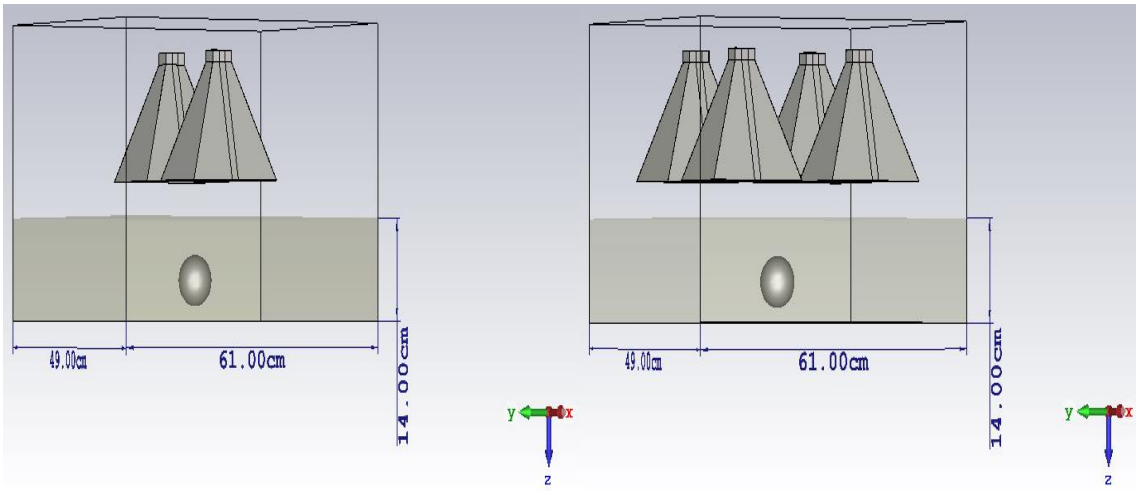

Figure 3.5 DRH bi-static and multi-static GPR system model

3.5.1 The Acquisition System

The models as shown in Figure 3.5 use the DRH antennas operating in transverse electromagnetic (TEM) mode, with 2 antennas for the bi-static system and 4 antennas (1 transmit, 3 receive simultaneously) for the multi-static system. The DRH antenna is selected due to its superior performance over other antennas for GPR, based on the study by (Hertl, Strycek 2007) which compared the mechanical and radiation properties of selected antennas from different classes of UWB antennas widely used for GPR operations for a 0.5-3 GHz bandwidth. The mechanical properties considered the antenna physical dimensions in mm, structure (planar, 3D or wire) and the design complexity (low, medium or high). The radiation properties considered the type of radiation (omni-directional, bi-directional or directional), polarization (linear or circular) and the gain in dBi. The antennas compared were the cone antenna (elementary monopole antennas), circular disc monopole (planar monopole antennas), bow-tie antenna (dipole antennas), Vivaldi antenna (tapered slot antennas), DRH (TEM horn antennas) and the Archimedean spiral antenna (frequency independent antennas). The

tests were conducted through simulation in CST Microwave Studio environment and the results, summarised in Table 3.1, showed that overall, the DRH and Vivaldi antennas were best suited for GPR applications, as the DRH antenna achieved a higher directivity and better side lobe control whereas the Vivaldi antenna was less complex and easier to construct. The dimensions of the bow-tie and DRH antennas used are up to 450 mm and 600 mm across respectively. These are larger than the handheld antennas considered here, which are based on physical handheld MD and GPR systems with dimensions not exceeding 400 mm (University of Manchester) and 30.5 cm (MINEHOUND) across any distance.

The DRH is designed using the Antenna Magus software for a centre frequency of 5.5 GHz and a frequency range of 1-10 GHz. The DRH has dimensions of 200 mm by 140 mm by 160 mm. The only difference between the bi-static and multi-static scenarios are the number and position of the antennas. It is assumed that the metal detector functionality of the GPR has been used to position the antenna array over the suspected mine, located at the point of rotational symmetry. This model and configuration are used for the analyses with the DRH as this is an attempt to validate the test rig at Manchester. For the bi-static case, only a single time-series measurement may be performed due to symmetry i.e. transmission from one antenna to the other. Due to reciprocity, the reverse propagation path yields the identical measurement. For the multi-static case, the four antennas are in a 2 by 2 grid centred on the target. Two measurements may be performed i.e. between adjacent and diagonally opposite pairs of antennas. In this case, the signal is transmitted from any single element while the other 3 elements receive the

signal simultaneously in a single input multiple output (SIMO) fashion. For a non-spherical target, the symmetry is broken, although reciprocity still holds.

Structure	Type	Dimensions (mm)	Design Complexity	Radiation Direction (dir)	Polarization	Gain (dBi) in the same direction		
						1GHz	2GHz	3GHz
Cone	3D	158*158*174	medium	omni	linear	3.2	4.4	4.0
Disc	planar	12*246*232	low	omni	linear	5.1	5.3	6.6
Bow-tie	wire	12*532*600	Medium	bi-dir	linear	3.3	5.2	6.8
Vivaldi	planar	405*12*318	medium	dir	linear	5.8	7.0	7.7
DRH	3D	450*218*218	high	dir	linear	10.3	10.3	11.9
Spiral	planar	12*218*218	Low	bi-dir	circular	3.9	5.8	5.5

Table 3.1 UWB antennas - mechanical and radiation properties (Hertl, Strycek 2007)

3.5.2 Results and Discussion

The DRH sensitivity analysis data are presented, with the numeric singular values for both systems in Table 3.2 and the right singular vectors for the bi-static and multi-static systems respectively in Tables 3.3 and 3.4. A logarithmic plot of the singular values is also presented in Figure 3.6. The slower decay of the singular values of the multi-static system is consistent with our expectation. The singular values similarly decay faster than exponentially, indicating the ill-posedness of the inverse problem. The larger singular values in the multi-static system suggests that, for a given noise floor, the multi-static system will provide a larger number of sub-surface parameters with greater certainty. Examination of the singular vectors shows which parameters can be identified by GPR. Several complicating factors are present such as different antenna gains in the mine direction and different antenna geometries w.r.t to the mine which influence the singular values and vectors. The first singular vector, for both systems, is linked to the contrast between the permittivity of the soil and the mine, as this determines the

strength of the signal scattered by the mine; principally reflected off the mines upper surface or propagated around the mine in a surface wave. At the frequencies considered, the mine is of a similar size or smaller than a wavelength, depending on the permittivity of the soil, and so a flat topped mined would yield a stronger reflection. Mie scattering from the spherical target includes surface waves that travel around the mine and then to the receiver. Other combinations of parameters yielded very small singular values e.g. increasing both the mine diameter and depth; as this combination leaves the mine's top surface in the same position. We can conclude that the most important component of the signal is due to single scattering from the mine i.e. a combination of reflection and surface wave. Measurements were least sensitive to the conductivity of the soil as the value chosen was low, typical of dry sand, and the path through the soil was short.

GPR System	**Singular Values,** $\sigma_i(1e-05*)$				
Bi-static	0.6113	0.3245	0.0846	0.0162	0
Multi-static	1.0930	0.8650	0.6530	0.1460	0

Table 3.2 Bi-static and multi-static GPR singular values

Parameters	**Bi-static Right Singular Vectors**				
σ^s	0	0	0	0	1
ε_r^s	-0.9995	-0.0229	0.0066	-0.0218	0
ε_r^m	0.0041	0.4858	0.7334	-0.4765	0
R^m	0.0194	-0.1491	-0.4666	-0.8716	0
z^m	-0.0256	0.8610	-0.4944	0.1168	0

Table 3.3 DRH Bi-static system right singular vectors

Parameters	**Multi-static Right Singular Vectors**				
σ^s	0	0	0	0	1
ε_r^s	0.5634	0.8262	-0.0001	0.0005	0
ε_r^m	-0.8262	0.5634	-0.0003	0.0052	0
R^m	-0.0001	0.0002	0.9999	0.0151	0
z^m	0.0040	-0.0034	-0.0151	0.9999	0

Table 3.4 DRH Multi-static system right singular vectors

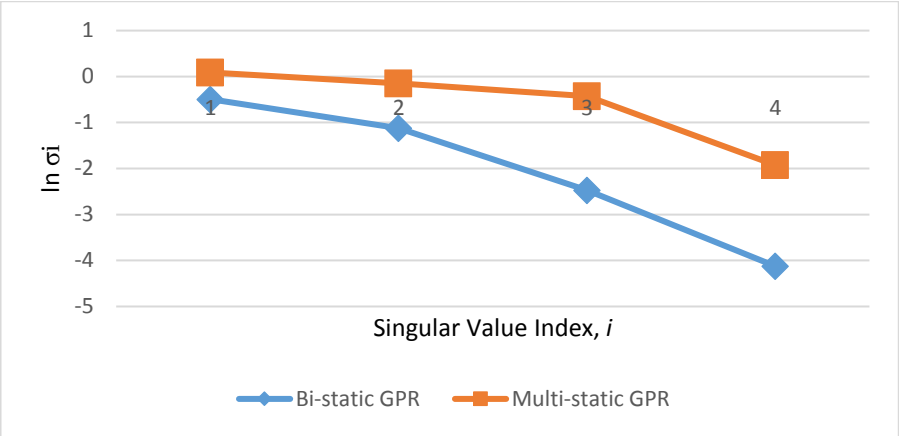

Figure 3.6 Logarithmic plot of DRH bi-static and multi-static GPR singular values

3.6 Sensitivity Analysis for the Vivaldi Antenna

This section presents the third and final sensitivity analysis comparing bi-static and multi-static handheld GPR systems using the Vivaldi antenna. Given the outcome of the Hertl study (Hertl, Strycek 2007), the Vivaldi antenna offers the best alternative to the DRH antenna. The Vivaldi antenna is lighter in weight, more portable and cheaper to manufacture than the DRH antenna. It is described as a "low cost" version of the TEM DRH antenna in (Neto, Monni et al. 2010). High gain antennas are difficult to achieve when electrically small, but with more broadcast radio power towards the subsurface target, are less susceptible to clutter not close to the target, and are less strongly coupled. Handheld MD and GPR fused systems with bi-static Vivaldi antennas have been evaluated in training fields in (Sato, Fujiwara et al. 2004) and a 10 element scanning array using the Vivaldi antenna was also tested in a controlled laboratory experiment (Sato, Fang et al. 2003). This section presents a sensitivity analysis for Vivaldi antenna systems, like the dipole systems presented in section 3.4. This includes a comparison of the sensitivity analyses for the mine placed in the middle or centre of the array and placed under the antenna next to the transmitting antenna, or either for the bistatic

system. The aim is also to compare the performance of the position of the mine w.r.t to the antennas.

3.6.1 Modelling and Simulation

The major difference from section 3.4 is the use of Vivaldi antennas instead of end fed dipoles. The Vivaldi antenna dimensions and structure are designed and optimised automatically using the Antenna Magus software for a centre frequency of 3.5 GHz (higher than that of the dipole systems at 2.5 GHz) which yielded an operating frequency range of 1-6 GHz (wider bandwidth than the dipole systems at 1.5 GHz). The Vivaldi antenna has a planar geometry with dimensions of 440 mm by 0.1 mm by 219 mm. The ground and mine parameters are identical to those used for the dipole system as seen in section 3.4.1. The Vivaldi antennas are placed in a linear (line) configuration for 1 to 4 RX antenna systems. Like the dipole system, the transmitting element is at the extreme left end of the array and the time series measured at each receive antenna are concatenated into a single data vector. This setup enables all the multi-static systems to be analysed with dimensions suitable for a handheld system. The line configuration is also assumed to potentially yield the best performance based on the results of the comparison of the dipole antenna system layouts also in section 3.4.2. The Vivaldi antenna system models are shown in Figure 3.7.

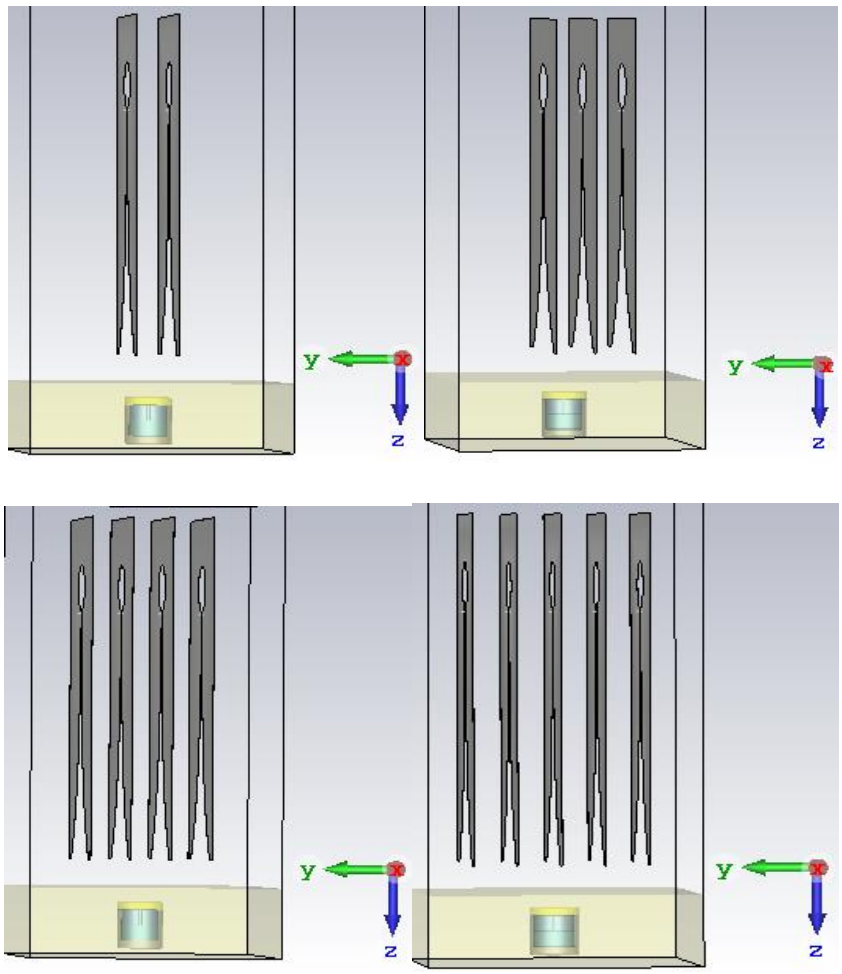

Figure 3.7 Different views of the Vivaldi antenna system models with 1-4 RXs

3.6.2 Results and Discussion

The results of the sensitivity analysis for the Vivaldi antenna are shown in Figures 3.8a and 3.8b with a logarithmic plot of the singular values for the different positions of the mine, i.e. in the middle and under an antenna respectively. The latter achieves the highest singular values, for the 2 RX system, and hence yields greater information. The singular values in the former decay more rapidly and reveals little differences between all the systems numerically as the singular values are very close, overlapping each other. As with the dipole system, the configuration with the mine in the middle of the array performs better and will be used throughout the rest of the thesis for any experiments

with the Vivaldi antenna. Furthermore, the impact of the system nonlinearity is observed conspicuously. Contrary to the dipole antenna sensitivity analysis, the 4 RX system does not yield the highest subsurface parameter sensitivity or information. Generally, the multi-static systems decay slower than the bi-static system as expected however the 2 RX system in this case exhibits the slowest decay rather than the 4 RX system. Therefore, the directional antenna radiation characteristics have a significant impact on parameter sensitivity and uncertainty estimation. A direct comparison between the dipole and Vivaldi GPR systems shows that the 2 RX Vivaldi system yields greater parameter sensitivity than the 4 RX dipole system and it is concluded that the Vivaldi system achieves a better performance by yielding more information about the subsurface under our experimental conditions, due to the directional radiation pattern.

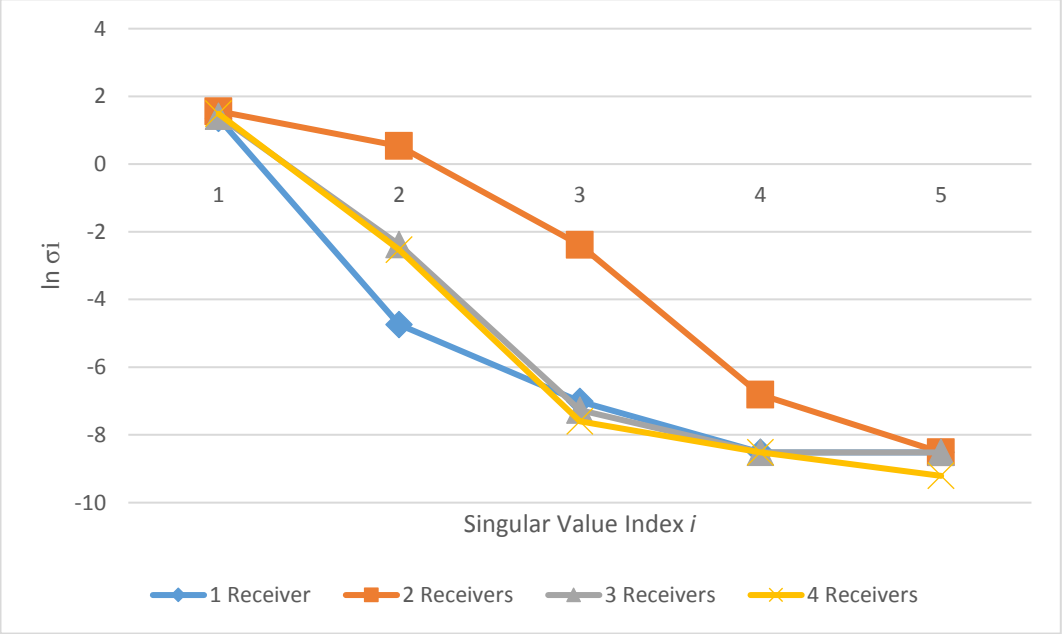

Figure 3.8a Singular values for the Vivaldi GPR system for 1-4 RXs for the mine placed in the middle of the array

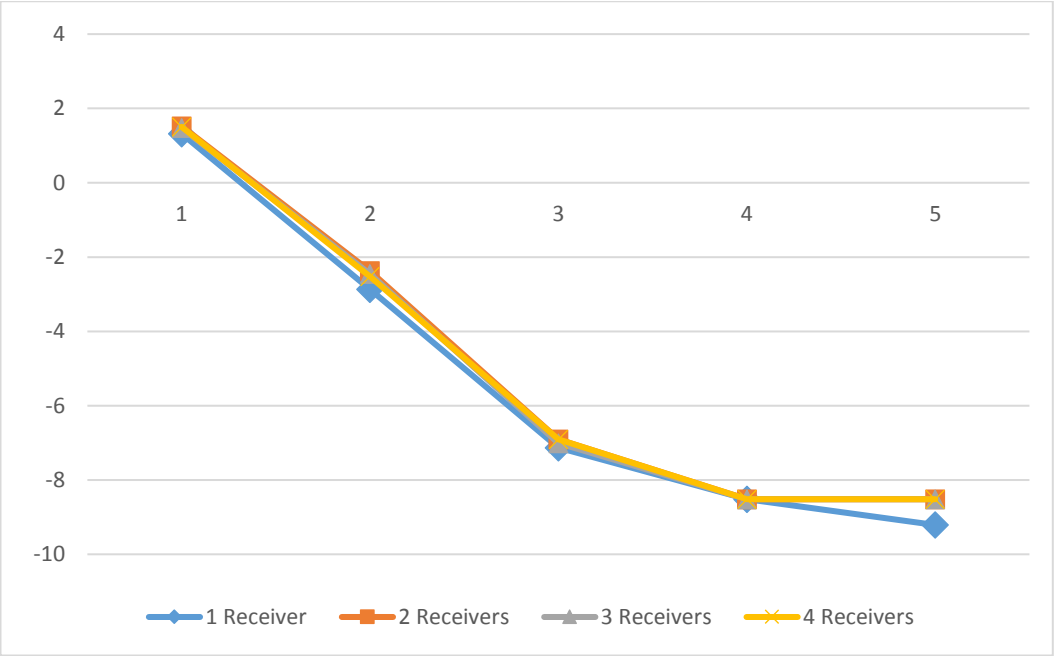

Figure 3.8b Singular values for the Vivaldi GPR system for 1-4 RXs for the mine placed under an antenna

3.7 POD Estimation

In this section, the POD for bi-static and multi-static GPR are calculated and compared to evaluate the performance of the systems for mine detection. The experiment is for a flat, homogeneous soil with a spherical, plastic mine, buried at a top surface depth of 130 mm and placed in the centre of the antenna array for the bi-static and multi-static GPR. The experiments are conducted for the dipole and Vivaldi antennas. The multi-static dipole GPR is the 4RX system while the multi-static Vivaldi GPR is the 2RX system.

POD is determined by calculating distinguishability, see 3.22, in each system for a range of positions of the mine in the ground. This is consistent with the conventional demining procedure described in chapter 1, and precludes FWI. The CST software is used to run simulations for a linear parameter sweep with the mine in different positions along the length, width and depth of the ground, corresponding to the three parameters of X-axis coordinate, Y-axis coordinate and Z-axis coordinate respectively. Five different samples

of these parameters yields a total number of 125 (5^3) simulations. See Appendices A and B for POD of the dipole system and Appendices C and D for POD of the Vivaldi system.

A threshold for distinguishability to determine a mine or no mine detection is set based on the distinguishability for the mine buried at 130 mm corresponding to an X-axis coordinate of 10.25, Y-axis coordinate of -25 and Z-axis (130 mm depth) coordinate of 36.5 as shown in Appendix A. Distinguishability values equal to or greater than the threshold indicate a mine detection while values below the threshold are indicative of a no mine detection. The POD figure is deduced from the percentage of mine detections out of the total number of detections or measurements (simulations). The POD values for the dipole and Vivaldi antenna systems are shown in Tables 3.5 and 3.6 respectively. Table 3.5 shows that the bi-static system achieves a 9% improvement in POD over the multi-static system for a 3D, flat, homogeneous dry sandy soil with a spherical, plastic mine. In chapter 4, the mine detection performance of the systems is evaluated using FWI in a cluttered domain to compare the bi-static and multi-static system performance for 1D data in a 3D domain.

GPR System	Mine Detections	No Mine Detections	POD
Bi-static Dipole	119	6	0.95
4RX Multi-static Dipole	107	18	0.86

Table 3.5 POD for Bi-static Dipole GPR and 4RX Multi-static GPR

GPR System	Mine Detections	No Mine Detections	POD
Bi-static Vivaldi	6	119	0.048
2RX Multi-static Dipole	8	117	0.064

Table 3.6 POD for Bi-static Vivaldi GPR and 2RX Multi-static GPR

3.8 FAR Reduction

The results of the sensitivity analyses conducted previously indicate that the presence or otherwise of an air void in the buried target can be detected from the singular value of the relative permittivity of free space when it is mapped to the right singular vector. Further results are shown in Section 6.2. When the relative permittivity of free space parameter has a singular value greater than zero, this is indicative of an air void and hence typical blast AP mine. However when the singular value is zero, there is no air void and the target can be considered a non-mine object. This can be used to reduce the FAR by enhancing target discrimination based on the parameter estimation of the mine air void. This is validated by attempting to verify a predetermined FAR value. Ten different sensitivity analyses are conducted using the 2RX Vivaldi multi-static GPR setup described in 3.6.1 and shown in Figure 3.7. Each setup has a mine-like object buried in a different position in the soil w.r.t the antennas and/or material from the others. Five of the buried targets contain air voids while 5 are solid objects of different materials, see Table 3.7. A FAR of 0.5 is expected if the singular values can be used to accurately determine a mine or no-mine decision based on the void parameter singular values. The results are also shown in Table 3.7. The targets with singular values greater than zero indicate sensitivity to the relative permittivity of free space and are designated as a mine detection while targets with singular values equal to zero are designated as a no mine detection. The FAR derived is equal to 0.5, which confirms the original known value. Therefore the singular values, and hence FWI, can be used to discriminate objects and reduce the FAR based on A-scan data. Chapter 6 provides a further investigation of the air void parameter estimation using the FWI algorithm for a heterogeneous domain.

Buried Target/ Relative Permittivity	Mine Position in x,y coordinates, depth (cm)	Air Void Singular Value	Detection Decision
Plastic Cylinder 1	10.25, -25, 2	0.0014	Mine
Plastic Cylinder 2	5.25, -25, 2	0.0014	Mine
Plastic Cylinder 3	10.25, -20, 2	0.0008	Mine
Plastic Cylinder 4	5.25, -20, 2	0.0009	Mine
Plastic Cylinder 5	10.25, -25, 4	0.0012	Mine
Plastic Cylinder 6	10.25, -25, 4	0	No mine
Quartz Cylinder	10.25, -25, 2	0	No mine
Graphite Cylinder	5.25, -25, 2	0	No mine
Iron Cylinder	10.25, -20, 2	0	No mine
Glass Cylinder	5.25, -20, 2	0	No mine

Table 3.7 Sensitivity analysis results to determine FAR

3.9 Conclusions

Three sensitivity analyses based on finite difference approximations to the Jacobian of the forward model, have been conducted for simulated 3D handheld GPR systems. Three types of antennas have been investigated to evaluate the amount of subsurface information that can be obtained from multi-static and bi-static handheld GPR systems for AP landmine detection. Generally, the analyses verify the finding of Watson (2014) that multi-static systems yield better distinguishability of AP mines than bi-static. However, contrary to the conclusion by Watson that the number of antenna elements of the multi-static array is not very important, the analysis based on the Vivaldi antenna shows that the multi-static system performance is not monotonic, with respect to the number of antenna elements. Additionally, the data shows that the improvements in

parameter sensitivity achieved with multi-static systems compared to the bi-static systems are small numerically, though distinct. Watson used a simple model with many unrealistic approximations. The current study uses a more accurate and realistic 3D EM high frequency numerical analysis in time domain to model and simulate handheld GPR systems. The analyses have been performed allowing the number and confidence of imaged parameters to be determined, for any noise floor. The 3D sensitivity analysis conducted also demonstrates the significant influence of antenna configuration and orientation on detection performance.

POD results based on distinguishability show that prior to FWI, for omni-directional antenna radiation, the bi-static system achieves a marginally better performance than the multi-static system whereas for directional antenna radiation, the multi-static system achieves a very small improved performance over the bi-static system of less than 2%. Nevertheless, the distinguishability values for the Vivaldi system were consistently greater than the dipole system, which is consistent with the sensitivity analysis data. The sensitivity data can also be used to reduce the FAR by discriminating between mine and non-mine targets based on the detection of the mine air void from the singular values and hence FWI parameter estimation. The free space relative permittivity parameter records a zero value in the absence of a void and a value greater than zero when there is a void.

Here, a flat ground surface and homogeneous soil has been assumed throughout. In practice, neither of these assumptions will be met as the inverse problem requires more parameters to describe processes leading to clutter signals.

Chapter 4 Non-Derivative Full-Wave Inversion

4.1 Introduction

This chapter provides further comparison of the quantitative information that can be obtained from bi-static and multi-static systems using a FWI analysis. The objectives are to validate the sensitivity results obtained in chapter 3 and evaluate the performance of bi-static and multi-static systems for FWI, including a cluttered domain. The former approach was also used by Watson to verify his comparison of bi-static and multi-static parameter sensitivity estimation using a simple model. His analysis assumed a 2D, flat, homogeneous domain with no clutter. Watson concluded that the multi-static system yielded more subsurface information that bi-static, with more information from more elements. Additionally, he states that the number of elements in the multi-static system or array is of little importance for GPR FWI.

Here, a FWI numerical analysis is reported for a 3D domain, with and without clutter, using a derivative-free optimization algorithm. The bi-static and multi-static system performance are evaluated by comparing the estimated subsurface parameters obtained in each case with the synthetic GPR data parameters. Given the similarity of the singular values obtained for the 2 and 3 RX multi-static systems in chapter 3, and the handheld system size constraint, the FWI multi-static system analysis in this chapter is limited to the 2 RX and 4 RX systems only. The derivative-free method for solving the FWI problem is used because it is computationally expensive to estimate the derivatives required for derivative based methods. Derivative-free (or non-derivative) methods

require less computation per iteration and are suitable for a limited number of variables, but may require more iterations. This chapter looks at the computations required to calculate FWI solutions for GPR bi-static and multi-static systems. The performance of non-derivative algorithms for a bounded domain are considered. The study is empirical with synthetic A-scan data, as used in the MINEHOUND dual sensor system, and not a full evaluation of the FWI algorithm. The analysis aims to quantitatively estimate the parameter sensitivity for bi-static and multi-static GPR systems using a nonlinear non-derivative optimization. This provides information on the reliability of target detection by each system in a real FWI evaluation. Therefore, the contribution to other studies on 3D GPR FWI for landmine detection is that a non-derivative nonlinear optimization method to solve FWI problems is used to compare bi-static and multi-static systems in a 3D, cluttered domain.

Furthermore, this chapter concludes with the introduction of a novel procedure for improving the estimation of the initial parameter vector for the iterative nonlinear optimization. The process uses a database of synthetic data based on the forward model for parameter sets randomly chosen within a local bounded domain. The data is used to determine an initial parameter vector for the actual optimization.

4.2 Nelder Mead Simplex Algorithm

A range of non-derivative nonlinear optimization algorithms may be used to solve the FWI optimisation problem when gradients do not exist or are expensive to compute. Local direct search methods may be used when there are a small number of variables and the objective function is computationally cheap to evaluate. Common examples

include the grid search, alternating variable search, Hook and Jeeves method, Rosenbrock's Method, Powell's Method and the Nelder and Mead's (Nelder Mead) Simplex Method (Gethins, Paulson 1995). Grid search, also known as brute-force, evaluates the objective function at every point within a rectangular grid and generally requires many more objective function evaluations than other methods. The alternating variable search performs 1D minimisations of each variable in turn, repeating as necessary. The Hook and Jeeves method looks for lower objective values by taking a fixed step in each variable direction. The variable step length is dynamically varied with each iteration to speed up convergence. Rosenbrock's method builds on the unsuccessful alternating variable search results by introducing improved updated search directions. Powell's method performs a direct search and generates multiple search patterns by updating previous coordinate directions. It is the most efficient of the methods listed so far. However, for more than five variables and poorly-conditioned problems, it may perform very poorly. The Nelder Mead simplex algorithm (Nelder, Mead 1965) is the most cited, robust and efficient of local direct search methods. The algorithm fundamentally relies on an initial number of points that create a simplex i.e. a set of points spanning a volume in the variable dimensionality considered. The objective function is evaluated at the vertices of the simplex during each iteration to determine the highest objective value, which is used to redefine another vertex that produces a new simplex. Additional new points are produced by moving the vertex with the highest objective value through a series of transformations using the centroid of the associated simplex, that include reflection, expansion, internal and external contractions (Rios, Sahinidis 2013). These steps are iterated until convergence is achieved. Convergence

can occur for non-smooth objective functions even when the first and second derivatives of the function are unobtainable (McKinnon 1998). Modifications to improve the efficiency of the algorithm have been suggested by other authors such as (Kelley 1999). The Nelder Mead simplex algorithm may be applied to the FWI optimisation problem, to estimate the uncertainty in parameter sensitivity of the handheld GPR bi-static and multi-static systems. The Nelder Mead Simplex algorithm is embedded in the CST Design Studio environment and so the 3D GPR forward model may be integrated with the optimization process on the same platform.

4.3 FWI Numerical Analysis

This section will use the end fed dipole antenna system for 1, 2 and 4 RXs as described in section 3.4. For the heterogeneous ground, we replace the homogenous ground with a rough surface. The ground is modelled with a surface roughness height in the form of a Gaussian distribution (Tajdini, Gonzalez-Valdes et al. 2015) (Gonzalez-Huici, Uschkerat 2010). Therefore, the box planar surface is modelled with random depressions and protrusions to simulate a ground surface with a random height, white noise, normally distributed with a mean value of zero (Daniels 2007). Additionally, subsurface clutter sources are modelled as several 3D rectangular blocks, grouped into two clusters, with each set having a different relative permittivity. One has a relative permittivity, $\varepsilon_{r,C1}$= 5 and the other with a relative permittivity, $\varepsilon_{r,C2}$= 4. This heterogeneous ground model is used throughout the thesis to represent a cluttered domain. An example bi-static dipole system and target subspace is shown in Figure 4.1. FWI is posed as a LSQ regularised optimisation problem, as in (3.2) i.e. the minimisation of $\|GPR_{meas} - GPR(\mathbf{X})\|^2$.

Watson performed a similar study for dipole antennas in a simplified 2D, homogenous domain only. Here both 3D homogenous and heterogeneous domains are investigated for the FWI solution.

The settings of the optimization for a flat, homogenous ground and a rough, heterogeneous ground are shown in Figures 4.2 and 4.3 respectively. The optimization is set to a maximum number of iterations of 20, due to the limited memory capacity available. The relative permittivity of free space is included in the parameters to represent the air void in the mine. The true value of 1 is assigned in the synthetic GPR data while an inaccurate value close to 1 is assigned to the initial parameter set. The aim is to see whether this value would converge to the true value. Further investigation of the air void is provided in chapter 6. The CST simulation hexahedral mesh used to produce synthetic GPR measurements is different from the mesh used in the forward model within the FWI objective function. This avoids the spuriously good results that can be the inverse crime artefact (Kaipio, Somersalo 2007) due to using the same mesh for both operations.

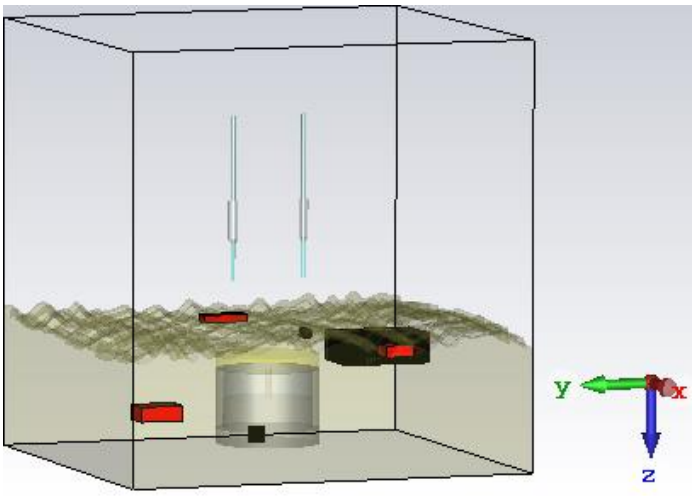

Figure 4.1 Bi-static dipole system for a heterogeneous ground

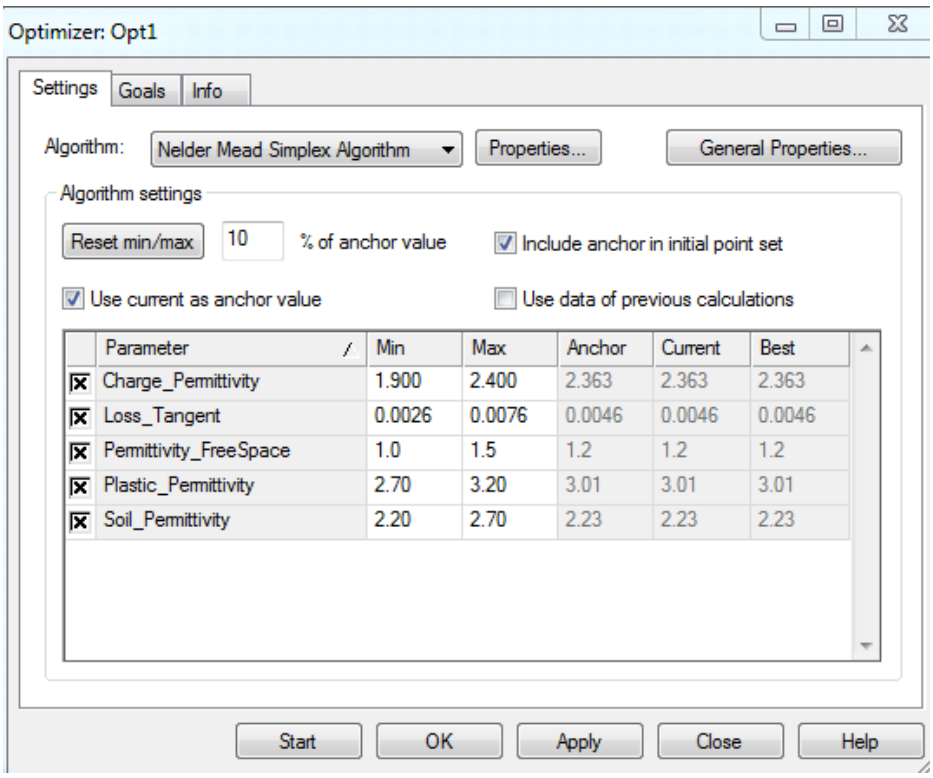

Figure 4.2 Optimizer settings for flat, homogenous ground

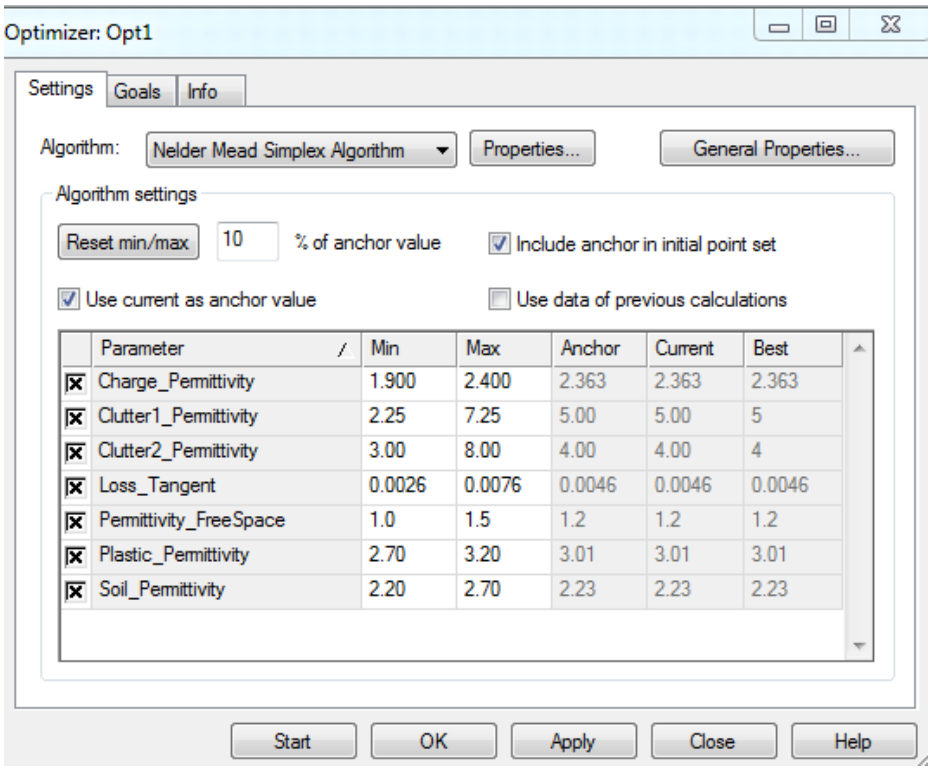

Figure 4.3 Optimizer settings for rough, heterogeneous ground

The parameter vector for the synthetic GPR data for the homogenous ground is;

$$GPR_{initial} = \left[\varepsilon_{r,t},\ \tan\sigma,\ \varepsilon_{0,}\ \varepsilon_{r,m},\ \varepsilon_{r,s}\right] = [2.163,\ 0.0036,\ 1,\ 2.8,\ 2.53] \quad (4.1)$$

where $\varepsilon_{r,t}$= relative permittivity of tetryl charge, $\tan\sigma$= loss tangent, $\varepsilon_{0,}$= relative permittivity of free space, $\varepsilon_{r,m}$= relative permittivity of plastic mine and $\varepsilon_{r,s}$= relative permittivity of dry sandy soil.

The parameter vector for the synthetic GPR data for the heterogeneous ground is;

$$GPR_{initial} = \left[\varepsilon_{r,t},\ \varepsilon_{r,C1},\ \varepsilon_{r,C2},\ \tan\sigma,\ \varepsilon_{0,}\ \varepsilon_{r,m},\ \varepsilon_{r,s}\right] = [2.163,\ 3.75,\ 6,\ 0.0036,\ 1,\ 2.8,\ 2.53] \quad (4.2)$$

where $\varepsilon_{r,t}$= relative permittivity of tetryl charge, $\varepsilon_{r,C1}$= relative permittivity of first clutter source, $\varepsilon_{r,C2}$= relative permittivity of second clutter source, $\tan\sigma$= loss tangent, $\varepsilon_{0,}$= relative permittivity of free space, $\varepsilon_{r,m}$= relative permittivity of plastic mine, $\varepsilon_{r,s}$= relative permittivity of dry sandy soil.

The initial subsurface parameter vector for the homogenous ground FWI is;

$$GPR_{initial} = \left[\varepsilon_{r,t},\ \tan\sigma,\ \varepsilon_{0,}\ \varepsilon_{r,m},\ \varepsilon_{r,s}\right] = [2.363,\ 0.0046,\ 1.2,\ 2.8,\ 2.23] \quad (4.3)$$

The initial vector for the heterogeneous ground FWI is;

$$GPR_{initial} = \left[\varepsilon_{r,t},\ \varepsilon_{r,C1},\ \varepsilon_{r,C2},\ \tan\sigma,\ \varepsilon_{0,}\ \varepsilon_{r,m},\ \varepsilon_{r,s}\right] = [2.363,\ 5,\ 4,\ 0.0046,\ 1.2,\ 3.01,\ 2.23] \quad (4.4)$$

4.3.1 Results and Discussion

To estimate the performance of the different antenna systems, a direct comparison is made between the estimated parameter values of interest produced by the FWI solutions and the true parameter values for both types of ground. All the solutions start form the same initial estimate and the best output is obtained after 20 iterations, due to computational constraints. The output indicates the error or uncertainty in the estimated parameters only and not the speed of convergence. For the optimization, the error in the subsurface parameters for each system in the different ground conditions is estimated with the FWI algorithm by determining the sum squared difference between the GPR data vector parameters and the FWI solution vector parameters. For the data analysis, the percentage errors between the true and estimated values for the parameters linked to the components of the mine are determined, to compare the performance of the multi-static systems with the bi-static system. These parameters are the charge relative permittivity, air void relative permittivity and mine relative permittivity. The results are shown in Tables 4.1 and 4.2. The percentage errors for these parameters are also included in brackets beside each parameter for each system.

In terms of uncertainty in parameter estimation, generally, the least uncertainty for the air void, charge permittivity and plastic mine permittivity is achieved with the multi-static system. However, the multi-static system with the most receivers does not yield the least uncertainty for these parameters in question in both types of soil conditions. For instance, in the homogeneous soil, the 4 RX multi-static system FWI yields a lower uncertainty than the bi-static system only for the air void and plastic mine permittivity and not for the charge permittivity. Nevertheless, the 2 RX multi-static system achieves

the least uncertainty for the charge permittivity. Whereas for the heterogeneous domain, the 2 RX multi-static system yields the least parameter uncertainty for the air void and plastic mine permittivity parameters while the 4 RX multi-static systems achieves the least uncertainty for the charge permittivity parameter. Numerically, the uncertainty based on the percentage errors shown in Tables 4.1 and 4.2 show that while lower uncertainty is produced by the multi-static systems in both soils, the margin of error and uncertainty is less than 5% for each parameter of interest. Therefore, multi-static systems can achieve more accurate mine detection than bi-static systems based on FWI. Nevertheless, the improvement is marginal and may not be cost effective. Furthermore, the results also show that the improved accuracy in detection with multi-static systems does not increase with the number of receivers. This 3D FWI numerical analysis is more realistic as the scattering on the soil surface and cylindrical mine introduce more degrees of freedom and complexity than a 2D numerical analysis. In the heterogeneous case the clutter signal is much larger than the mine signal and the parameterisation does not sufficiently describe the clutter and so the optimisation easily converges to the wrong solution. Some method is required to reduce the effects of the clutter signal. Therefore, better imaging with multi-static systems for a real GPR system based on FWI is dependent on an optimised antenna design as well as clutter reduction. Otherwise, the multi-static may not offer a cost effective solution or may not yield an improvement in detection over the bi-static system.

Subsurface Parameters	GPR Data Parameter Values	FWI Solution Estimated Parameter Values		
		Bi-static (% Error)	Multi-static 2RXs (% Error)	Multi-static 4RXs (%Error)
Charge relative permittivity	2.16	2.29 **(6)**	2.27 **(5.1)**	2.3 **(6.5)**
Loss tangent	0.0036	0.0026	0.0034	0.0069
Air void relative permittivity	1.0	1.49 **(49)**	1.5 **(50)**	1.45 **(45)**
Mine relative permittivity	2.8	3.069 **(9.6)**	3.185 **(13.8)**	3.032 **(8.3)**
Soil relative permittivity	2.53	2.2	2.2	2.6

Table 4.1 Summary of GPR and FWI solution parameter values for homogenous ground (% error for the charge relative permittivity, air void relative permittivity and mine relative permittivity are indicated in brackets beside the estimated parameter values)

Subsurface Parameters	GPR Data Parameter Values	FWI Solution Estimated Parameter Values		
		Bi-static (% Error)	Multi-static 2RXs (% Error)	Multi-static 4RXs (%Error)
Charge relative permittivity	2.16	2.4 **(11.1)**	2.39 **(10.6)**	2.31 **(6.9)**
Clutter1 relative permittivity	3.75	2.25	2.25	2.25
Clutter2 relative permittivity	6.0	7.28	6.67	8.0
Loss tangent	0.0036	0.0058	0.0066	0.0068
Air void relative permittivity	1.0	1.35 **(35)**	1.29 **(29)**	1.39 **(39)**
Mine relative permittivity	2.8	3.04 **(8.6)**	2.96 **(5.7)**	3.16 **(12.9)**
Soil relative permittivity	2.53	2.27	2.33	2.2

Table 2.2 Summary of GPR and FWI solution parameter values for heteregeneous ground (% error for the charge relative permittivity, air void relative permittivity and mine relative permittivity are indicated in brackets beside the estimated parameter values)

4.4 Improvement of the Initial Parameter Set

The steepest descent and direct search methods for iterative nonlinear optimisation, all require an initial parameter set which is updated iteratively according to the chosen method. The GPR FWI problem is also a local minimisation problem that is nonlinear as well as ill-posed. A good initial parameter set that is as close as possible to the true solution is desirable to ensure convergence to the global minimum and less computational expense. A more general approach would be to employ global optimization techniques prior to the local optimization. However, for the GPR problem this would be computationally prohibitive as calculation of the forward model is very expensive, and the number of evaluations required for optimisation needs to be kept small for the algorithm to be useful in the field. One way of achieving this is to use a pre-calculated database of forward modelling solutions. The database can contain the simulated GPR measurements for many potential solution parameter vectors. The relative insensitivity of GPR to many parameters allows the solution space to be characterised by a relatively small number of solutions. These need only be calculated once and may be stored in a remote high-performance computer to which the handheld device can communicate. When the GPR device makes a measurement in the field, only the measurement need be communicated to the computation centre, where FWI optimisation takes place.

At the computation centre, the objective function may be calculated for each potential solution parameter vector in the database, $\mathbf{P}_i \;\; i = 1, \Lambda \;, N$:

$$Obj_i = \left| GPR(P_i) - GPR \right|^2 \tag{4.5}$$

It is assumed that the parameter vectors and objective function values have been sorted from lowest objective value to highest, and so the best of the pre-calculated solution parameter vectors is $\mathbf{P}_1$, which is also selected as the initial parameter set for the substantive optimization. Therefore, the parameter vector for the FWI solution is chosen by interpolation from the database of parameter vectors and measured time-series. Hence a single database is generated during a single campaign but can be used repeatedly for GPR data from the same source environment or location. The database campaign could be generated during the training phase of a demining operation prior to the actual clearance operation. The forward model meshing or grid would be set to the lowest tolerance level as only a coarse analysis is required to avoid a high computational expense. A higher tolerance is set for the forward model grid for the optimization.

The database can be generated for any chosen number of parameter combinations and sample space or bounded conditions. More forward model solutions would be expected to increase the probability of a better initial estimate of the parameter set. For this experiment, the 4 RX end fed dipole system for a heterogeneous domain is used. Due to memory constraints, only eleven forward model solutions are chosen. This was done by selecting values between the minimum and maximum values for each parameter with equal step lengths of 0.005 for the loss tangent, 0.5 for the clutter permittivities and 0.05 for all other parameters. These are shown in Table 4.3. This yields a database of eleven sets of A-scan data and the objective function of each of these data for any measured GPR would be determined. The parameter set for the time-series (A-scan) that achieves the lowest objective function value would be considered as the closest to the true solution or global minimum and selected as the initial optimization parameter

set. Figure 4.4 presents the objective function value for all the eleven forward problem solutions.

Parameter	Min	Max	1	2	3	4	5	6	7	8	9	10	11
ε^{T}	1.90	2.40	1.90	1.95	2.00	2.05	2.10	2.15	2.20	2.25	2.30	2.35	2.40
ε^{C1}	2.25	7.25	2.25	2.75	3.25	3.75	4.25	4.75	5.25	5.75	6.25	6.75	7.25
ε^{C2}	3.00	8.00	3.00	3.50	4.00	4.50	5.00	5.50	6.00	6.50	7.00	7.50	8.00
$\tan\sigma\ (e-03)$	2.6	7.6	2.6	3.1	3.6	4.1	4.6	5.1	5.6	6.1	6.6	7.1	7.6
ε_0	1.00	1.50	1.00	1.05	1.10	1.15	1.20	1.25	1.30	1.35	1.40	1.45	1.50
$\varepsilon_{r,m}$	2.70	3.20	2.70	2.75	2.80	2.85	2.90	2.95	3.00	3.05	3.10	3.15	3.20
$\varepsilon_{r,s}$	2.20	2.70	2.20	2.25	2.30	2.35	2.40	2.45	2.50	2.55	2.60	2.65	2.70

Table 4.3 Forward model parameter sets for database generation

It can be seen in Figure 4.4 that the lowest objective function value is obtained at simulation run eight which corresponds to a value of 0.001708. The parameter set for this forward model measurement, GPR_F can be selected from Table 4.3 and is given by

$$GPR_F = [\varepsilon_{r,t},\ \varepsilon_{r,C1},\ \varepsilon_{r,C2},\ \tan\sigma,\ \varepsilon_{0,}\ \varepsilon_{r,m},\ \varepsilon_{r,s}] = [2.25,\ 5.75,\ 6.50,\ 0.0061,\ 1.35,\ 3.05,\ 2.55] \quad (4.6)$$

Therefore, this parameter set is selected as the initial parameter set for the iterative FWI solution, for the bi-static dipole system for a heterogeneous domain under test. The FWI optimization solution for the parameter set given in (4.6) is then obtained for 20 iterations and compared directly with the FWI solution for the initial parameter set in (4.4). The result is shown in Figure 4.5.

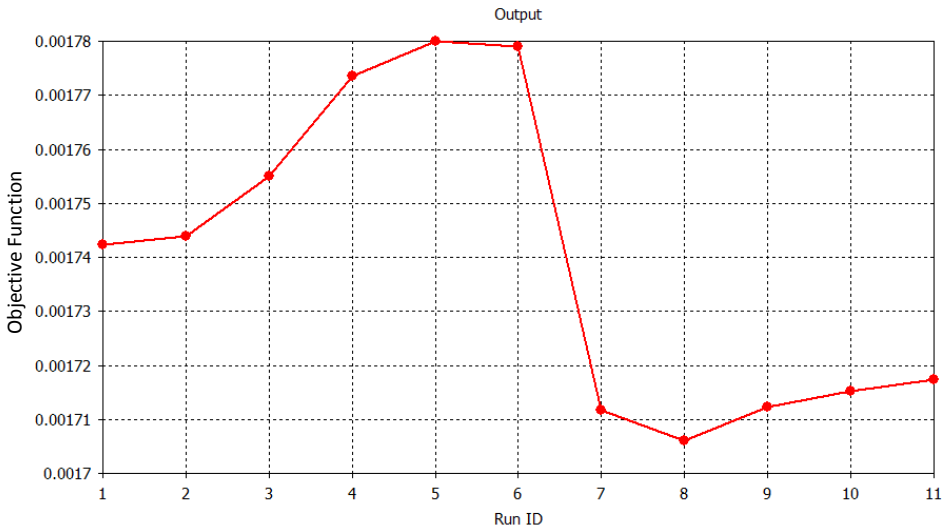

Figure 4.4 Objective function values for eleven forward problem solutions

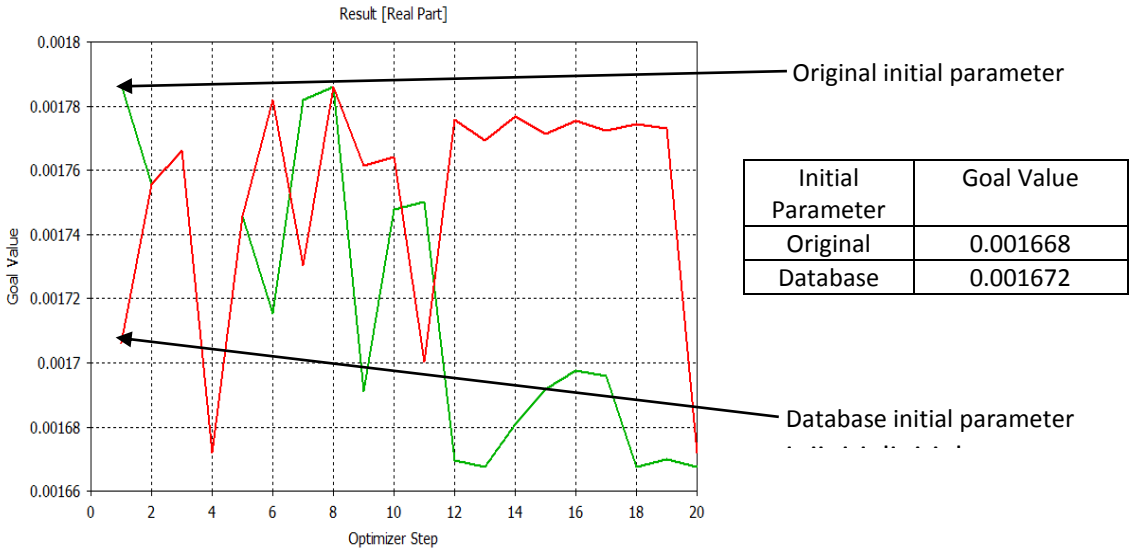

Initial Parameter	Goal Value
Original	0.001668
Database	0.001672

Figure 4.5 FWI solution for a. original parameter set (GREEN) versus database parameter set (RED) b. Summary of goal values

The Nelder Mead Simplex method requires O(*n*) function evaluations to determine the simplex and the general shape of the objective function in the region of the simplex. This is particularly true when the parameters vary across a wide range of scales, as in this case, or the linearised objective is poorly conditioned. The comparison of the FWI solution for the original initial parameter set and the one derived from the database generation (Figure 4.5) shows that the latter does not achieve an improvement in the

accuracy of convergence as the absolute error is marginally less than the original solution. However, the results also show that the database generated initial parameter FWI solution is closer to the true solution. This could potentially lead to a more efficient optimization using a more powerful algorithm. Derivative based methods would benefit from this improvement and achieve convergence with less computational expense and fewer iterations as a local minimum would be realised more efficiently. The procedure achieves the goal of improving the initial parameter estimation or guess. The CST integrated Nelder-Mead optimisation does not allow the user to specify the entire simplex and objective function values. If this had been the case, the initial 10 iterations exploring the simplex could have been entirely avoided by selecting all the simplex points from the database.

4.5 Conclusion

An empirical study has been undertaken to compare 3D FWI imaging using multi-static and bi-static systems in homogeneous and heterogeneous media. The results show that multi-static systems achieve greater subsurface parameter sensitivity for the landmine target only marginally, by less than 5% for the parameters linked to the mine's components. Additionally, in a 2D study (Watson, 2014), all multi-static systems outperformed the bi-static systems. However, this 3D analysis also shows that the improvement in performance with increasing numbers of antennas is not simple or linear due to cross-coupling and antenna patterns. This underlines the need for optimisation of the antenna system configuration and size (number of elements), to achieve better performance than a bi-static system. Clutter reduction is also required to

obtain good estimates of the true parameters. The effect of clutter significantly limits the accuracy of parameter estimation. Finally, a novel procedure has been proposed to determine the initial parameter vector for the FWI solution which yields an initial forward problem solution that is closer to the true GPR data solution. The procedure requires numerous forward problem solutions stored prior to a deeming campaign but has the potential to significantly reduce the computational expense of the FWI as well as the accuracy for an ideal local minimisation. In general, the multi-static system achieves only a small improvement in performance over the bi-static system, which may not be cost effective.

Chapter 5 GPR Distinguishability and Antenna Tilting for Handheld GPR

5.1 Introduction

In this chapter, distinguishability for bi-static and multi-static systems is estimated in the presence of clutter, followed by a novel investigation of the impact of tilted antenna orientation for handheld GPR. A preliminary evaluation of initial clutter reduction for multi-static systems in a cluttered domain is evaluated through the effect on distinguishability. Additionally, the effect of tilting the antennas towards the mine target is evaluated.

Clutter returns from surface roughness and inhomogeneity are known to produce much larger changes in the measured GPR return signal than those produce by the presence of a mine. Distinguishability of a mine is reduced by clutter noise. The handheld GPR antenna system is simulated in a high clutter environment to estimate GPR performance with preliminary de-clutter processing. A conventional ground return subtraction technique is tested to compare the amount of information that can be obtained from bi-static and multi-static GPR systems for a portable handheld platform. Subtraction algorithms have been used extensively for GPR data signal processing and pre-processing. However, this is a novel empirical study that considers A-scan data for a multi-static handheld system in time domain, based on FWI. Secondly, sensitivity analysis is used to quantify the impact of antenna tilting. Although the antennas have wide main beams, the target is very close and so changing the orientation of the antenna

towards the expected target position can have a significant effect. This aspect will be limited to a bi-static configuration of bow-tie antennas based on commercially available GPR systems (Warren 2009)(Giannakis 2016) and the DRH system utilised in section 3.5, which is based on the experimental set-up at the University of Manchester (Podd, Peyton et al. 2015). Antenna tilting for GPR systems has been presented in (Stickley, Longstaff et al. 1996) for a step frequency GPR with SAR processing to detect buried objects with AT mine dimensions. Giannakis (2016) remarks that achieving this with a FDTD numerical solver is prohibitive. However, this report presents this analysis in the time domain using the FIT EM numerical solver of the CST STUDIO SUITE environment.

5.2 Mean Scan Subtraction

Mean scan subtraction is the most commonly used technique for removing background noise and the ground surface reflections for GPR. Typically, the mean or weighted average of the total received A-scans is determined and then the result is subtracted from each individual A-scan of interest (Abujarad, Jostingmeier et al. 2004). The resulting waveform is given by

$$\overline{A}_i(t) = A_i(t) - \frac{1}{N_s}\sum_{i=1}^{N_s} A_i(t) \tag{5.1}$$

where $A_i(t)$ is the A-scan, i is an index to the A-scans expected to be affected by similar clutter and N_s is the total number of scans. The rationale is that the A-scan from nearby points will have similar clutter signals but the signal due to a mine or other localised anomaly will appear in just a few A-scans. Averaging tends to reinforce the coherent clutter signal but reduce the anomalous mine signal. Subtracting the average aims to

cancel the clutter signal while leaving the mine signal. The method relies upon having coherent clutter returns across a sizable number of measured A-scans.

There are several variations of this method. Windowed average subtraction removes the weighted mean of A-scans about the area of interest only and not the entire A-scan data. Complex average subtraction is equivalent to the mean subtraction described with the mean scan determined without a mine or target. Background subtraction attempts to use a filtering scheme or time weighting to subtract the ground reflections from the A-scans.

5.3 Landmine Distinguishability

In this section, distinguishability is determined in bi-static and multi-static systems after a mean subtraction signal processing method is applied to suppress clutter, for varying mine depths in the ground. The simulations use the Vivaldi antenna bi-static system and multi-static system (1 TX and 2RX in a SIMO driving sequence), configured in a straight line as used for the sensitivity analysis in chapter 3. The cluttered ground model described in section 4.3 is used for this experiment with the exception that the dipole antennas are replaced with the bi-static and multi-static (2RXs) Vivaldi antennas (described in chapter 3). The setup for both models is shown Figure 5.1. The mine in this case is a plastic cylinder of permittivity $\varepsilon_{r,m}$ = 2.8. All other parameters remain unchanged. Complex average subtraction is applied for clutter reduction and therefore both systems are also simulated without a mine to obtain the A-scan for a no mine case for each of the systems. This is a numerical experiment rather than a process that could be used in practice; although where the surface is flat then uniform measurements could

be made in positions where the MD gave no indication of a mine. In this case a single A-scan waveform for each measurement is obtained therefore $N_s = 1$ in equation (5.1) and the new equation is given by

$$\overline{A}_i(t) = A_i(t) - A_0(t) \tag{5.2}$$

where $A_0(t)$ is the A-scan without a mine.

Distinguishability is a scalar calculated using equation (3.13): $\left\| GPR^B(\mathbf{X}_s) - GPR^B(\mathbf{X}_0) \right\|^2$, which is equivalent to the L2 objective function, i.e. the sum squared difference between the pre-processed A-scan with a mine, $GPR^B(\mathbf{X}_s)$ and the A-scan without a mine, $GPR^B(\mathbf{X}_0)$. Distinguishability may also be calculated numerically from the differences in GPR received power for an impulse radar. For this simulated analysis, it is assumed that distinguishability is small when there is no mine i.e. the difference $GPR^B(\mathbf{X}_s)$ - $GPR^B(\mathbf{X}_0)$ corresponds to noise. Therefore, a value greater than the noise power, indicates a mine whereas a smaller value indicates no evidence of a mine. Additionally, a higher value is indicative of less uncertainty in subsurface parameter estimation. This is hypothetical, but enables a direct comparison of the distinguishability provided by the two systems. The distinguishability can also be calculated for the bi-static and multi-static systems when mines are buried with their tops at three different depths: 0.3 cm, 2.3 cm and 2.8 cm respectively. These depths represent typical pressure activated blast mines buried shallowly or just under the ground surface. The depth values and intervals are also constrained by the height (9 cm) of the ground (box) to ensure that the entire mine is positioned in the soil without having any portions protruding outside the simulation

domain. Again, 9 cm is used considering the investigation is limited to the detection of pressure activated mines and not their clearance, which requires a 13 cm clearance or excavation depth based on UN standards. The distinguishability values are expressed as a power (W), see Table 5.1, for the bi-static and multi-static systems, indicating higher received signal power in the multi-static system for any of the mine depths. It is noted that the values are larger for increased mine depths due to the nature of the antenna radiation pattern. A typical impulse GPR receiver noise floor level is given as -44 dBm (Daniels 2007), which translates at a power of approximately 3.98×10^{-8} W. The hypothetical noise levels for the given distinguishability values are presented in Table 5.2, and compared to this noise floor and power.

The noise level in the multi-static system is considerably less than that of the bi-static system and is also above the assumed noise floor of -44 dBm. Therefore, any value of distinguishability less than -44 dBm or the equivalent power of 3.98e-08 W indicates a no mine detection and vice versa. The mean subtraction clutter suppression method alone is conventionally used as an initial technique for clutter reduction. A combination of schemes may be applied to improve clutter reduction to enable better target discrimination, which ought to be considered in future work. However, the GPR systems can be calibrated and designed to process these distinguishability values to aid the decisions of the operators or demining personnel. These results do not include a determination of POD and the mine depth is at 5 cm, for a typical pressure operated blast mine. The improved performance of the multi-static system over the bi-static system in this case demonstrates the significant impact of directional antenna radiation in detecting mines. Therefore, multi-static systems can achieve greater mine

distinguishability for cluttered environments with optimised directional antennas and effective clutter reduction. Further studies would require a determination of POD with real data and measurements as this study is limited to an evaluation of performance of multi-static systems using a hypothetical estimation of distinguishability for a cluttered domain.

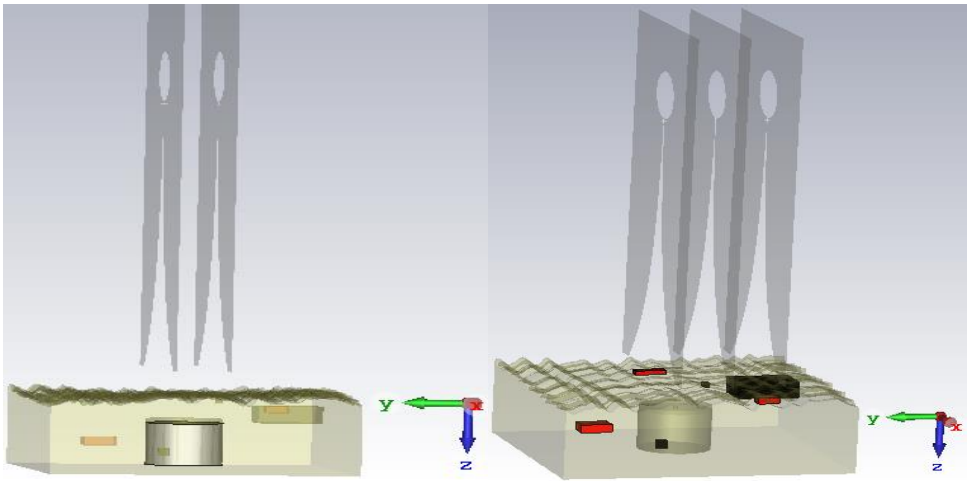

Figure 5.1 Vivaldi bi-static and multi-static systems with clutter viewed from different directions

Antenna System	**Mine Depth, *cm***		
	0.3	2.3	2.8
	Distinguishability, W		
Bi-static	3.1E-05	3.1E-07	6.39E-06
Multi-static	4.7E-04	4.6E-04	4.94E-04

Table 5.1 Distinguishability of bi-static and multi-static GPR systems

Antenna System	**Mine Depth, *cm***		
	0.3	2.3	2.8
	Noise level, dBm		
Bi-static	-15.1	-35.1	-21.94
Multi-static	-3.28	-3.37	-3.06

Table 5.2 Noise level for bi-static and multi-static GPR systems based on distinguishability

5.4 Antenna Tilting Performance

To maximise mine distinguishability, it is important that the GPR system delivers as much EM energy through the ground to the mine, as possible. Due to the cluttered and

inhomogeneous nature of the ground, this becomes difficult to achieve because of refraction, multiple scattering, attenuation and other limitations of the physics of propagation of the EM waves in a near field or reactive field region. For landmine detection, the antennas must not be placed in direct contact with the ground to avoid an inadvertent activation of a mine that may be lying on the ground surface or very shallowly buried. Although the antennas investigated here are electrically small, they have some directivity with typical main lobe widths of 32.6 degrees for the DRH antenna and 48.7 degrees for the bow-tie antenna. Particularly for the rectangular DRH, the antenna patterns are complex, with nulls and side-lobes along the diagonal directions. The system is made more complex to design due to the cross-coupling between antennas. More highly directional antennas are expected to broadcast more energy into the ground than omni-directional antennas. The direction of the radiation with regards to the target of interest is also important as it affects the ability of the receive antenna to measure sufficient energy scattered by the mine. Therefore, if the relative position of a target is known, it is desirable to orientate the antennas to focuses the broadcast power towards the target and to collect as much of the mine scattered energy as possible. Theoretically, tilting of directional antennas is expected to achieve an improvement in mine detection. In Stickley et al (1996), non-metallic, shallow, subsurface objects are detected with SAR processing; with the antennas tilted in the direction of movement. However, for handheld GPR systems, the literature does not provide a comparison of the performance of tilted and vertically aligned antennas for landmine detection. Giannakis (2016) states this as a future investigation in his work, but states that this is difficult to achieve with FDTD simulation methods. Most industry

standard EM simulation systems force antennas to be aligned along axis directions as this greatly simplifies the meshing required in the simulation process. However, this thesis achieved a simulated tilted antenna design using FIT time domain analysis within CST, to determine the impact on performance through a sensitivity analysis. This is undertaken for a bi-static bow-tie antenna system to allow direct comparison with the work of Giannakis. This will also be compared with the performance of a bi-static DRH system. Bow-tie antennas are known to be used commercially for GPR systems (Warren 2009) whereas the DRH antennas exhibit more highly directional radiation characteristics. A direct comparison of the bow-tie and horn antennas has been conducted experimentally for general GPR applications in (Pieraccini, Rojhani et al. 2017). Firstly, the sensitivities are calculated for the two antenna systems in a conventional vertical configuration. Then the analysis is repeated for the antennas tilted 30^{o} away from vertical towards the expected mine location under the centre of the antenna array. The models are illustrated in Figure 5.2. They are independent, and the aim is to compare the sensitivity for a tilted and non-tilted configuration for each system individually. The cylindrical mine and DRH antenna design are identical to those described in chapter 3. PML boundary conditions are also applied. The bow-tie system is designed with Antenna Magus for a centre frequency of 1.92 GHz which yields an operating frequency range of 960 MHz to 2880 MHz. The DRH antenna, as specified in chapter 3, has a centre frequency of 5.5GHz and operating frequency range of 1-10 GHz.

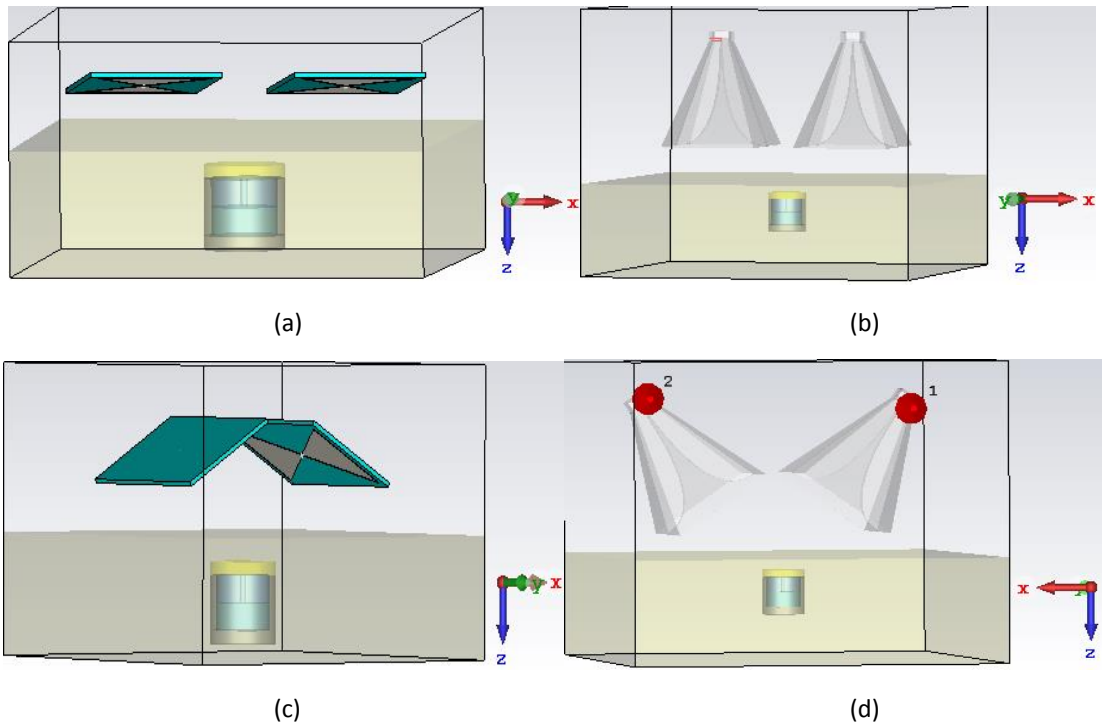

Figure 5.2 Bow-tie and DRH bi-static systems: (a) Bow-tie non-tilted, (b) DRH non-tilted, (c) Bow-tie tilted, and (d) DRH tilted

5.4.1 Results

The results of the sensitivity analysis are shown in Table 5.3 and Table 5.4 for the bow-tie system and DRH system respectively. In addition to the Tables, Figure 5.3 shows that the impact of tilting the antennas is significant only in the DRH system and results in a distinct improvement in parameter sensitivity and information about the subsurface. Antenna tilting also achieves enhanced parameter sensitivity in the bow-tie system but only marginally. These results are reasonable due to the higher directionality of the DRH antenna. Tilting leads to a small increase in the amount of broadcast energy reaching the mine and scattering back to the receive antenna.

GPR System	Singular Values, σ_i				
Bow-tie no Tilt	7.9195	0.0134	0.0007	0.0002	0.0001
Bow-tie Tilted	8.2610	0.0126	0.0008	0.0003	0.0001

Table 5.3 Singular values for the non-tilted and tilted bow-tie system

GPR System	Singular Values, σ_i				
DRH no Tilt	3.2760	0.0167	0.0007	0.0002	0.0001
DRH Tilted	5.7832	0.1039	0.0030	0.0004	0.0003

Table 5.4 Singular values for the non-tilted and tilted DRH system

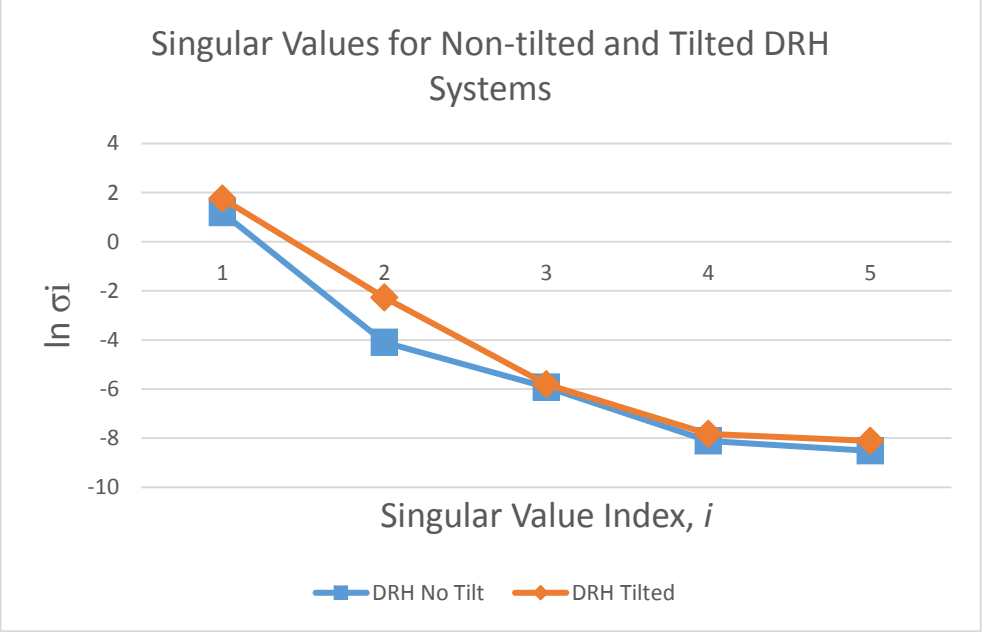

Figure 5.3 Logarithmic plot singular values for non-tilted and tilted DRH antennas

5.5 Conclusion

The investigation to estimate distinguishability in a cluttered 3D GPR domain for bi-static and multi-static systems, suggests that with clutter reduction, multi-static systems yield greater distinguishability for mine detection. In this case we have applied mean subtraction, which is conventionally and typically used to reduce background noise and air-ground reflections, to compare the performance of handheld bi-static and multi-static systems in a cluttered domain based on A-scan data. The GPR data is limited to the A-scan because this study is based on the MINEHOUND system which is an impulse radar that processes single A-scans. It is concluded that for A-scan data, multi-static,

directional antennas with an optimised number of elements and configuration would improve mine detection based on distinguishability compared to bi-static antennas in the presence of clutter.

The data from the experiments comparing tilted and non-tilted, bi-static antenna systems confirm that significant detection performance improvement can be achieved with directional antennas angled towards the expected mine position, also for A-scan data. Also, more focused antenna radiation would result in a further enhancement over broader antenna radiation. Additionally, the antenna geometry imposes constraints on tilting especially for a multi-static system. For a given GPR system with an optimised antenna orientation, tilted directional antennas is expected to yield an improvement in the POD and FAR for landmine detection over conventional, non-tilted systems.

Chapter 6 Enhanced Feature Extraction Based on Full Wave Inversion (FWI)

6.1 Introduction

This chapter proposes the exploitation of the mine air void or cavity which is present in most pressure activated blast type AP landmines. Such mines are the most widely used because they are easy and cheap to construct (Prado, Cabrita et al. 2013). Typically, they contain small voids or cavities required for the pressure controlled mechanism that activates the mine. To identify these voids, a further region is introduced into the subsurface parameterisation specifying a contrasting permittivity volume inside the mine. Initially this volume in the forward model is assumed to have a relative permittivity of other than one, which is the relative permittivity of free space. If the FWI returns a relative permittivity closer or equal to one then this is evidence that a void exists and so the object is less likely to be a mine, and vice-versa. A numerical estimation of this parameter would be obtained from the A-scan FWI solution quantitative data. This would enhance the FWI based target discrimination by providing more information in addition to, or prior to, the reconstructed image. This inference is drawn from a consideration of the nonlinear seismo-acoustic technique (NSAT) developed by Donskoy (Donskoy 1998).

This thesis is interested in investigating if the void detection feature of the NSAT can be exploited with GPR sensor data to improve target classification. The aim is to determine if a handheld GPR system can detect the void in a mine based on the A-scan FWI

quantitative data. This investigation shall be undertaken by evaluating sensitivity analysis data and a FWI numerical analysis data.

6.2 Void Sensitivity Analysis

The sensitivity analysis performed in chapter three for the 4 RX end fed dipole model and the bi-static DRH model described in sections 3.4 and 3.5 respectively are repeated here, but more parameters are introduced, see Table 6.1. The sensitivity analysis for the DRH antenna system has already been reported in (Sule, Paulson 2017b). The mine surrogate dimensions and internal composition are shown in Figure 6.1. Three different sensitivity analyses are performed for both antenna systems for different air void volumes of 76.96 cm^3, 38.48 cm^3 and 0 cm^3 (no void). This yields 6 sensitivity analyses. Only the air void depth (or height) is changed to obtain the different volumes. The mine diameter is therefore unchanged throughout the experiments. For the sensitivity analysis, the void is assigned the accurate relative permittivity of free space of one.

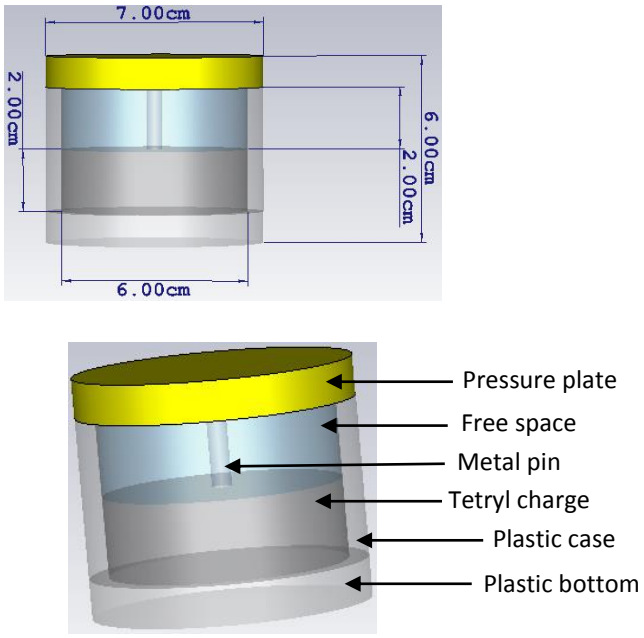

Figure 6.1 Antipersonnel mine components and dimensions

Parameter	Value
Tetryl charge relative permittivity, ε_r^T	2.163 ($1\,\mathrm{gcm}^{-3}$ density)
Antenna height above ground, h	5cm
Soil loss tangent, $\tan\delta$	0.0036
Metal Pin conductivity, σ^M	5.96e+07 S/m
Pressure plate conductivity, σ^P	3.56e+07 S/m
Void relative permittivity, ε_0	1
Plastic relative permittivity, ε_r^P	2.8
Soil relative permittivity, ε_r^S	2.53

Table 6.1 AP mine parameters

6.2.1 Sensitivity Analysis Results

It is expected that EM waves will be reflected off the top and bottom boundaries between the mine material and the void, due to the step change in intrinsic impedance. The amount of reflected power will be closely related to the area of the boundaries. The singular values corresponding to the void parameter in the right singular vectors for the multi-static (4RXs) end fed dipole model and bi-static DRH model sensitivity are shown in Tables 6.2 and 6.3 respectively. Therefore, the sensitivity analyses data are indicative of the presence or absence of an air void in the mine. The volume of the air cavity is not directly proportional to the singular values in either case, however the DRH antenna system provides a more accurate indication of the changes in volume. The dipole antenna system provides an observable response to the air cavity when the volume is halved from the initial value. It is possible that given the presence of buried clutter objects and ground surface reflections this void sensitivity may not be sufficiently achieved as the clutter easily obscures the backscattered signals from the mine. However, this initial analysis shows that both antenna systems can determine the presence or complete absence of an air void in the mine. This provides the confidence

to proceed to a more elaborate FWI analysis that also considers a cluttered domain to obtain a more accurate estimation of this result that could be useful for real GPR system mine feature extraction.

Size of Void	Void, ε_0 Singular Values, σ_i
Initial Volume ($76.96 cm^3$)	0.027
Half Volume ($38.48 cm^3$)	0.018
Zero Volume	0

Table 6.2 Singular values for void parameter for bi-static DRH antenna system

Size of Void	Void, ε_0 Singular Values, σ_i
Initial Volume ($76.96 cm^3$)	7.449
Half Volume ($38.48 cm^3$)	7.509
Zero Volume	0

Table 6.3 Singular values for void parameter for multi-static dipole antenna system

6.3 Void Feature Extraction for Empirical FWI Data

This section builds on the sensitivity analysis from the previous section to investigate the possibility of detecting an air void in an AP mine using FWI. The aim is to verify the results obtained from the sensitivity data, determining whether the mine void can be detected from FWI data. Here the Vivaldi antenna system reported in the previous chapters is used in a bi-static configuration, and the data used to estimate subsurface parameters using FWI. The bi-static system is used due to limit the computational expense also the fact that the results from previous chapters reveal only marginal improvements observed with the multi-static systems. As before, the meshing for the GPR synthetic data and forward model are set differently to avoid an inverse crime. Two FWI solutions will be obtained: first for a flat, homogenous ground and then for a rough, heterogeneous ground. The former is expected to provide an initial estimation of the

void parameter data and the latter a more realistic estimation for a cluttered domain. The simulated models are shown in Figure 6.2. The estimated subsurface parameters of the FWI solutions are compared to the subsurface parameters derived from the synthetic GPR measurement to evaluate the information provided by the GPR measurement. The nonlinear optimization settings using the Nelder Mead Simplex algorithm are shown in Figures 6.3 and 6.4. for a flat, homogenous ground and rough, heterogeneous ground respectively. The parameter vector set for the GPR for the homogeneous and heterogeneous ground are equivalent to (4.1) and (4.2) while the parameter vector set for the initial forward model for the homogeneous and heterogeneous ground are equivalent to (4.3) and (4.4), with the only exception that the initial void relative permittivity is set to 1.25 instead of 1.2.

The maximum number of iterations for the uncluttered (homogenous) system are set to 20 iterations whereas for the cluttered (heterogeneous) system it is set to 30 iterations. All the other settings are equivalent for both experiments.

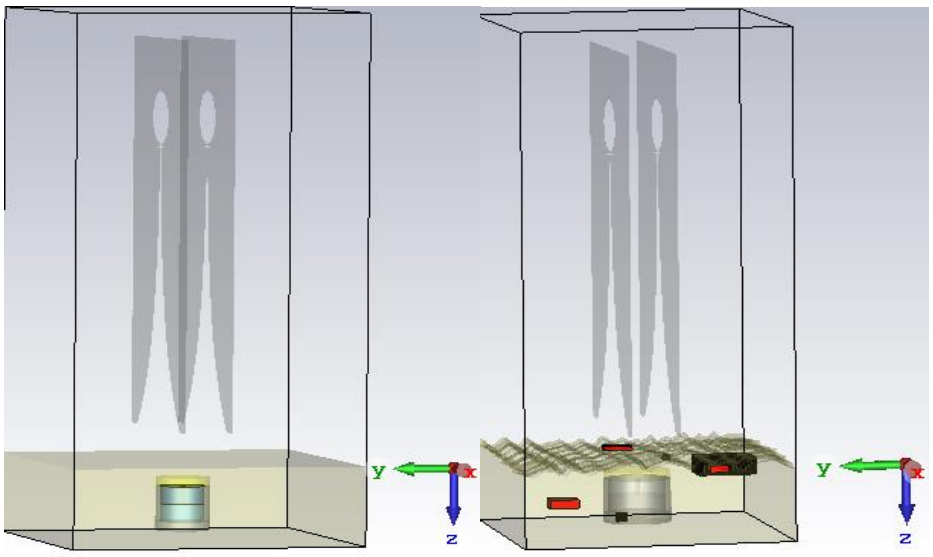

(a) (b)

Figure 6.2 Vivaldi bi-static systems (a) flat, homogenous ground (b) rough, heterogeneous ground

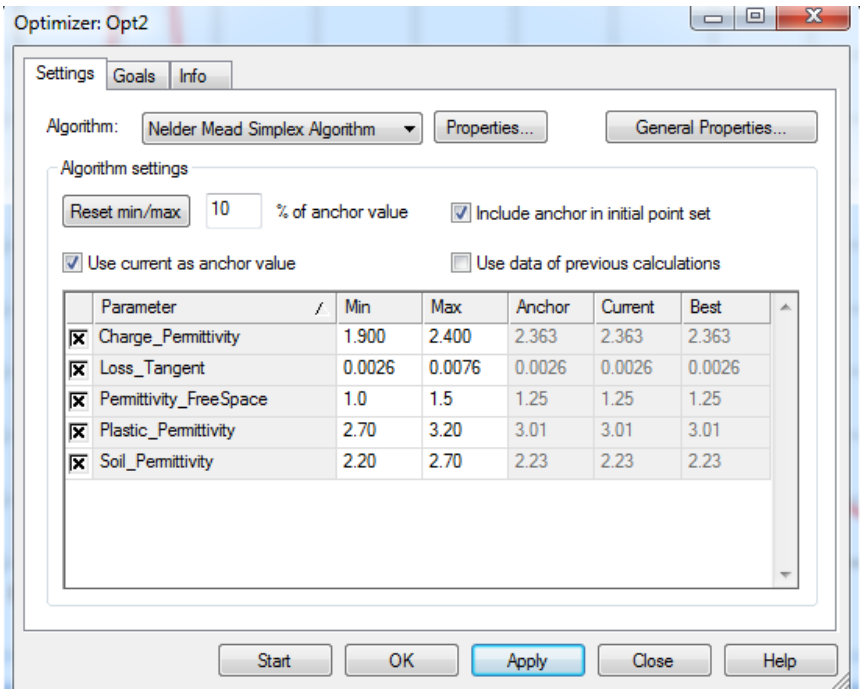

Figure 6.3 FWI optimization settings for flat, homogenous soil

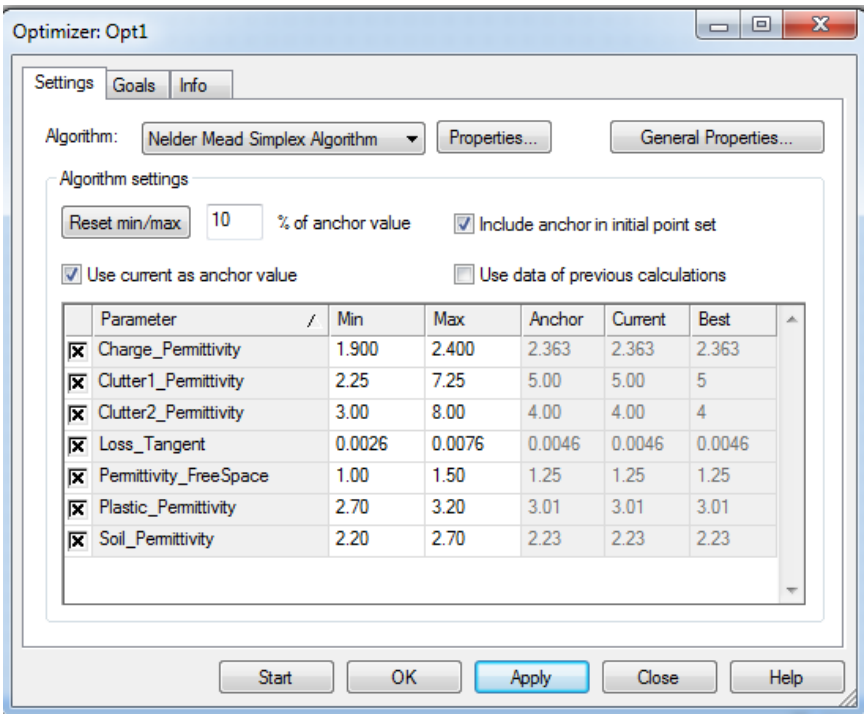

Figure 6.4 FWI optimization settings for rough, cluttered soil

6.3.1 Initial Empirical FWI Results

The results for the FWI solutions for the flat, homogenous ground and rough, heterogeneous ground are presented in Tables 6.4 and 6.5 respectively. In both tests

the void and mine relative permittivities are well estimated. For the homogenous ground the FWI solution yields the actual void relative permittivity of 1 whereas for the heterogeneous ground the estimated value is 1.03 to two significant figures. For the plastic relative permittivity parameter, there is a small uncertainty in the actual and estimated values, which are 2.8 and 2.7 for the homogenous ground and 2.8 and 2.75 for the heterogeneous ground respectively. There is larger uncertainty in the heterogeneous ground parameter estimation, which has more parameters, as well as scattering and complexity. Nevertheless, the parameters associated with the mine achieve very good convergence in both cases. Therefore, the empirical FWI quantitative data is indicative of the air cavity in the mine in these simulated experiments. The next step is a further investigation of a comparison of convergence for a mine with and without a void. This is shown in the following sub-section.

Subsurface Parameters	**GPR Actual Parameter Values**	**FWI Estimated Parameter Values**
Charge relative permittivity	2.163	1.956
Loss tangent	0.0036	0.0026
Air void relative permittivity	1	1
Mine relative permittivity	2.8	2.7
Soil relative permittivity	2.53	2.25

Table 6.4 GPR actual parameters and FWI estimated parameters for flat, homogeneous ground

Subsurface Parameters	GPR Actual Parameter Values	FWI Estimated Parameter Values
Charge relative permittivity	2.163	2.252
Clutter1 relative permittivity	3.75	2.7
Clutter2 relative permittivity	6.0	3.0
Loss tangent	0.0036	0.0068
Air void relative permittivity	1	1.03
Mine relative permittivity	2.8	2.75
Soil relative permittivity	2.53	2.21

Table 6.5 GPR actual parameters and FWI estimated parameters for rough, heterogeneous ground

6.3.2 Further FWI Results

As a follow on to the previous analysis, an investigation is conducted here to determine whether the FWI quantitative data can indicate when a mine possesses no void at all with some reasonable degree of certainty or accuracy for a cluttered domain. Two different FWI experiments are conducted for the heterogeneous ground model. Experiment 1 computes the L2 norm objective for a synthetic GPR based on the domain shown in Figure 6.2b, described in chapter 5. However, the bounded domain for the air void relative permittivity is changed from a range of 1-1.5 as shown in Figure 6.4 to a wider range of 1-3, to see if convergence can still be achieved for a larger search space. The tetryl charge relative permittivity bounds are also adjusted to 1-3 instead of 1.9-2.4 used previously, also shown in Figure 6.4. For experiment 2, the same procedure in Experiment 1 is repeated with the only difference being that the mine is replaced with a solid plastic cylindrical buried target with equivalent dimensions as the mine in experiment 1, with no void or other internal components. See Figure 6.5. For both experiments, the synthetic GPR data subsurface parameters are the same and

equivalent to those used in the previous section, i.e. (4.2). The FWI optimization results for the experiments are presented in Tables 6.6 and 6.7 respectively.

Based on the results of the first experiment presented in Table 6.6, the FWI solution shows that the void relative permittivity and the plastic mine relative permittivity parameters converge very close to the actual value while the other parameters converge less accurately. Specifically, the estimated air void parameter is 1.1 compared to an actual value of 1. However, based on the results of the second experiment presented in Table 6.7, the air void relative permittivity value converges to 2.3, compared to the true value of 1. Based on these observations, it is demonstrated that the empirical simulated GPR FWI solution is indicative of the presence or absence of an air void in the buried target. This feature extraction can be used to discriminate between a mine and non-mine targets.

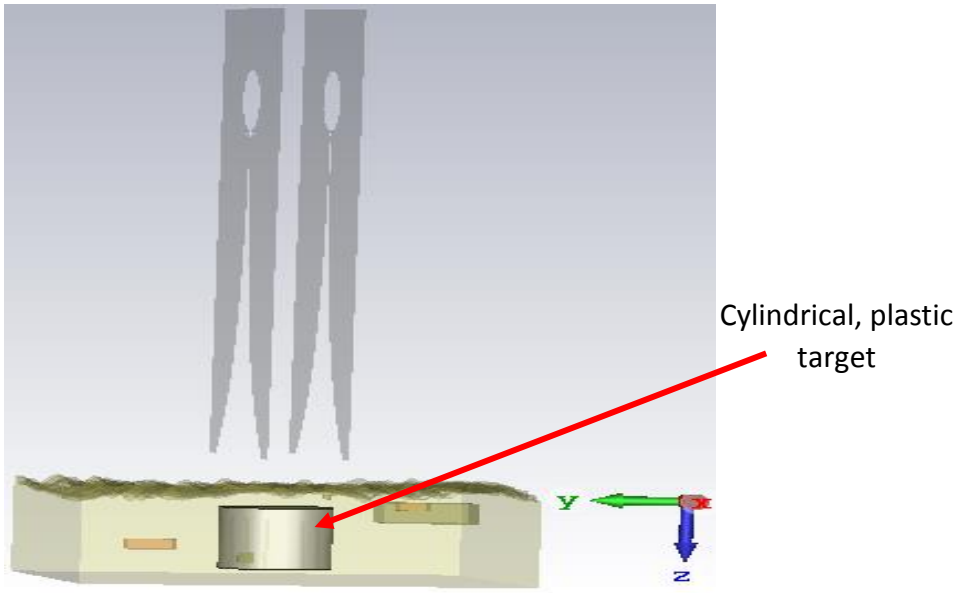

Figure 6.5 GPR model for a block plastic cylindrical mine-like target

Subsurface Parameters	GPR Actual Parameter Values	FWI Estimated Parameter Values
Charge relative permittivity	2.163	2.409
Clutter1 relative permittivity	3.75	2.7
Clutter2 relative permittivity	6.0	3.0
Loss tangent	0.0036	0.0068
Air void relative permittivity	1	1.1
Mine relative permittivity	2.8	2.75
Soil relative permittivity	2.53	2.21

Table 6.6 Experiment 1 results: GPR actual parameters and FWI estimated parameters for model with internal components

Subsurface Parameters	GPR Actual Parameter Values	FWI Estimated Parameter Values
Charge relative permittivity	2.163	2.302
Clutter1 relative permittivity	3.75	4.45
Clutter2 relative permittivity	6.0	4.96
Loss tangent	0.0036	0.0070
Air void relative permittivity	1	2.3
Mine relative permittivity	2.8	3.1
Soil relative permittivity	2.53	2.28

Table 6.7 Experiment 2 results: GPR actual parameters and FWI estimated parameters for plastic buried target with no internal components

6.4 Discussion and Conclusion

This study suggests that, for ideal or controlled conditions, GPR FWI quantitative data can be used to classify a typical mine based on the numerical estimation of the free space relative permittivity which denotes the presence or otherwise of a void in the detected target. This is applicable to blast type AP mines that are pressure activated and which contain a small void in most cases. The void parameter sensitivity for the plastic

mine-like target and the actual mine surrogate strongly suggest the capability for target discrimination based on the void internal component of such AP mines. Similarly, this feature extraction and classification approach is also robust and potentially applicable to pressure denoted mines made of different materials other than plastic, which is ideal for consideration in future work.

This analysis assumes the use of a dual or multiple MD and GPR handheld system, such as the MINEHOUND. After positive MD and GPR signals are obtained, it is assumed a mine has been detected. Apart from imaging the target to extract features, the quantitative FWI data could also be fused with the other data to enhance detection based on the extraction of the void feature. This would potentially improve the detection decision of the operator or clearing team. This study has used a pattern search non-derivative optimization method. A gradient based method may converge in fewer iterations, but the added overhead of derivative calculation may mean that solution may not be faster. A priori data is critical to the success of FWI as iterative solution is heavily reliant on an accurate forward model with good approximations of the unknown parameters of the mine and ground.

This chapter has drawn on the characteristics of the NSAT developed by Donskoy (Donskoy 1998, Donskoy, Ekimov et al. 2002) to empirically demonstrate the ability of a handheld GPR system to detect AP mines through A-scan data signal processing based on feature extraction and classification of the void present in most pressure activated blast mines. The method used is GPR FWI that includes a void parameter which is given by the relative permittivity of free space.

Chapter 7 Research Conclusions, Limitations and Future Work

7.1 Conclusions

This thesis has built on previous studies of GPR FWI for landmine detection. An empirical sensitivity study has shown that only a small number of subsurface parameters can be estimated from GPR data consistent with a handheld device. FWI parameter estimation has been implemented using a non-derivative nonlinear optimization scheme. The performance of bi-static and multi-static, handheld GPR systems that operate in a sensor fused system with a MD, have been compared. The results, all based on an impulsive GPR A-scan data, have been used to characterise antenna performance and target discrimination based on parameter sensitivity, feature extraction and classification. The project aimed to increase the POD and reduce the FAR or false positives, typically present in humanitarian demining operations. This has been achieved through several contributions.

A 3D EM parameter sensitivity study, to compare optimised bi-static and multi-static, handheld GPR antenna arrays for a flat homogeneous ground, was presented in chapter 3. The required FWI objective function Hessian and Jacobian matrices were estimated using finite differences. Other studies do not consider antenna radiation characteristics, crosstalk, orientation, and full 3D numerical model analysis, as this report has. It provides verification of the improved performance of multi-static systems over bi-static systems. Additionally, it is found that this improvement is not necessarily linear and is

subject to optimisation of the antenna orientation, number of elements and radiation patterns with reference to the target.

A comparison of bi-static and multi-static GPR systems based on a 3D empirical FWI analysis for both homogeneous and heterogeneous media was presented in chapter 4. This led to a further verification of the suggestion that more receivers can achieve greater parameter sensitivity and acquisition of subsurface information as reported in chapter 3, albeit in a non-linear fashion. Additionally, the 3D EM modelling shows that the optimum number of elements is influenced heavily by the antenna radiation properties and its interactions with the ground surface and subsurface. Therefore, optimisation of the number of antenna elements for a given multi-static system configuration is necessary to achieve performance superior to that of a bi-static system. Previous 2D FWI studies reported that the antenna element number is not very important in achieving an improved performance with multi-static systems over bi-static systems. A 2D EM analysis is also insufficient for a real GPR system and mine detection application where the ground, target and clutter are all in 3D. This study also proposed that a database of forward model solutions for different parameter vectors, may be used to produce an improved initial parameter for the FWI optimisation that is closer to the global minimum. This is in addition to reducing the computational expense of the optimization.

Chapter 5 compared bi-static and multi-static handheld systems in a cluttered domain to determine distinguishability. Multi-static systems achieve greater target distinguishability, which gives a numerical estimation of the POD for the GPR systems. A

novel sensitivity analysis of systems with tilted antennas for a bi-static setup was also conducted. Antenna tilting produces a significant improvement in subsurface parameter sensitivity for even mildly directional antennas.

Finally, a novel feature extraction technique for FWI was presented, which detects the void in a typical blast type pressure activated mine through empirical determination of the void relative permittivity. The results show that this parameter can be estimated accurately and therefore be fused with the reconstructed image to improve the reliability of detection and reduce false positives. Such a procedure is robust to different mine materials. The void data acquisition would enhance detection decision making based on an expanded decision level fusion of FWI data for a MD and GPR sensor fused handheld system.

7.2 Limitations

This work was based on numerical modelling and simulation using industry standard numerical EM simulation software. Despite the reported accuracy of the FIT which is comparable to the FDTD method, the results obtained from this methodology are empirical and require substantial verification under controlled physical experimental conditions and ultimately with data from real GPR measurements. There are also many specific assumptions and constraints associated with the results obtained.

1. The forward model can benefit from more a priori data and other site-observable parameters which have not been included in this work. Features such as water puddles, vegetation or land cover and soil layer heterogeneity are present in many real sites. A major assumption has been that the mine axis is vertical. In

practice, the mine could be tilted or have a horizontal axis orientation, which would influence the sensitivity and FWI data significantly.

2. Surface roughness has been modelled as random height variation. However, in a real situation surface roughness will often be due to objects such as bricks with irregular features. Subsurface clutter has been modelled by the inclusion of blocks of different permittivity, which is consistent with many buried objects, but requires further characterisation to enable the application of a broader range of clutter reduction techniques. To some extent these choices are mitigated by the limited resolution of the GPR system.
3. The soil type under test is dry sandy soil with a fixed relative permittivity and hence the data obtained do not apply for a variety of other soil types and with different moisture content or wet soil in general.
4. The AP mine parameters, dimensions and internal structure, though representative of ideal parameters for a surrogate mine, are limited in the context of the numerous types of AP blast mines, fuse mechanisms, material components and variations in size, physical structure and buried depth.
5. Few operating frequency ranges and centre frequencies have been simulated and therefore only a limited frequency response has been investigated.
6. The acquisition system analysis has been limited to the antenna system and does not include the electronic transmitter and receiver systems. The studies could also benefit from use of a wider range of UWB antennas suitable for GPR.

7. The analysis was limited to simpler antenna designs and the tolerance of the meshing properties was kept to a level consistent with the limited computing memory available.

7.3 Future Work

Several areas of future study or work are identified to validate the results obtained in this thesis and improve handheld GPR system design based on FWI for landmine detection.

Principally, the FWI experiments and implementation need to be conducted with real data; GPR measurements obtained from a physical laboratory setup or more importantly, a mine test field; to determine the true performance of handheld multi-static systems, the FWI imaging performance and the detection of the void in a mine using GPR FWI. This study has been empirical, with synthetic data. Although the 3D analysis provides a more realistic estimation of the performance of multi-static systems using FWI, real measurements are required to really test system design. The sensitivity analysis could also benefit from real data, to enable a more realistic analysis of the relationships between parameters based on the singular vectors. In view of this, a forward model that includes data and parameters acquired from real or test clearance sites is required for the FWI as this is a critical component for successful GPR data inversion. This includes a more accurate modelling and characterisation of clutter, both above and beneath the ground, which is also required for a more accurate evaluation of clutter reduction techniques. A critical goal for future work in this regard should include the investigation of clutter reduction for 3D sensitivity and FWI analysis. Additionally,

the relationships between the singular values and singular vectors could be evaluated more accurately.

Furthermore, there is potential for a study devoted to the FWI optimisation. The most beneficial size and use of a data base of measurements needs to be quantified. Understanding of the topology of the FWI objective function is likely to yield more highly efficient optimisation algorithms tuned to this application.

The antennas in this research were designed with a software tool for selected centre frequency specifications. Given the importance of the antenna system configuration and properties, novel antenna design aimed at enhanced side lobe suppression, reduction of cross-coupling and increased bandwidth is expected to achieve a positive impact on the GPR system performance.

This study was limited to an impulsive radar with A-scan processing and a focus on the centre frequency impulse response. More GPR measurements and analysis with data from scanning measurements (SAR) or multiple frequency responses may be conducted, and the performances compared.

FWI optimisation is computationally expensive and a handheld system with the required computing hardware is unlikely. However, a co-radar system with a satellite communications link to high power computing resource is a potential solution. This would involve the transmission of the recorded GPR data to a remote supercomputer (SC) or high-performance computer (HPC) and a retrieval of the FWI solution to the originating terminal. This could make FWI feasible with current technology for mine clearance operations and compensates for the lack of current portable supercomputing

systems. However, certain conditions and considerations would have to be factored. The clearing protocol may need to be adapted to this technology. Secondly, the satellite link propagation delay would need to be low enough to allow for concurrent use of the retrieved data for online demining operations on site. If GPR data were collected simultaneously with each target identified by the MD, then remote HPCs could have many minutes to perform the FWI solution. Finally, the cost of utilisation of the satellite link for the demining operation must not be prohibitive, compared to the cost of off-line FWI with on-site or remote computing resources.

BIBLIOGRAPHY

ABUJARAD, F., JOSTINGMEIER, A. and OMAR, A., 2004. Clutter removal for landmine using different signal processing techniques, *Ground Penetrating Radar, 2004. GPR 2004. Proceedings of the Tenth International Conference on* 2004, IEEE, pp. 697-700.

BARBOUR, B.A., JONES, M.W., BARNES, H.B. and LEWIS, C.P., 1998. Passive IR polarization sensors: A new technology for mine detection, *Aerospace/Defense Sensing and Controls* 1998, International Society for Optics and Photonics, pp. 96-103.

BRUSCHINI, C., GROS, B., GUERNE, F., PIECE, P. and CARMONA, O., 1998. Ground penetrating radar and imaging metal detector for antipersonnel mine detection. *Journal of Applied Geophysics,* **40**(1), pp. 59-71.

BUSCH, S., VAN DER KRUK, J., BIKOWSKI, J. and VEREECKEN, H., 2012. Quantitative conductivity and permittivity estimation using full-waveform inversion of on-ground GPR data. *Geophysics,* .

CARIN, L., GENG, N., MCCLURE, M., SICHINA, J. and NGUYEN, L., 1999. Ultra-wide-band synthetic-aperture radar for mine-field detection. *Antennas and Propagation Magazine, IEEE,* **41**(1), pp. 18-33.

CLARK, G.A., HERNANDEZ, J., DELGRANDE, N., SHERWOOD, R., LU, S., SCHAICH, P. and DURBIN, P., 1991. Computer vision for locating buried objects, *Signals, Systems and Computers, 1991. 1991 Conference Record of the Twenty-Fifth Asilomar Conference on* 1991, IEEE, pp. 1235-1239.

COLLINS, L.M., HUETTEL, L.G., SIMPSON, W.A. and TANTUM, S.L., 2002. Sensor fusion of EMI and GPR data for improved landmine detection, *Proc. SPIE* 2002, pp. 873.

COUNTS, T., GURBUZ, A.C., SCOTT, W.R., MCCLELLAN, J.H. and KIM, K., 2007. Multistatic ground-penetrating radar experiments. *Geoscience and Remote Sensing, IEEE Transactions on,* **45**(8), pp. 2544-2553.

DANIELS, D., J., ed, 2007. *Ground Penetrating Radar.* 2nd Edition edn. Stevenage, Herts: The Institution of Engineering and Technology, London, United Kingdom.

DANIELS, D., J., 1999. Resolution of UWB Signals. *IEE Proceedings on Radar Sonar and Navigation,* **146**, pp. 189.

DANIELS, D.J., 2014. The impact of antenna design on short range radar performance, *Antenna Measurements & Applications (CAMA), 2014 IEEE Conference on* 2014, IEEE, pp. 1-4.

DANIELS, D.J., 2008. A review of landmine detection using GPR, European *Radar Conference, EuRAD*, pp. 280-283.

DANIELS, D.J., 2006. A review of GPR for landmine detection. *Sensing and Imaging: An international journal,* **7**(3), pp. 90-123.

DANIELS, D.J., 2004. GPR for landmine detection, an invited review paper, *Ground Penetrating Radar, Proceedings of the Tenth International Conference on*, pp. 7-10.

DANIELS, D.J., CURTIS, P., AMIN, R. and HUNT, N., 2005. MINEHOUND™ production development, *Proc. of SPIE Vol* 2005, pp. 489.

DANIELS, D.J., CURTIS, P., HUNT, N., BRAUNSTEIN, J. and MERZ, A., 2007. MINEHOUND: transition to production, *Defense and Security Symposium*, International Society for Optics and Photonics, pp. 65531B-65531B-10.

DANIELS, D., BRAUNSTEIN, J. and NEVARD, M., 2015. Using minehound in Cambodia and Afghanistan. *Journal of Conventional Weapons Destruction,* **18**(2), pp. 14.

DANIELS, D. and CURTIS, P., 2006. MINEHOUND trials in Bosnia, Angola and Cambodia, *Proceedings of the SPIE Defense and Security Conference*, pp. 17-23.

DANIELS, D., GUNTON, D. and SCOTT, H., 1988. Introduction to subsurface radar, *IEE Proceedings (Communications, Radar and Signal Processing)*, IET, pp. 278-320.

DE HOOP, A.T., VAN DEN BERG, PETER M and REMIS, R.F., 2002. Absorbing boundary conditions and perfectly matched layers-an analytic time-domain performance analysis. *IEEE Transactions on Magnetics,* **38**(2), pp. 657-660.

DE JONGH, R., LIGTHART, L., KAPLOUN, I., SCHUKIN, A. and YAROVOY, A., 1999. Design and analysis of new GPR antenna concepts. *Tijdschrift-Nederlands Elektronica En Radiogenootschap,* **64**, pp. 26-32.

DE PAUW, D.J. and VANROLLEGHEM, P.A., 2006. Avoiding the finite difference sensitivity analysis deathtrap by using the complex-step derivative approximation technique.

DOHENY, R.C., BURKE, S., CRESCI, R., NGAN, P. and WALLS, R., 2005. *Handheld standoff mine detection system (HSTAMIDS) field evaluation in Thailand,* .

DOHENY, R.C., BURKE, S., CRESCI, R., NGAN, P., WALLS, R. and CHERNOFF, J., 2006. Handheld standoff mine detection system (HSTAMIDS) field evaluation in Namibia. *Proc. SPIE Detection and Remediation Technologies for Mines and Minelike Targets XI,* , pp. 62172K-1.

DONSKOY, D., EKIMOV, A., SEDUNOV, N. and TSIONSKIY, M., 2002. Nonlinear seismo-acoustic land mine detection and discrimination. *The Journal of the Acoustical Society of America,* **111**(6), pp. 2705-2714.

DONSKOY, D., 1998. Nonlinear seismo-acoustic technique for land mine detection and discrimination, *Detection of Abandoned Land Mines, Second International Conference on the (Conf. Publ. No. 458)*, IET, pp. 244-248.

DUBEY, A.C., HARVEY, J.F., BROACH, J.T. and GEORGE, V., 2001. Detection and Remediation Technologies for Mines and Minelike Targets VI., SPIE.

DUMANIAN, A.J. and RAPPAPORT, C.M., 2005. Enhanced detection and classification of buried mines with an UWB multistatic GPR, *IEEE Antennas and Propagation Society International Symposium*, pp. 88-91.

EARP, S., HUGHES, E., ELKINS, T. and VICKERS, R., 1996. Ultra-wideband ground-penetrating radar for the detection of buried metallic mines. *IEEE Aerospace and Electronic Systems Magazine,* **11**(9), pp. 30-39.

ELLEFSEN, K.J., MAZZELLA, A.T., HORTON, R.J. and MCKENNA, J.R., 2011. Phase and amplitude inversion of crosswell radar data. *Geophysics,* **76**(3), pp. J1-J12.

ERLANGGA, Y.A. and HERRMANN, F.J., 2008. An iterative multilevel method for computing wavefields in frequency-domain seismic inversion. *SEG Technical Program Expanded Abstracts,* Society of Exploration Geophysicists, pp. 1956-1960.

ERNST, J.R., GREEN, A.G., MAURER, H. and HOLLIGER, K., 2007. Application of a new 2D time-domain full-waveform inversion scheme to crosshole radar data. *Geophysics,* **72**(5), pp. J53-J64.

FIKE, J.A., JONGSMA, S., ALONSO, J.J. and VAN DER WEIDE, E., 2011. Optimization with gradient and hessian information calculated using hyper-dual numbers. *AIAA paper,* **3807**, pp. 2011.

GETHINS, T. and PAULSON, K., 1995. *Module 8625: Optimisation.* 2 edn. Oxford: Oxford Brookes University.

GIANNAKIS, I., 2016. Realistic numerical modelling of ground penetrating radar for landmine detection, University of Edinburgh.

GIANNOPOULOS, A. and DIAMANTI, N., 2008. Numerical modelling of ground-penetrating radar response from rough subsurface interfaces. *Near Surface Geophysics,* **6**(6), pp. 357-369.

GONZALEZ-HUICI, M.A. and USCHKERAT, U., 2010. GPR modeling for landmine detection, *Electromagnetic Theory (EMTS), 2010 URSI International Symposium on* 2010, pp. 152-155.

GUNATILAKA, A.H. and BAERTLEIN, B.A., 2001. Feature-level and decision-level fusion of noncoincidently sampled sensors for land mine detection. *IEEE Transactions on Pattern Analysis and Machine Intelligence,* **23**(6), pp. 577-589.

HABIB, M., K., 2007. Humanitarian Demining: Reality and the Challenge of Technology-The State of the Arts. *International Journal of Advanced Robotic Systems,* **4**(2), pp. 151-172.

HABIB, M.K., 2008. *Humanitarian demining: The problem, difficulties, priorities, demining technology and the challenge for robotics.* INTECH Open Access Publisher.

HERTL, I. and STRYCEK, M., 2007. UWB antennas for ground penetrating radar application, *Applied Electromagnetics and Communications, ICECom, 19th International Conference on* 2007, pp. 1-4.

HERTL, I. and STRÝČEK, M., 2009. Effective time-domain antenna modeling based on impulse-matching method, *EUROCON*, pp. 33-38.

HIBBS, A.D., BARRALL, G.A., CZIPOTT, P.V., LATHROP, D.K., LEE, Y., MAGNUSON, E.E., MATTHEWS, R. and VIERKOTTER, S.A., 1998. Land mine detection by nuclear quadrupole resonance, *Aerospace/Defense Sensing and Controls*, International Society for Optics and Photonics, pp. 522-532.

HO, K., COLLINS, L.M., HUETTEL, L.G. and GADER, P.D., 2004. Discrimination mode processing for EMI and GPR sensors for hand-held land mine detection. *IEEE Transactions on Geoscience and Remote Sensing,* **42**(1), pp. 249-263.

HYVÄRINEN, A. and OJA, E., 2000. Independent component analysis: algorithms and applications. *Neural Networks,* **13**(4), pp. 411-430.

IOTT, J., HAFTKA, R.T. and ADELMAN, H.M., 1985. Selecting step sizes in sensitivity analysis by finite differences. NASA.

JAMALI, A.A. and MARKLEIN, R., 2011. Design and optimization of ultra-wideband TEM horn antennas for GPR applications, *General Assembly and Scientific Symposium, XXXth URSI*, pp. 1-4.

KAIPIO, J. and SOMERSALO, E., 2007. Statistical inverse problems: discretization, model reduction and inverse crimes. *Journal of Computational and Applied Mathematics,* **198**(2), pp. 493-504.

KARASUWA, A.S., EASTMENT, J.D. and OTUNG, I.E., 2016. Cross-polarisation discrimination-induced interference in dual-polarised high-capacity satellite communication systems. *The Journal of Engineering,* **1**(1),.

KARIM, M., MALEK, M., JAMLOS, M., SENG, L. and SAUDIN, N., 2013. Design of Ground Penetrating Radar antenna for buried object detection, *IEEE RF and Microwave Conference (RFM),* pp. 253-257.

KELLEY, C., 1999. Detection and Remediation of Stagnation in the Nelder--Mead Algorithm Using a Sufficient Decrease Condition. *SIAM journal on optimization,* **10**(1), pp. 43-55.

KIM, D.M., KIM, S.H., LEE, S. and KIM, K., 2009. Combined metal detector and ground-penetrating radar sensor experiments in a variety of soil conditions, *Geoscience and Remote Sensing Symposium, IEEE International, IGARSS*, pp. IV-601-IV-604.

KLOTZSCHE, A., VAN DER KRUK, J., MELES, G.A., DOETSCH, J., MAURER, H. and LINDE, N., 2010. Full-waveform inversion of cross-hole ground-penetrating radar data to characterize a gravel aquifer close to the Thur River, Switzerland. *Near Surface Geophysics,* **8**(6), pp. 635-649.

KLOTZSCHE, A., VAN DER KRUK, J., MELES, G. and VEREECKEN, H., 2012. Crosshole GPR full-waveform inversion of waveguides acting as preferential flow paths within aquifer systems. *Geophysics,* **77**(4), pp. H57-H62.

KNOX, M., RUNDEL, C. and COLLINS, L., 2017. Sensor fusion for buried explosive threat detection for handheld data, *SPIE Defense Security*, International Society for Optics and Photonics, pp. 101820D-101820D-8.

KURODA, S., TAKEUCHI, M. and KIM, H.J., 2007. Full-waveform inversion algorithm for interpreting crosshole radar data: A theoretical approach. *Geosciences Journal,* **11**(3), pp. 211-217.

LIAO, Y., NOLTE, L.W. and COLLINS, L.M., 2007. Decision fusion of ground-penetrating radar and metal detector algorithms—A robust approach. *IEEE Transactions on Geoscience and Remote Sensing,* **45**(2), pp. 398-409.

LOPERA, O. and MILISAVLJEVIC, N., 2007. Prediction of the effects of soil and target properties on the antipersonnel landmine detection performance of ground-penetrating radar: A Colombian case study. *Journal of Applied Geophysics,* **63**(1), pp. 13-23.

LOPERA, O., SLOB, E.C., MILISAVLJEVIC, N. and LAMBOT, S., 2007. Filtering soil surface and antenna effects from GPR data to enhance landmine detection. *IEEE Transactions on Geoscience and Remote Sensing,* **45**(3), pp. 707-717.

MACDONALD, J., LOCKWOOD, J.R. and MCFEE, J.E.A., 2003. *Alternatives for Landmine Detection.* Santa Monica, CA: Science and Technology Policy Institute Prepared for the Office of Science and Technology Policy.

MANKINS, J.C., 1995. Technology readiness levels. *White Paper, April,* **6**, NASA.

MASARIK, M.P., BURNS, J., THELEN, B.T., KELLY, J. and HAVENS, T.C., 2016. Enhanced buried UXO detection via GPR/EMI data fusion, *SPIE Defense Security*, International Society for Optics and Photonics, pp. 98230R-98230R-9.

MCKINNON, K.I., 1998. Convergence of the Nelder--Mead Simplex Method to a Nonstationary Point. *SIAM Journal on Optimization,* **9**(1), pp. 148-158.

MELES, G.A., GREENHALGH, S.A., GREEN, A.G., MAURER, H. and VAN DER KRUK, J., 2012. GPR full-waveform sensitivity and resolution analysis using an FDTD adjoint method. *IEEE Transactions on Geoscience and Remote Sensing,* **50**(5), pp. 1881-1896.

MELES, G.A., VAN DER KRUK, J., GREENHALGH, S.A., ERNST, J.R., MAURER, H. and GREEN, A.G., 2010. A new vector waveform inversion algorithm for simultaneous updating of conductivity and permittivity parameters from combination crosshole/borehole-to-surface GPR data. *IEEE Transactions on Geoscience and Remote Sensing,* **48**(9), pp. 3391-3407.

MILLER, E., 1994. Time-domain modeling in electromagnetics. *Journal of Electromagnetic Waves and Applications,* **8**(9-10), pp. 1125-1172.

MITCHELL, O.R., HERRICK, T.J., SUMMERS, D.A., RECHTIEN, R.D., DREWNIAK, J.L., SOMU, S.R., SRINIVASAN, S., RAO, V., MOSS, R.H. and DUBROFF, R.E., 1998. New sensors and sensor fusion for a ground-based land mine detection system, *Proceedings of SPIE: Detection and Remediation Technologies for Mines and Minelike Targets III*, Society of Photo-Optical Instrumentation Engineers SPIE.

MOHAMED, H., ELSADEK, H. and ABDALLAH, E.A., 2012. Design of compact DRH antenna For GPR transmitter application, *Antennas and Propagation (MECAP), Middle East Conference on* 2012, IEEE, pp. 1-4.

MONITORING AND RESEARCH COMMITTEE, ICBL- CMC GOVERNANCE BOARD, 2016. *Landmine Monitor 2016.* Geneva: y International Campaign to Ban Landmines – Cluster Munition Coalition (ICBL-CMC).

MUNTEANU, I. and HIRTENFELDER, F., 2005. Convergence of the finite integration technique on various mesh types, *German Microwave Conference, GeMiC*.

NATAF, F., 2013. *Absorbing boundary conditions and perfectly matched layers in wave propagation problems, Direct and Inverse problems in Wave Propagation and*

Applications, 14, de Gruyter, pp.219-231, 2013, Radon Ser. Comput. Appl. Math., 978-3-11-028228-3

NELDER, J.A. and MEAD, R., 1965. A simplex method for function minimization. *The computer journal,* **7**(4), pp. 308-313.

NETO, A., MONNI, S. and NENNIE, F., 2010. UWB, non dispersive radiation from the planarly fed leaky lens antenna—Part II: Demonstrators and measurements. *IEEE Transactions on Antennas and Propagation,* **58**(7), pp. 2248-2258.

NOCEDAL, J. and WRIGHT, S., 2006. *Numerical optimization.* Springer Science & Business Media.

OBERRÖHRMANN, M., KLOTZSCHE, A., VEREECKEN, H. and VAN DER KRUK, J., 2013. Optimization of acquisition setup for cross-hole GPR full-waveform inversion using checkerboard analysis. *Near Surface Geophysics,* **11**(2), pp. 197-209.

OLOUMI, D., MOUSAVI, P., PETTERSSON, M. and ELLIOTT, D.G., 2013. A modified TEM horn antenna customized for oil well monitoring applications. *Antennas and Propagation, IEEE Transactions on,* **61**(12), pp. 5902-5909.

OZDEMIR, C., YILMAZ, B., KECELI, S.I., LEZKI, H. and SUTCUOGLU, O., Ultra Wide Band Horn Antenna Design for Ground Penetrating Radar: A Feeder Practice, *15th International Radar Symposium*, pp. 1-4.

PANZNER, B., JOSTINGMEIER, A. and OMAR, A., 2010. A compact double-ridged horn antenna for ground penetrating radar applications, *Microwave Radar and Wireless Communications (MIKON), 18th International Conference on* 2010, pp. 1-4.

PIERACCINI, M., ROJHANI, N. and MICCINESI, L., 2017. Comparison between horn and bow-tie antennas for Ground Penetrating Radar, *Advanced Ground Penetrating Radar (IWAGPR), 9th International Workshop on* 2017, pp. 1-5.

PLESSIX, R., 2006. A review of the adjoint-state method for computing the gradient of a functional with geophysical applications. *Geophysical Journal International,* **167**(2), pp. 495-503.

PODD, F.J., PEYTON, A.J. and ARMITAGE, D.W., 2015. GPR combined with a positioning system to detect anti-personnel landmines, *Advanced Ground Penetrating Radar (IWAGPR), 8th International Workshop on* 2015, pp. 1-4.

POULAIN, D.E., SCHAUB, S.A., ALEXANDER, D.R. and KRAUSE, J.K., 1998. Detection and location of buried objects using active thermal sensing, *Aerospace/Defense Sensing and Controls*, International Society for Optics and Photonics, pp. 861-866.

PRADO, J., CABRITA, G. and MARQUES, L., 2013. Bayesian sensor fusion for land-mine detection using a dual-sensor hand-held device, *Industrial Electronics Society, IECON, 39th Annual Conference of the IEEE*, pp. 3887-3892.

RAPPAPORT, C., EL-SHENAWEE, M. and ZHAN, H., 2003. Suppressing GPR clutter from randomly rough ground surfaces to enhance nonmetallic mine detection. *Subsurface Sensing Technologies and Applications,* **4**(4), pp. 311-326.

RIOS, L.M. and SAHINIDIS, N.V., 2013. Derivative-free optimization: a review of algorithms and comparison of software implementations. *Journal of Global Optimization,* , pp. 1-47.

RIYANTI, C., KONONOV, A., ERLANGGA, Y.A., VUIK, C., OOSTERLEE, C.W., PLESSIX, R. and MULDER, W.A., 2007. A parallel multigrid-based preconditioner for the 3D heterogeneous high-frequency Helmholtz equation. *Journal of Computational physics,* **224**(1), pp. 431-448.

SAI, B. and LIGTHART, L.P., 2004. GPR phase-based techniques for profiling rough surfaces and detecting small, low-contrast landmines under flat ground. *Geoscience and Remote Sensing, IEEE Transactions on,* **42**(2), pp. 318-326.

SATO, M., 2009. Principles of mine detection by ground-penetrating radar. *Anti-personnel Landmine Detection for Humanitarian Demining.* Springer, pp. 19-26.

SATO, M., FANG, G. and ZENG, Z., 2003. Landmine detection by a broadband GPR system, *Geoscience and Remote Sensing Symposium, IGARSS. Proceedings, IEEE International*, pp. 758-760.

SATO, M., FENG, X. and FUJIWARA, J., 2005. Handheld GPR and MD sensor for landmine detection, *Antennas and Propagation Society International Symposium, IEEE*, pp. 104-107.

SATO, M., FUJIWARA, J., FENG, X., ZHOU, Z. and KOBAYASHI, T., 2004. Evaluation of a Hand-held GPR MD sensor system (ALIS), *Proc. of the IARP International workshop on Robotics and Mechanical Assistance in Humanitarian Demining*, pp 21-26

SILVESTROV, I. and TCHEVERDA, V., 2011. SVD analysis in application to full waveform inversion of multicomponent seismic data, *Journal of Physics: Conference Series*, IOP Publishing, pp. 012014.

SKOLNIK, M., 2008. *Radar Handbook.* Third edn. USA: McGraw-Hill.

SOLDOVIERI, F., LOPERA, O. and LAMBOT, S., 2011. Combination of advanced inversion techniques for an accurate target localization via GPR for demining applications. *IEEE Transactions on Geoscience and Remote Sensing,* **49**(1), pp. 451-461.

STANLEY, R.J., GADER, P.D. and HO, K., 2002. Feature and decision level sensor fusion of electromagnetic induction and ground penetrating radar sensors for landmine detection with hand-held units. *Information fusion,* **3**(3), pp. 215-223.

STEINWAY, W.J., DUVOISIN, H.A., TOMASSI, M., THOMAS, J., BETTS, G., MORRIS, C., KAHN, B., STERN, P., KRYWICK, S. and JOHNSON, K., 1998. Multi-sensor system for mine detection, *Geoscience and Remote Sensing Symposium Proceedings, IGARSS, IEEE International*, pp. 228-230.

STICKLEY, G., LONGSTAFF, I. and RADCLIFFE, M., 1996. Synthetic aperture radar for the detection of shallow buried objects, *EUREL International Conference. The Detection of Abandoned Land Mines: A Humanitarian Imperative Seeking a Technical Solution,* pp 160-163.

SULE, S.D. and PAULSON, K.S., 2017a. A comparison of bistatic and multistatic handheld ground penetrating radar (GPR) antenna performance for landmine detection, *Radar Conference (RadarConf), IEEE*, pp. 1211-1215.

SULE, S.D. and PAULSON, K.S., 2017b. Enhanced feature extraction for landmine detection using handheld ground penetrating radar (GPR) based on full wave inversion (FWI), *Radar Symposium (IRS), 18th International*, pp. 1-6.

SULE, S.D. and PAULSON, K.S., 2017c. Performance measurements for full wave inversion (FWI) based multistatic handheld ground penetrating radar (GPR) for landmine detection, *Circuits, System and Simulation (ICCSS), International Conference on*, pp. 45-48.

TAJDINI, M.M., GONZALEZ-VALDES, B., MARTINEZ-LORENZO, J.A., MORGENTHALER, A.W. and RAPPAPORT, C.M., 2015. Efficient 3D forward modeling of GPR scattering from rough ground, *Antennas and Propagation & USNC/URSI National Radio Science Meeting, IEEE International Symposium on*, pp. 1686-1687.

TAKAHASHI, K. and SATO, M., 2008. A hand-held dual-sensor system using impulse GPR for demining, *IEEE International Conference on Ultra-Wideband*, pp. 157-160.

TANTUM, S.L., MORTON, K.D., COLLINS, L.M. and TORRIONE, P.A., 2012. Investigation of the effects of operator technique on handheld sensor data for landmine detection, *SPIE Defense, Security, and Sensing*, International Society for Optics and Photonics, pp. 83571B-83571B-8.

TEBCHRANY, E., SAGNARD, F., BALTAZART, V., TAREL, J.P. and DÉROBERT, X., 2014. Assessment of statistical-based clutter reduction techniques on ground-coupled GPR

data for the detection of buried objects in soils, *Ground Penetrating Radar (GPR), 15th International Conference on*, pp. 604-609.

TEIXEIRA, F.L., 2008. Time-domain finite-difference and finite-element methods for Maxwell equations in complex media. *IEEE Transactions on Antennas and Propagation,* **56**(8), pp. 2150-2166.

TEIXEIRA, F., 2001. Time-Domain Analysis. *Wiley Encyclopedia of Electrical and Electronics Engineering,* .

TESFAMARIAM, G.T., 2013. *Signal Processing Techniques for Landmine Detection Using Impulse Ground Penetrating Radar (ImGPR),* Technische Universität Darmstadt.

TEXAS RESEARCH INSTITUTE AUSTIN, INC., 2017-last update, TRI/Austin - NDE Toolbox [Homepage of Texas Research Institute Austin, Inc.], [Online]. Available: http://nditoolbox.chriscoughlin.com/quickstart.html [11/12, 2017].

UNITED NATIONS, 2003. *International Mine Action Standards.* IMAS 09.10 Second Edition, Amendment 5, June 2013 edn. New York: UNITED NATIONS MINE ACTION SERVICE.

UNITED NATIONS, 1997 (standard section 5, paragraph 10). *International Mine Action Standards.* New York: UNITED NATIONS.

VIRIEUX, J. and OPERTO, S., 2009. An overview of full-waveform inversion in exploration geophysics. *Geophysics,* **74**(6), pp. WCC1-WCC26.

WALTZ, E. and LLINAS, J., 1990. *Multisensor data fusion.* Artech house Boston.

WARREN, C., 2009. *Numerical modelling of high-frequency ground-penetrating radar antennas,* University of Edinburgh.

WATSON, F., 2016. Towards 3D full-wave inversion for GPR, *Radar Conference (RadarConf), IEEE*, pp. 1-6.

WATSON, F. and LIONHEART, W., 2014. SVD analysis of GPR full-wave inversion, *Ground Penetrating Radar (GPR), 15th International Conference on*, pp. 484-490.

WATSON, F.M., 2016. *Better imaging for landmine detection: an exploration of 3D full-wave inversion for ground-penetrating radar*, University of Manchester.

WITTEN, T., 2005. Buried mine detection using gamma rays produced by neutrons, *Proc. SPIE*, pp. 795-802.

WITTEN, T.R., 1998. Present state of the art in ground-penetrating radars for mine detection, *Proc. SPIE*, pp. 576-586.

YAMAZAKI, S., NAKANE, H. and TANAKA, A., 2002. Basic analysis of a metal detector. *IEEE Transactions on instrumentation and measurement,* **51**(4), pp. 810-814.

APPENDIX A: MULTI-STATIC DIPOLE GPR POD DATA

Simulation/ Measurement Number	X-axis coordinate of mine	Y-axis coordinate of mine	Z-axis coordinate of mine/Depth, cm (Z= 21 = 0 cm)	Distinguishability, Threshold = 0.000447671	Mine or No Mine Detection
1	2.75	-17.5	29	0.000446918	No mine
2	2.75	-17.5	32.75	0.000446733	No mine
3	2.75	-17.5	36.5	0.000446698	No mine
4	2.75	-17.5	40.25	0.000446677	No mine
5	2.75	-17.5	44	0.000446679	No mine
6	2.75	-21.25	29	0.000454922	Mine
7	2.75	-21.25	32.75	0.000454559	Mine
8	2.75	-21.25	36.5	0.000454304	Mine
9	2.75	-21.25	40.25	0.000454288	Mine
10	2.75	-21.25	44	0.000454315	Mine
11	2.75	-25	29	0.000448137	Mine
12	2.75	-25	32.75	0.000448650	Mine
13	2.75	-25	36.5	0.000448594	Mine
14	2.75	-25	40.25	0.000448514	Mine
15	2.75	-25	44	0.000448484	Mine
16	2.75	-28.75	29	0.000451214	Mine
17	2.75	-28.75	32.75	0.000450585	Mine
18	2.75	-28.75	36.5	0.000450792	Mine
19	2.75	-28.75	40.25	0.000450986	Mine
20	2.75	-28.75	44	0.000451005	Mine
21	2.75	-32.5	29	0.000448826	Mine
22	2.75	-32.5	32.75	0.000449406	Mine
23	2.75	-32.5	36.5	0.000449096	Mine
24	2.75	-32.5	40.25	0.000448924	Mine
25	2.75	-32.5	44	0.000448991	Mine
26	6.5	-17.5	29	0.000462058	Mine
27	6.5	-17.5	32.75	0.000461683	Mine
28	6.5	-17.5	36.5	0.000461491	Mine
29	6.5	-17.5	40.25	0.000461505	Mine
30	6.5	-17.5	44	0.000461542	Mine
31	6.5	-21.25	29	0.000470080	Mine
32	6.5	-21.25	32.75	0.000469121	Mine
33	6.5	-21.25	36.5	0.000469137	Mine
34	6.5	-21.25	40.25	0.000469269	Mine
35	6.5	-21.25	44	0.000469327	Mine

36	6.5	-25	29	0.000463683	Mine
37	6.5	-25	32.75	0.000463086	Mine
38	6.5	-25	36.5	0.000462961	Mine
39	6.5	-25	40.25	0.000462968	Mine
40	6.5	-25	44	0.000462974	Mine
41	6.5	-28.75	29	0.000465025	Mine
42	6.5	-28.75	32.75	0.000464966	Mine
43	6.5	-28.75	36.5	0.000465422	Mine
44	6.5	-28.75	40.25	0.000465546	Mine
45	6.5	-28.75	44	0.000465496	Mine
46	6.5	-32.5	29	0.000463964	Mine
47	6.5	-32.5	32.75	0.000463865	Mine
48	6.5	-32.5	36.5	0.000463352	Mine
49	6.5	-32.5	40.25	0.000463390	Mine
50	6.5	-32.5	44	0.000463521	Mine
51	10.25	-17.5	29	0.000446853	No mine
52	10.25	-17.5	32.75	0.000446050	No mine
53	10.25	-17.5	36.5	0.000445830	No mine
54	10.25	-17.5	40.25	0.000445876	No mine
55	10.25	-17.5	44	0.000445921	No mine
56	10.25	-21.25	29	0.000454162	Mine
57	10.25	-21.25	32.75	0.000453207	Mine
58	10.25	-21.25	36.5	0.000453351	Mine
59	10.25	-21.25	40.25	0.000453519	Mine
60	10.25	-21.25	44	0.000453563	Mine
61	10.25	-25	29	0.000448487	Mine
62	10.25	-25	32.75	0.000447714	Mine
63	10.25	-25	36.5	0.000447671	Threshold
64	10.25	-25	40.25	0.000447721	Mine
65	10.25	-25	44	0.000447721	Mine
66	10.25	-28.75	29	0.000449529	Mine
67	10.25	-28.75	32.75	0.000449674	Mine
68	10.25	-28.75	36.5	0.000450149	Mine
69	10.25	-28.75	40.25	0.000450228	Mine
70	10.25	-28.75	44	0.000450175	Mine
71	10.25	-32.5	29	0.000448873	Mine
72	10.25	-32.5	32.75	0.000448513	Mine
73	10.25	-32.5	36.5	0.000448037	Mine
74	10.25	-32.5	40.25	0.000448134	Mine
75	10.25	-32.5	44	0.000448265	Mine
76	14	-17.5	29	0.000444402	No mine
77	14	-17.5	32.75	0.000444333	No mine
78	14	-17.5	36.5	0.000444205	No mine

79	14	-17.5	40.25	0.000444192	No mine
80	14	-17.5	44	0.000444232	No mine
81	14	-21.25	29	0.000452644	Mine
82	14	-21.25	32.75	0.000451807	Mine
83	14	-21.25	36.5	0.000451695	Mine
84	14	-21.25	40.25	0.000451781	Mine
85	14	-21.25	44	0.000451833	Mine
86	14	-25	29	0.000446435	No mine
87	14	-25	32.75	0.000446228	No mine
88	14	-25	36.5	0.000446048	No mine
89	14	-25	40.25	0.000446032	No mine
90	14	-25	44	0.000446030	No mine
91	14	-28.75	29	0.000448311	Mine
92	14	-28.75	32.75	0.000448004	Mine
93	14	-28.75	36.5	0.000448400	Mine
94	14	-28.75	40.25	0.000448558	Mine
95	14	-28.75	44	0.000448528	Mine
96	14	-32.5	29	0.000446751	No mine
97	14	-32.5	32.75	0.000446974	No mine
98	14	-32.5	36.5	0.000446483	No mine
99	14	-32.5	40.25	0.000446433	No mine
100	14	-32.5	44	0.000446551	No mine
101	17.75	-17.5	29	0.000447227	No mine
102	17.75	-17.5	32.75	0.000446753	No mine
103	17.75	-17.5	36.5	0.000446695	No mine
104	17.75	-17.5	40.25	0.000446684	No mine
105	17.75	-17.5	44	0.000446663	No mine
106	17.75	-21.25	29	0.000454490	Mine
107	17.75	-21.25	32.75	0.000454561	Mine
108	17.75	-21.25	36.5	0.000454376	Mine
109	17.75	-21.25	40.25	0.000454292	Mine
110	17.75	-21.25	44	0.000454276	Mine
111	17.75	-25	29	0.000447817	Mine
112	17.75	-25	32.75	0.000448423	Mine
113	17.75	-25	36.5	0.000448590	Mine
114	17.75	-25	40.25	0.000448534	Mine
115	17.75	-25	44	0.000448479	Mine
116	17.75	-28.75	29	0.000451410	Mine
117	17.75	-28.75	32.75	0.000450734	Mine
118	17.75	-28.75	36.5	0.000450726	Mine
119	17.75	-28.75	40.25	0.000450923	Mine
120	17.75	-28.75	44	0.000450968	Mine
121	17.75	-32.5	29	0.000448657	Mine

122	17.75	-32.5	32.75	0.000449246	Mine
123	17.75	-32.5	36.5	0.000449164	Mine
124	17.75	-32.5	40.25	0.000448942	Mine
125	17.75	-32.5	44	0.000448956	Mine

APPENDIX B: BI-STATIC DIPOLE GPR POD DATA

Simulation/ Measurement Number	X-axis coordinate of mine	Y-axis coordinate of mine	Z-axis coordinate of mine/Depth, cm (Z= 21 = 0 cm)	Distinguishability Threshold = 0.00027058	Mine or No Mine Detection
1	2.75	-17.5	29	0.000272715	Mine
2	2.75	-17.5	32.75	0.000273331	Mine
3	2.75	-17.5	36.5	0.000273341	Mine
4	2.75	-17.5	40.25	0.000273232	Mine
5	2.75	-17.5	44	0.000273177	Mine
6	2.75	-21.25	29	0.000277102	Mine
7	2.75	-21.25	32.75	0.000276825	Mine
8	2.75	-21.25	36.5	0.000276646	Mine
9	2.75	-21.25	40.25	0.000276588	Mine
10	2.75	-21.25	44	0.000276580	Mine
11	2.75	-25	29	0.000271425	Mine
12	2.75	-25	32.75	0.000271073	Mine
13	2.75	-25	36.5	0.000270964	Mine
14	2.75	-25	40.25	0.000270950	Mine
15	2.75	-25	44	0.000270953	Mine
16	2.75	-28.75	29	0.000277118	Mine
17	2.75	-28.75	32.75	0.000276842	Mine
18	2.75	-28.75	36.5	0.000276653	Mine
19	2.75	-28.75	40.25	0.000276595	Mine
20	2.75	-28.75	44	0.000276598	Mine
21	2.75	-32.5	29	0.000272714	Mine
22	2.75	-32.5	32.75	0.000273331	Mine
23	2.75	-32.5	36.5	0.000273336	Mine
24	2.75	-32.5	40.25	0.000273238	Mine
25	2.75	-32.5	44	0.000273183	Mine
26	6.5	-17.5	29	0.000281764	Mine
27	6.5	-17.5	32.75	0.000281652	Mine
28	6.5	-17.5	36.5	0.000281436	Mine
29	6.5	-17.5	40.25	0.000281349	Mine
30	6.5	-17.5	44	0.000281333	Mine
31	6.5	-21.25	29	0.000284975	Mine
32	6.5	-21.25	32.75	0.000284806	Mine
33	6.5	-21.25	36.5	0.000284776	Mine
34	6.5	-21.25	40.25	0.000284783	Mine
35	6.5	-21.25	44	0.000284797	Mine

36	6.5	-25	29	0.000279040	Mine
37	6.5	-25	32.75	0.000279066	Mine
38	6.5	-25	36.5	0.000279059	Mine
39	6.5	-25	40.25	0.000279066	Mine
40	6.5	-25	44	0.000279067	Mine
41	6.5	-28.75	29	0.000284966	Mine
42	6.5	-28.75	32.75	0.000284797	Mine
43	6.5	-28.75	36.5	0.000284777	Mine
44	6.5	-28.75	40.25	0.000284783	Mine
45	6.5	-28.75	44	0.000284791	Mine
46	6.5	-32.5	29	0.000281749	Mine
47	6.5	-32.5	32.75	0.000281629	Mine
48	6.5	-32.5	36.5	0.000281409	Mine
49	6.5	-32.5	40.25	0.000281326	Mine
50	6.5	-32.5	44	0.000281309	Mine
51	10.25	-17.5	29	0.000273303	Mine
52	10.25	-17.5	32.75	0.000273019	Mine
53	10.25	-17.5	36.5	0.000272810	Mine
54	10.25	-17.5	40.25	0.000272752	Mine
55	10.25	-17.5	44	0.000272748	Mine
56	10.25	-21.25	29	0.000276177	Mine
57	10.25	-21.25	32.75	0.000276128	Mine
58	10.25	-21.25	36.5	0.000276130	Mine
59	10.25	-21.25	40.25	0.000276134	Mine
60	10.25	-21.25	44	0.000276146	Mine
61	10.25	-25	29	0.000270599	Mine
62	10.25	-25	32.75	0.000270599	Mine
63	10.25	-25	36.5	0.000270580	Threshold
64	10.25	-25	40.25	0.000270566	No Mine
65	10.25	-25	44	0.000270558	No Mine
66	10.25	-28.75	29	0.000276220	Mine
67	10.25	-28.75	32.75	0.000276177	Mine
68	10.25	-28.75	36.5	0.000276176	Mine
69	10.25	-28.75	40.25	0.000276190	Mine
70	10.25	-28.75	44	0.000276191	Mine
71	10.25	-32.5	29	0.000273311	Mine
72	10.25	-32.5	32.75	0.000273030	Mine
73	10.25	-32.5	36.5	0.000272817	Mine
74	10.25	-32.5	40.25	0.000272760	Mine
75	10.25	-32.5	44	0.000272760	Mine
76	14	-17.5	29	0.000272125	Mine
77	14	-17.5	32.75	0.000272273	Mine
78	14	-17.5	36.5	0.000272086	Mine

79	14	-17.5	40.25	0.000271987	Mine
80	14	-17.5	44	0.000271967	Mine
81	14	-21.25	29	0.000275770	Mine
82	14	-21.25	32.75	0.000275459	Mine
83	14	-21.25	36.5	0.000275376	Mine
84	14	-21.25	40.25	0.000275370	Mine
85	14	-21.25	44	0.000275380	Mine
86	14	-25	29	0.000269829	No Mine
87	14	-25	32.75	0.000269751	No Mine
88	14	-25	36.5	0.000269744	No Mine
89	14	-25	40.25	0.000269751	No Mine
90	14	-25	44	0.000269766	No Mine
91	14	-28.75	29	0.000275707	Mine
92	14	-28.75	32.75	0.000275393	Mine
93	14	-28.75	36.5	0.000275314	Mine
94	14	-28.75	40.25	0.000275307	Mine
95	14	-28.75	44	0.000275313	Mine
96	14	-32.5	29	0.000272107	Mine
97	14	-32.5	32.75	0.000272255	Mine
98	14	-32.5	36.5	0.000272075	Mine
99	14	-32.5	40.25	0.000271966	Mine
100	14	-32.5	44	0.000271941	Mine
101	17.75	-17.5	29	0.000272597	Mine
102	17.75	-17.5	32.75	0.000273199	Mine
103	17.75	-17.5	36.5	0.000273413	Mine
104	17.75	-17.5	40.25	0.000273362	Mine
105	17.75	-17.5	44	0.000273307	Mine
106	17.75	-21.25	29	0.000276839	Mine
107	17.75	-21.25	32.75	0.000276987	Mine
108	17.75	-21.25	36.5	0.000276831	Mine
109	17.75	-21.25	40.25	0.000276738	Mine
110	17.75	-21.25	44	0.000276705	Mine
111	17.75	-25	29	0.000271512	Mine
112	17.75	-25	32.75	0.000271321	Mine
113	17.75	-25	36.5	0.000271143	Mine
114	17.75	-25	40.25	0.000271075	Mine
115	17.75	-25	44	0.000271066	Mine
116	17.75	-28.75	29	0.000276770	Mine
117	17.75	-28.75	32.75	0.000276921	Mine
118	17.75	-28.75	36.5	0.000276755	Mine
119	17.75	-28.75	40.25	0.000276662	Mine
120	17.75	-28.75	44	0.000276642	Mine
121	17.75	-32.5	29	0.000272583	Mine

122	17.75	-32.5	32.75	0.000273177	Mine
123	17.75	-32.5	36.5	0.000273392	Mine
124	17.75	-32.5	40.25	0.000273349	Mine
125	17.75	-32.5	44	0.000273292	Mine

APPENDIX C: MULTI-STATIC VIVALDI GPR SYSTEM POD DATA

Simulation/ Measurement Number	X-axis coordinate of mine	Y-axis coordinate of mine	Z-axis coordinate of mine/Depth, cm, (Z= 21 = 0 cm)	Distinguishability, Threshold = 7.6379E-07	Mine or No Mine Detection
1	2.75	-17.5	29	9.7619E-08	No mine
2	2.75	-17.5	32.75	9.6660E-08	No mine
3	2.75	-17.5	36.5	1.0755E-07	No mine
4	2.75	-17.5	40.25	1.1001E-07	No mine
5	2.75	-17.5	44	9.6506E-08	No mine
6	2.75	-21.25	29	1.8740E-07	No mine
7	2.75	-21.25	32.75	2.1183E-07	No mine
8	2.75	-21.25	36.5	2.2131E-07	No mine
9	2.75	-21.25	40.25	2.1158E-07	No mine
10	2.75	-21.25	44	2.0596E-07	No mine
11	2.75	-25	29	1.5740E-07	No mine
12	2.75	-25	32.75	1.6063E-07	No mine
13	2.75	-25	36.5	1.7691E-07	No mine
14	2.75	-25	40.25	1.7232E-07	No mine
15	2.75	-25	44	1.5417E-07	No mine
16	2.75	-28.75	29	1.4063E-07	No mine
17	2.75	-28.75	32.75	1.3404E-07	No mine
18	2.75	-28.75	36.5	1.4388E-07	No mine
19	2.75	-28.75	40.25	1.4352E-07	No mine
20	2.75	-28.75	44	1.3302E-07	No mine
21	2.75	-32.5	29	1.7183E-07	No mine
22	2.75	-32.5	32.75	1.7427E-07	No mine
23	2.75	-32.5	36.5	1.9218E-07	No mine
24	2.75	-32.5	40.25	1.9441E-07	No mine
25	2.75	-32.5	44	1.8149E-07	No mine
26	6.5	-17.5	29	2.4410E-07	No mine
27	6.5	-17.5	32.75	2.3818E-07	No mine
28	6.5	-17.5	36.5	2.5703E-07	No mine
29	6.5	-17.5	40.25	2.5681E-07	No mine
30	6.5	-17.5	44	2.3689E-07	No mine
31	6.5	-21.25	29	4.1158E-07	No mine
32	6.5	-21.25	32.75	4.2805E-07	No mine
33	6.5	-21.25	36.5	4.4805E-07	No mine
34	6.5	-21.25	40.25	4.4047E-07	No mine
35	6.5	-21.25	44	4.2962E-07	No mine

36	6.5	-25	29	3.0169E-07	No mine
37	6.5	-25	32.75	3.0905E-07	No mine
38	6.5	-25	36.5	3.2853E-07	No mine
39	6.5	-25	40.25	3.2838E-07	No mine
40	6.5	-25	44	3.0629E-07	No mine
41	6.5	-28.75	29	2.5789E-07	No mine
42	6.5	-28.75	32.75	2.5264E-07	No mine
43	6.5	-28.75	36.5	2.6882E-07	No mine
44	6.5	-28.75	40.25	2.6806E-07	No mine
45	6.5	-28.75	44	2.5404E-07	No mine
46	6.5	-32.5	29	3.1600E-07	No mine
47	6.5	-32.5	32.75	3.1525E-07	No mine
48	6.5	-32.5	36.5	3.4173E-07	No mine
49	6.5	-32.5	40.25	3.4086E-07	No mine
50	6.5	-32.5	44	3.2684E-07	No mine
51	10.25	-17.5	29	7.0467E-07	No mine
52	10.25	-17.5	32.75	6.9342E-07	No mine
53	10.25	-17.5	36.5	6.9858E-07	No mine
54	10.25	-17.5	40.25	7.0282E-07	No mine
55	10.25	-17.5	44	6.8156E-07	No mine
56	10.25	-21.25	29	8.3920E-07	Mine
57	10.25	-21.25	32.75	8.4153E-07	Mine
58	10.25	-21.25	36.5	8.4173E-07	Mine
59	10.25	-21.25	40.25	8.5406E-07	Mine
60	10.25	-21.25	44	8.3987E-07	Mine
61	10.25	-25	29	7.6477E-07	Mine
62	10.25	-25	32.75	7.6881E-07	Mine
63	10.25	-25	36.5	7.6379E-07	Threshold
64	10.25	-25	40.25	7.7979E-07	Mine
65	10.25	-25	44	7.5988E-07	No mine
66	10.25	-28.75	29	6.2599E-07	No mine
67	10.25	-28.75	32.75	6.1390E-07	No mine
68	10.25	-28.75	36.5	6.1588E-07	No mine
69	10.25	-28.75	40.25	6.2220E-07	No mine
70	10.25	-28.75	44	6.1011E-07	No mine
71	10.25	-32.5	29	6.9324E-07	No mine
72	10.25	-32.5	32.75	6.8708E-07	No mine
73	10.25	-32.5	36.5	6.9794E-07	No mine
74	10.25	-32.5	40.25	7.0262E-07	No mine
75	10.25	-32.5	44	6.9004E-07	No mine
76	14	-17.5	29	1.0644E-07	No mine
77	14	-17.5	32.75	1.0576E-07	No mine
78	14	-17.5	36.5	1.1502E-07	No mine

79	14	-17.5	40.25	1.0898E-07	No mine
80	14	-17.5	44	9.8689E-08	No mine
81	14	-21.25	29	2.5831E-07	No mine
82	14	-21.25	32.75	2.8432E-07	No mine
83	14	-21.25	36.5	2.8890E-07	No mine
84	14	-21.25	40.25	2.7371E-07	No mine
85	14	-21.25	44	2.7079E-07	No mine
86	14	-25	29	2.1784E-07	No mine
87	14	-25	32.75	2.2734E-07	No mine
88	14	-25	36.5	2.3501E-07	No mine
89	14	-25	40.25	2.2650E-07	No mine
90	14	-25	44	2.1117E-07	No mine
91	14	-28.75	29	1.2649E-07	No mine
92	14	-28.75	32.75	1.2264E-07	No mine
93	14	-28.75	36.5	1.2693E-07	No mine
94	14	-28.75	40.25	1.1740E-07	No mine
95	14	-28.75	44	1.1268E-07	No mine
96	14	-32.5	29	1.5311E-07	No mine
97	14	-32.5	32.75	1.5576E-07	No mine
98	14	-32.5	36.5	1.6991E-07	No mine
99	14	-32.5	40.25	1.6192E-07	No mine
100	14	-32.5	44	1.5627E-07	No mine
101	17.75	-17.5	29	4.9869E-08	No mine
102	17.75	-17.5	32.75	4.9146E-08	No mine
103	17.75	-17.5	36.5	5.2987E-08	No mine
104	17.75	-17.5	40.25	5.0178E-08	No mine
105	17.75	-17.5	44	4.5268E-08	No mine
106	17.75	-21.25	29	1.5343E-07	No mine
107	17.75	-21.25	32.75	1.8263E-07	No mine
108	17.75	-21.25	36.5	1.8056E-07	No mine
109	17.75	-21.25	40.25	1.6597E-07	No mine
110	17.75	-21.25	44	1.6791E-07	No mine
111	17.75	-25	29	1.1391E-07	No mine
112	17.75	-25	32.75	1.2666E-07	No mine
113	17.75	-25	36.5	1.3438E-07	No mine
114	17.75	-25	40.25	1.1923E-07	No mine
115	17.75	-25	44	1.1104E-07	No mine
116	17.75	-28.75	29	9.4575E-08	No mine
117	17.75	-28.75	32.75	9.2191E-08	No mine
118	17.75	-28.75	36.5	9.8637E-08	No mine
119	17.75	-28.75	40.25	8.8776E-08	No mine
120	17.75	-28.75	44	8.5934E-08	No mine
121	17.75	-32.5	29	1.2483E-07	No mine

122	17.75	-32.5	32.75	1.2622E-07	No mine
123	17.75	-32.5	36.5	1.3944E-07	No mine
124	17.75	-32.5	40.25	1.3429E-07	No mine
125	17.75	-32.5	44	1.3009E-07	No mine

APPENDIX D: BI-STATIC VIVALDI GPR SYSTEM POD DATA

Simulation/ Measurement Number	X-axis coordinate of mine	Y-axis coordinate of mine	Z-axis coordinate of mine/Depth, cm, (Z= 21 = 0 cm)	Distinguishability, Threshold = 7.4684E-07	Mine or No Mine Detection
1	2.75	-17.5	29	7.4444E-08	No mine
2	2.75	-17.5	32.75	7.1103E-08	No mine
3	2.75	-17.5	36.5	7.4544E-08	No mine
4	2.75	-17.5	40.25	7.8504E-08	No mine
5	2.75	-17.5	44	6.8268E-08	No mine
6	2.75	-21.25	29	1.7224E-07	No mine
7	2.75	-21.25	32.75	1.8283E-07	No mine
8	2.75	-21.25	36.5	1.7996E-07	No mine
9	2.75	-21.25	40.25	1.9039E-07	No mine
10	2.75	-21.25	44	1.7584E-07	No mine
11	2.75	-25	29	1.7238E-07	No mine
12	2.75	-25	32.75	1.8533E-07	No mine
13	2.75	-25	36.5	1.8398E-07	No mine
14	2.75	-25	40.25	1.9247E-07	No mine
15	2.75	-25	44	1.7659E-07	No mine
16	2.75	-28.75	29	8.5108E-08	No mine
17	2.75	-28.75	32.75	7.3407E-08	No mine
18	2.75	-28.75	36.5	7.9054E-08	No mine
19	2.75	-28.75	40.25	7.8841E-08	No mine
20	2.75	-28.75	44	7.1497E-08	No mine
21	2.75	-32.5	29	8.1652E-08	No mine
22	2.75	-32.5	32.75	7.5394E-08	No mine
23	2.75	-32.5	36.5	8.0397E-08	No mine
24	2.75	-32.5	40.25	8.0183E-08	No mine
25	2.75	-32.5	44	7.3497E-08	No mine
26	6.5	-17.5	29	2.0405E-07	No mine
27	6.5	-17.5	32.75	1.9559E-07	No mine
28	6.5	-17.5	36.5	2.0752E-07	No mine
29	6.5	-17.5	40.25	2.116E-07	No mine
30	6.5	-17.5	44	1.9564E-07	No mine
31	6.5	-21.25	29	3.7592E-07	No mine
32	6.5	-21.25	32.75	3.8365E-07	No mine
33	6.5	-21.25	36.5	3.9486E-07	No mine
34	6.5	-21.25	40.25	4.0382E-07	No mine
35	6.5	-21.25	44	3.826E-07	No mine

36	6.5	-25	29	3.1169E-07	No mine
37	6.5	-25	32.75	3.2119E-07	No mine
38	6.5	-25	36.5	3.3281E-07	No mine
39	6.5	-25	40.25	3.4118E-07	No mine
40	6.5	-25	44	3.197E-07	No mine
41	6.5	-28.75	29	1.9044E-07	No mine
42	6.5	-28.75	32.75	1.783E-07	No mine
43	6.5	-28.75	36.5	1.8826E-07	No mine
44	6.5	-28.75	40.25	1.9326E-07	No mine
45	6.5	-28.75	44	1.7767E-07	No mine
46	6.5	-32.5	29	1.9619E-07	No mine
47	6.5	-32.5	32.75	1.8395E-07	No mine
48	6.5	-32.5	36.5	1.9588E-07	No mine
49	6.5	-32.5	40.25	1.9775E-07	No mine
50	6.5	-32.5	44	1.8475E-07	No mine
51	10.25	-17.5	29	5.7551E-07	No mine
52	10.25	-17.5	32.75	5.5917E-07	No mine
53	10.25	-17.5	36.5	5.6702E-07	No mine
54	10.25	-17.5	40.25	5.7589E-07	No mine
55	10.25	-17.5	44	5.5755E-07	No mine
56	10.25	-21.25	29	8.0177E-07	Mine
57	10.25	-21.25	32.75	7.9345E-07	Mine
58	10.25	-21.25	36.5	8.0037E-07	Mine
59	10.25	-21.25	40.25	8.1652E-07	Mine
60	10.25	-21.25	44	7.9272E-07	Mine
61	10.25	-25	29	7.4668E-07	No mine
62	10.25	-25	32.75	7.4134E-07	No mine
63	10.25	-25	36.5	7.4684E-07	Threshold
64	10.25	-25	40.25	7.6208E-07	Mine
65	10.25	-25	44	7.3955E-07	No mine
66	10.25	-28.75	29	5.2812E-07	No mine
67	10.25	-28.75	32.75	5.0623E-07	No mine
68	10.25	-28.75	36.5	5.1163E-07	No mine
69	10.25	-28.75	40.25	5.2347E-07	No mine
70	10.25	-28.75	44	5.0467E-07	No mine
71	10.25	-32.5	29	5.3078E-07	No mine
72	10.25	-32.5	32.75	5.1169E-07	No mine
73	10.25	-32.5	36.5	5.1885E-07	No mine
74	10.25	-32.5	40.25	5.2617E-07	No mine
75	10.25	-32.5	44	5.1066E-07	No mine
76	14	-17.5	29	7.8558E-08	No mine
77	14	-17.5	32.75	7.1571E-08	No mine
78	14	-17.5	36.5	7.7401E-08	No mine

79	14	-17.5	40.25	7.7754E-08	No mine
80	14	-17.5	44	6.8341E-08	No mine
81	14	-21.25	29	2.2968E-07	No mine
82	14	-21.25	32.75	2.3782E-07	No mine
83	14	-21.25	36.5	2.3944E-07	No mine
84	14	-21.25	40.25	2.4222E-07	No mine
85	14	-21.25	44	2.2977E-07	No mine
86	14	-25	29	2.2059E-07	No mine
87	14	-25	32.75	2.2868E-07	No mine
88	14	-25	36.5	2.3171E-07	No mine
89	14	-25	40.25	2.3309E-07	No mine
90	14	-25	44	2.1949E-07	No mine
91	14	-28.75	29	8.6001E-08	No mine
92	14	-28.75	32.75	7.0229E-08	No mine
93	14	-28.75	36.5	7.485E-08	No mine
94	14	-28.75	40.25	7.3509E-08	No mine
95	14	-28.75	44	6.5238E-08	No mine
96	14	-32.5	29	8.1609E-08	No mine
97	14	-32.5	32.75	7.0805E-08	No mine
98	14	-32.5	36.5	7.8021E-08	No mine
99	14	-32.5	40.25	7.5299E-08	No mine
100	14	-32.5	44	6.8891E-08	No mine
101	17.75	-17.5	29	3.5988E-08	No mine
102	17.75	-17.5	32.75	3.3578E-08	No mine
103	17.75	-17.5	36.5	3.4008E-08	No mine
104	17.75	-17.5	40.25	3.4064E-08	No mine
105	17.75	-17.5	44	2.85E-08	No mine
106	17.75	-21.25	29	1.3725E-07	No mine
107	17.75	-21.25	32.75	1.4948E-07	No mine
108	17.75	-21.25	36.5	1.4163E-07	No mine
109	17.75	-21.25	40.25	1.4903E-07	No mine
110	17.75	-21.25	44	1.3681E-07	No mine
111	17.75	-25	29	1.4E-07	No mine
112	17.75	-25	32.75	1.5558E-07	No mine
113	17.75	-25	36.5	1.4867E-07	No mine
114	17.75	-25	40.25	1.5276E-07	No mine
115	17.75	-25	44	1.3973E-07	No mine
116	17.75	-28.75	29	4.8903E-08	No mine
117	17.75	-28.75	32.75	4.2517E-08	No mine
118	17.75	-28.75	36.5	4.4319E-08	No mine
119	17.75	-28.75	40.25	3.9716E-08	No mine
120	17.75	-28.75	44	3.6469E-08	No mine
121	17.75	-32.5	29	4.8416E-08	No mine

122	17.75	-32.5	32.75	4.3478E-08	No mine
123	17.75	-32.5	36.5	4.4952E-08	No mine
124	17.75	-32.5	40.25	4.1418E-08	No mine
125	17.75	-32.5	44	3.9381E-08	No mine